Quantification of the Relationship between Surrogate Fuel Structure and Performance

R. P. Lindstedt
R. K. Robinson

Imperial College of Science, Technology and Medicine
Department of Mechanical Engineering
Exhibition Road
London, United Kingdom SW7 2AZ

Report Date: July 2012

Final Report from 21 July 2009 to 20 July 2012

REPORT DOCUMENTATION PAGE		Form Approved OMB No. 0704-0188

Public reporting burden for this collection of information is estimated to average 1 hour per response, including the time for reviewing instructions, searching existing data sources, gathering and maintaining the data needed, and completing and reviewing the collection of information. Send comments regarding this burden estimate or any other aspect of this collection of information, including suggestions for reducing the burden, to Department of Defense, Washington Headquarters Services, Directorate for Information Operations and Reports (0704-0188), 1215 Jefferson Davis Highway, Suite 1204, Arlington, VA 22202-4302. Respondents should be aware that notwithstanding any other provision of law, no person shall be subject to any penalty for failing to comply with a collection of information if it does not display a currently valid OMB control number. **PLEASE DO NOT RETURN YOUR FORM TO THE ABOVE ADDRESS.**

1. REPORT DATE *(DD-MM-YYYY)* 31 July 2012	2. REPORT TYPE Final Report	3. DATES COVERED *(From – To)* 21 July 2009 – 20 July 2012

4. TITLE AND SUBTITLE	5a. CONTRACT NUMBER
Quantification of the Relationship between Surrogate Fuel Structure and Performance	**FA8655-09-1-3089**
	5b. GRANT NUMBER
	Grant 09-3089
	5c. PROGRAM ELEMENT NUMBER
	61102F

6. AUTHOR(S)	5d. PROJECT NUMBER
R. P. Lindstedt R. K. Robinson	
	5d. TASK NUMBER
	5e. WORK UNIT NUMBER

7. PERFORMING ORGANIZATION NAME(S) AND ADDRESS(ES) Imperial College of Science, Technology and Medicine Department of Mechanical Engineering Exhibition Road London, United Kingdom SW7 2AZ	8. PERFORMING ORGANIZATION REPORT NUMBER N/A

9. SPONSORING/MONITORING AGENCY NAME(S) AND ADDRESS(ES) EOARD Unit 4515 BOX 14 APO AE 09421	10. SPONSOR/MONITOR'S ACRONYM(S) AFRL/AFOSR/RSW (EOARD)
	11. SPONSOR/MONITOR'S REPORT NUMBER(S) **AFRL-AFOSR-UK-TR-2012-0033**

12. DISTRIBUTION/AVAILABILITY STATEMENT

Approved for public release; distribution is unlimited.

13. SUPPLEMENTARY NOTES

Government Purpose Rights

14. ABSTRACT
The project commenced in August 2009 and the current final report outlines some of the progress made during the grant period. The overall objective of the research has been to contribute to a quantitative understanding of combustion processes to a degree that permits a rational link between the structure of the fuel and observed performance.
This effort explored the geometries and energetics of a group of bimolecular hydrogen exchange reactions involved in the combustion of nPB. Energies from a wide selection of methods were compared with the CCSD(T)/aug-cc-pVDZ//M06-2X/6-311++G(3df,3pd) level of theory, the most accurate achievable for molecules the size of nPB. It was established that the energies produced at M06-2X/6-31G(2df,p) level provide a comparatively good match. Thermodynamic data, based on the G4 calculations, was also produced in the form of JANAF polynomials for the compounds involved. Kinetic rate data was determined for a range of temperatures using TST and TST/SCT. For the current bimolecular reactions no variational character was found and we recommend the use of the TST/SCT determination obtained at the M06-2X/6-31G(2df,p) level. However, for reaction (6), a disagreement of -6.9 kJ mol-1 in the barrier height, as compared to the CC calculation, has been highlighted and we therefore recommend the rate based on TST using CCSD(T)/aug-cc-pVDZ energies. Some agreement was found between our calculations and older reaction class based determinations. However, for the CH3 based extractions significant deviations were noted. Finally, the current exercise has allowed the identification of candidate functionals and basis sets that describe the nPB system with sufficient accuracy.

15. SUBJECT TERMS

EOARD, Fuels, Thermodynamics, Combustion

16. SECURITY CLASSIFICATION OF:			17. LIMITATION OF ABSTRACT	18, NUMBER OF PAGES	19a. NAME OF RESPONSIBLE PERSON Gregg Abate
a. REPORT UNCLAS	b. ABSTRACT UNCLAS	c. THIS PAGE UNCLAS	SAR	103	19b. TELEPHONE NUMBER *(Include area code)* +44 (0)1895 616021

Standard Form 298 (Rev. 8/98)
Prescribed by ANSI Std. Z39-18

Imperial College London

Quantification of the Relationship Between Surrogate Fuel Structure and Performance

Final Report on Grant FA8655-09-1-3089

R.P. Lindstedt and R.K. Robinson

Department of Mechanical Engineering, Imperial College London, Exhibition Road, London, SW7 2AZ, UK

Principal Investigator R. P. Lindstedt

July 2012

Contract Information

Grant Number	FA8655-09-1-3089
Title of Research	Quantification of the Relationship Between Surrogate Fuel Structure and Performance
Principal Investigator	R P Lindstedt
Organization	Imperial College London

Summary

The project commenced in August 2009 and the current final report outlines some of the progress made during the grant period.

The overall objective of the research has been to contribute to a quantitative understanding of combustion processes to a degree that permits a rational link between the structure of the fuel and observed performance.

A particular challenge is to establish to what extent theoretical rate constant calculations can augment reaction class based methods for realistic fuel components or breakdown products of direct relevance to aviation fuels. Given the complexities of molecules of practical interest, a compromise between the different elements of such calculation procedures is required. The impact of uncertainties, for example associated with transition state energies obtained with different levels of theory, on rate constants also typically remains to be formally assessed. Furthermore, practical systems often feature elevated pressures while laboratory data used for mechanism validation is often obtained at sub-atmospheric conditions. Accordingly, the absence of fall-off effects for pressure dependent reactions can be expected to add significantly to uncertainties to the point where such effects may become dominant. Hence, a balanced approach accounting for a wide range of error sources is in our view appropriate.

Aromatics form an integral part of typical aviation fuels with n-propyl benzene (nPB) selected as a representative molecule for inclusion in EU and US surrogate blends and with cyclopentadiene (CPD) a key intermediate in the oxidation of virtually all aromatic fuel components as well as a potential source of poly-aromatic hydrocarbons (PAH). Despite the practical relevance of such fuel molecules, kinetic and thermodynamic data, obtained using comparatively accurate *ab initio* methods (e.g. quantum mechanical methods combined with transition state theory), have not to date been compared with currently used reaction class based estimates or comparatively simple computational chemistry methods. The use of *ab initio* methods for comparatively complex molecules also requires an assessment of the relative benefits of higher levels of theory as it is typically necessary to balance a desire to understand individual reactions with the need to consider more complete reaction sequences.

Two systems of particular interest to aviation fuels, cyclopentadiene (cf. R.K. Robinson and R.P. Lindstedt, Combustion and Flame, 158 (2011) 666-686) and n-propyl benzene, were considered as suitable target molecules and pursued, as outlined below, along with an interest in creating a consistent thermochemical database at the G4 and G4MP2 levels of theory. One conclusion of the work is that these composite methods – if used in a consistent manner – provide data of sufficient quality for a wide

selection of stable molecule and radicals. The adopted calculation method for the determination of such data is outlined in Appendix 1 in the context of cyclopentadiene along with comparisons with literature data from sources such as the Argonne Active Thermochemical Tables and NIST/JANAF databases.

The issue is further explored in the context of the n-propyl benzene system, as outlined in Appendix 2, where the issue of the energetics of transition states is also addressed at some length. The current final report examines six hydrogen extractions from the n-propyl side chain in an effort that is almost complete. Potential energy surfaces (PES) were determined using a wide range of different approaches with results presented relative to data obtained using the CCSD(T)/aug-cc-pVDZ//M062X/6-311++G(3df,3pd) method. Rate parameters were hence determined using transition state theory (TST) with small curvature tunnelling (SCT) combined with energetics obtained at (i) the M062X/6-31G(2df,p) and (ii) the CCSD(T)/aug-cc-pVDZ levels. Results were found to agree comparatively well with differences in barrier heights less than 8 kJ/mol, resulting in comparatively modest differences in reaction rates, while substantial deviations can arise with respect to even very recent reaction class based estimates.

The selection of the fuel components was based on discussions with the Surrogate Fuels Energy IPT (PI: Egolfopoulous, USC) and MURI (PI: Dryer, Princeton) projects and the authors wish the express their gratitude for the interactions with these groups.

Appendix 1: Summary of Work on the Cyclopentadiene System

On the Chemical Kinetics of Cyclopentadiene Oxidation

R.K. Robinson, R.P. Lindstedt*

Department of Mechanical Engineering, Imperial College London, South Kensington Campus, London, SW7 2AZ, UK

Abstract

The cyclopentadiene/cyclopentadienyl system forms a critical part in the oxidation chemistry of aromatic fuel components used in surrogate fuels and the importance of the cyclopentadienyl radical in poly-aromatic hydrocarbon (PAH) growth has also been noted due to its site dependent reactivity. The latter aspect has been subject to a number of studies along with the initial pyrolysis steps. By contrast, few studies have been performed of the corresponding oxidation chemistry under conditions of relevance to combustion applications. Thermochemical data for oxidation reactions featuring the cyclopentadienyl radical with O, OH, HO_2 and O_2 were determined at the G3B3 and G4/G4MP2 levels in combination with an analysis of internal rotations using density functional theory and with the Jahn–Teller effect treated as a pseudo-rotation. The calculated potential energy surfaces were subsequently used in a consistent manner for the determination of pressure dependent reaction rate parameters through the Rice-Ramsperger-Kassel-Marcus/master-equation approach with Eckart quantum tunnelling corrections applied to reactions involving hydrogen transfers. The accuracy of the method was further investigated by comparisons of computed rate parameters for selected pyrolysis reactions with alternative determinations. The resulting chemistry was incorporated into an evaluation framework for the study of cyclopentadiene oxidation using recent experimental flow reactor data and principal uncertainties in reaction pathways assessed.

Keywords: Kinetics—Cyclopentadienyl—RRKM—Oxidation—*ab initio*

1. Background

The oxidation of cyclopentadiene (CPD) remains of central importance to the chemistry of aromatics in combustion applications as exemplified by a number of studies covering the chemistry of benzene, toluene and other substituted

---

*Corresponding author. Fax: +44 20 75945696.
Email address: p.lindstedt@imperial.ac.uk (R.P. Lindstedt)

aromatics. However, experimental studies using cyclopentadiene as a fuel are scarce. The CPD oxidation data sets obtained by Butler [1] and Butler and Glassman [2] using a flow reactor therefore present a particularly welcome basis from which to investigate the major oxidation and mass growth channels. Such an analysis is presented below along with updated thermochemistry for key reactions, selected on the basis of earlier studies of related systems (e.g. [3–8]), involved in the oxidation of the cyclopentadienyl radical (CPDyl) via O_2, HO_2, O and OH attack. In particular, Zhong and Bozzelli [4] performed a comprehensive study of the oxidation of the cyclopentadienyl radical with results used in a number of subsequent chemical kinetic models for combustion applications (e.g. [9, 10]). The thermochemical parameters were obtained from literature values or calculated using group additivity. Enthalpies for radical species were determined from the enthalpy of the parent molecules and taking into account C-H or O-H bond enthalpies. Entropies and heat capacities were calculated using the hydrogen bond increment technique. The effects of changes in vibrational frequencies, internal rotations and symmetry that occur with the loss of the H atom were taken into account. The fate of cyclopentadienone (CPDone) was not investigated. However, Wang and Brezinsky [11] performed a study of the thermal decomposition of using a hybrid G2MP2 based method, while Alzueta et al. [9], DiNaro et al. [12] and Ristori et al. [13] investigated benzene oxidation under conditions related to the current study. In particular, Alzueta et al. [9] discussed the challenges associated with the CPDone chemistry.

In the current study, Density Functional Theory (DFT) and composite energy calculations were performed at the G4/G4MP2 level using Gaussian09 [14] with molecules initially subjected to a low level minimisation to determine their basic configurations. If a molecule was found to have many rotatable bonds, or if the structure appeared to be strained, a conformational analysis was performed with DFT calculations using the Becke-3–Lee–Yang–Parr (B3LYP) [15, 16] functional with the 6-31G(d) basis set used to locate stationary points along the potential energy surface (PES). Vibrational frequency calculations were carried out at the same level of theory to identify the latter as either saddle points or

2

minima. If a reaction passed through at least one transition state then intrinsic reaction coordinate (IRC) calculations were performed starting from each maxima in order to link reactants and products with calculations allowed to follow the energy profile in both directions. The number and size of each step was optimised to allow enough movement to identify the reactants and products and therefore to confirm that the correct transition state had been located. The resulting structures were then used as the basis for high accuracy calculations using either G4 or G4MP2 composite methods [17] with G3B3 [18] calculations also performed for comparison purposes and to highlight parameters associated with large uncertainties. The rates of reaction were subsequently computed using microcanonical Rice-Ramsperger-Kassel-Marcus/master-equation (RRKM/ME) theory [19].

The initial pyrolysis steps, including the thermal decomposition of C_5H_6 and C_5H_5, have been the subject of a number of studies. Roy et al. [20], Kern et al. [21] and Moskaleva and Lin [22] investigated the thermal decomposition of cyclopentadiene using experimental and computational methods and, more recently, Harding et al. [23] performed CASPT2/cc-pvdz calculations and used variable reaction coordinate transition state theory to deduce reaction rate data. The decomposition of the cyclopentadienyl radical is of key importance in the current system [8]. Kern et al. [21] produced rate constants using RRKM theory with vibrational frequencies calculated at the B3LYP/6-311G(d,p) level for radicals and the B3LYP/6-31G(d,p) level for the transition state resulting in a barrier of 259 kJ mol^{-1}. The high pressure limit rate was investigated by Roy et al. [20] using transition state theory with data from *ab initio* calculations at the PUMP2 level and a barrier height of 230 kJ mol^{-1} was found. Moskaleva and Lin [22] used a combination of methods, including CASTP2 and G2M, to calculate energies and other molecular properties and used multichannel RRKM calculations to derive reaction rate data. The determined rate is significantly slower than the experimental data presented by Kern et al. [21] though in better agreement with that obtained by Knyazev and Slagle [24]. The C_5H_6 + H = C_5H_5 + H_2 reaction was estimated by Emdee et al. [3] and revised by Roy

3

and Frank [25]. Bacskay and Mackie [26] carried out a more detailed study using a combination of CASSCF/CASPT2 and RRKM theory. Moskaleva and Lin [27] characterised the PES of the reaction at the G2M level and applied multichannel variational Rice-Ramsperger-Kassel-Marcus theory (VRRKM) to obtain rate data and suggested that the formation of C_5H_7 isomers is likely to become important at lower temperatures. The current methodology was also applied to these reactions with a view to provide further comparisons of results with a wider range of alternative methods.

A number of studies have also considered aromatic ring addition reactions [6, 28–30] and progress made in the analysis of sequences linking C_5 and C_6 ring structures via the $C_5H_5 + CH_3$ (e.g. Moskaleva et al. [31] and Sharma and Green [32]) and $C_5H_5 + C_2H_2$ (e.g. Cavallotti et al. [33]) channels. However, some of the key aspects of the chemistry remain conjectural or subject to significant uncertainties. This includes the pathways from the cyclopentadienyl radical to indene and naphthalene [5, 6, 28, 30, 34]. Marinov et al. [35, 36] formulated a global reaction step based on the assumption that the initial adduct formation is rate limiting though it has been shown that in an oxidative environment such a fast global reaction step has a strong tendency to over–estimate second ring formation when applied to the modelling of aromatic fuels as well as cyclopentene flames [5, 6]. By contrast, a rate determined on the basis of the stabilisation of the C_5H_5–C_5H_4 intermediate, according to the PES determined by Melius et al. [34], was found to reproduce some experimental data sets well [5, 34]. Related channels have recently been studied using DFT and RRKM methods by Mebel and Kislov [37]. The study suggests that a channel featuring the formation of 9-H-fulvalenyl prior to conversion to fulvalene and naphthalene is viable at combustion temperatures.

The current work provides (i) improved thermochemistry for a set of key oxidation reactions featuring the cyclopentadienyl radical through application of G3B3/G4MP2/G4 methods and (ii) an updated evaluation framework for assessing the accuracy of the determined rate constants. The work further (iii) explores the ability of the adopted G4/G4MP2 and RRKM/ME approach

4

to reproduce flow reactor data for the oxidation of cyclopentadiene and (iv) assesses the impact of updated formation channels leading to poly-aromatic hydrocarbon (PAH) and mono–substituted aromatics (MSA). Finally, (v) the impact of uncertainties in major reaction pathways on the ability to predict observed trends is assessed.

2. Thermochemistry Considerations

The G4MP2 composite method consists of a geometry optimisation at the B3LYP/6-31G(2df,p) level in order to obtain the equilibrium structure with the harmonic frequencies scaled by a correction factor of 0.9854 in order to account for know deficiencies [18]. The frequencies are then used to calculate the zero point energy (ZPE). In the G3 theory HF/6-31G* was used for the ZPE and the new procedure is likely to be more reliable. Also in contrast to previous G series composite methods, the Hartree–Fock energy limit is calculated and a series of single point energy calculations are carried out at various levels of theory (CCSD(FC,T)/6-31G(d), MP2(FC)/G3MP2LargeXP and MP2(FC)/6-31G(d)). The resulting energies are combined and a higher-level correction obtained by taking into account remaining deficiencies. The total energy is obtained by adding the previously calculated ZPE. Durant and Rohlfing [38] reported that B3LYP density functional methods provide improved geometries and vibrational frequencies in comparison to MP2 and Hartree-Fock *ab initio* methods. Heats of formation were also calculated at the G3B3 level and, for a selection of species, at the G4 level in order to further assess uncertainties.

Internal rotations can significantly influence thermochemical properties and rotors were investigated for the relevant species. Each molecule underwent a series of scans in which internal rotors were rotated though $360\,^{\circ}$ in $15\,^{\circ}$ steps. At each step, the molecular structure was optimised and the energy of the molecule calculated at the B3LYP/6-31G(d) level. An in-house code (SCANCALC) was used to fit the calculated energy profile to the series $V = \frac{1}{2}\Sigma V_n(1 - cos(n\Theta))$, with n ranging from 1 to 6. The computations also produced internal rota-

5

tional constants. Vibrational frequencies, enthalpies of formation, moments of inertia and molecular symmetry numbers were extracted and, if required, data for low frequency vibrations were omitted and modelled as hindered internal rotors. The NASA statistical mechanics program Properties and Coefficients 99 (PAC99) [39] was then used with the rigid rotor harmonic oscillator (RRHO) approximation to calculate thermodynamic data for enthalpy, heat capacity, entropy and Gibbs free energy in the standard JANAF polynomial form covering the range 200 K to 6000 K with the enthalpy at 298 K anchored to the G4/G4MP2 value.

The thermodynamic properties of C_5H_5 are of fundamental importance and some uncertainties prevail. The G4 method provides a heat of formation of 257.8 kJ mol^{-1} at 298 K, G4MP2 253.3 kJ mol^{-1}, G3B3 261.5 kJ mol^{-1} and the G3 method a somewhat higher value of 268.4 kJ mol^{-1}. Alternative determinations have been obtained using a range of methods, including CBS-QB3, with values ranging from 266.5 kJ mol^{-1} [32], 292.9 kJ mol^{-1} [40], 266.1 kJ mol^{-1} [41], 239.2 kJ mol^{-1} [4], 259.4 kJ mol^{-1} [42] and 273.2 kJ mol^{-1} [21]. Experimental studies have produced a value of 263.6 kJ mol^{-1} [34, 43] with a value of 242.7 kJ mol^{-1} suggested in the review by Puttemans et al. [44]. The G4 value of 257.8 kJ mol^{-1} was adopted in the current work. Enthalpies of formation for other species show smaller differences and the G4 method was used for species involved in the decomposition of CPD with the G4MP2 method used for the less sensitive oxidation system.

The entropy of the cyclopentadienyl radical can affect the direction of reaction steps such as the formation of larger aromatics. The radical displays first-order Jahn–Teller behaviour, the most symmetric D_{5h} conformation of C_5H_5 belongs to a degenerate electronic state, therefore two more stable C_{2v} symmetry conformations can be found. The conformers ($^2B_1$ and $^2A_2$) have an a low frequency interconnect mode. The contribution of the Jahn–Teller effect was modelled by introducing a pseudo-rotation. Katzer and Sax [45] developed a general numerical method for calculating accurate pseudo-rotation constants and the recommended value of 230 cm^{-1} for this molecule was used. At the B3LYP/6-

31G(2df,p) level, vibration frequencies of the $^2B_1$ and $^2A_2$ conformations differ by less than 3% and the frequencies from the $^2B_1$ conformer were used for the thermochemistry calculations. A resulting entropy value of 271.3 J mol^{-1} K^{-1} was obtained at 298 K. Literature values include 289.6 J mol^{-1} K^{-1} from the Burcat thermodynamic tables [46], 274.1 J mol^{-1} K^{-1} obtained by Zhong and Bozzelli [4] using a group additivity and 267.8 J mol^{-1} K^{-1} by Sharma and Green [32] using the CBS-QB3 method. Thermochemical data for key species are shown in Table 1.

3. Calculation of Rate Constants

Zhong and Bozzelli [4] computed high pressure limit rate constants with pressure dependencies calculated using the bimolecular quantum Rice–Ramsperger–Kassel (QRRK) method with a modified strong collision approach for falloff. The QRRK methodology used three vibrational frequencies plus one external rotation for the density of states. Hindered internal rotors were also modelled as vibrations. For instance, the 27 vibrational frequencies of 2,4-cyclopentadieneoxy (C_5H_5O) were represented by three frequencies 686.2, 1618.6 and 3562.9 cm^{-1} with degeneracies of 14.037, 10.258 and 2.705 [4]. If the current corrected G4MP2 vibrations are used in this manner then values of 729.3, 1643.7 and 3189.9 cm^{-1} would result from averages of vibrations 1 to 14, 15 to 24 and 25 to 27 (degeneracies of 14, 10 and 3), suggesting possible under-/over-estimations of low/high-frequency vibrations in the earlier work.

Structures relating to the selected reaction channels are shown in Fig. 1 and a summary of results from the PES calculations can be found in Table 2. Rate constants in the temperature range 500 K to 2500 K were calculated at 1 atm, 10 atm and at the high pressure limit using microcanonical Rice-Ramsperger-Kassel-Marcus/master-equation (RRKM/ME) theory [19] with the rate constants determined from Eq. (1),

$$k(E) = l^+ \left(\frac{G^+(E)}{hN(E + E_0)} \right) \tag{1}$$

7

where $G^+(E)$ is the total number of states of the transition structure and l^+ is the reaction path degeneracy, N is the density of states of the reactant at energy $E + E_0$ and h is Planck's constant. It was assumed that once a reaction had advanced past the highest energy point, sufficient energy was present in the system to allow rearrangement to products without stabilisation of intermediates. Therefore the rate–determining step was considered to be the step with the largest energy barrier before this point. For reactions where the products are higher in energy than the reactants, the rate determining step was taken to be the step with the highest barrier. All reactions are discussed further below.

Lennard–Jones parameters σ (Å) and ϵ (K), used to estimate the frequency of collisions, were obtained from databases or calculated from a method based on molar volumes and compressibility [47]. The calculation requires critical temperatures, critical volumes and acentric factors for each species and data for related molecules was used for cases where literature values could not be found. For C_5H_5 values of $\sigma = 5.18$ Å and $\epsilon = 357$ K were used with similar values for related species. Argon was used as a bath gas collider with values of $\sigma = 3.44$ Å and $\epsilon = 119.44$ K. Studies of the decomposition of cyclopentadienyl have used various values of $\langle \Delta E \rangle_{down}$ to model pressure fall-off. Kern et al. [21] and Tokmakov et al. [48] used a value of 450 cm^{-1}, while Bacskay and Mackie [26] preferred a value of 400 cm^{-1}. Studies of related systems include the work by Miller et al. [49], where a temperature dependent expression $\langle \Delta E \rangle_{down} = 80 \cdot$ $(T[K]/300)^{0.7}$ cm^{-1} was used in a study of reactions on the C_3H_5 potential, while Miller and Klippenstein [50] used $\langle \Delta E \rangle_{down} = 400 \cdot (T[K]/300)^{0.7}$cm^{-1} in a study of propargyl radical recombination on the C_6H_6 potential. Detailed knowledge with respect to $\langle \Delta E \rangle_{down}$ is lacking and in the current work a value of 400 cm^{-1} was applied using the standard form of the exponential down model [51]. The master equation was used to model pressure fall-off and a maximum energy limit (E_{max}) of 1000 kJ mol^{-1} was used for the energy integration to ensure convergence at high temperatures. Eckart [52] quantum tunnelling corrections were applied to reactions involving hydrogen transfers.

The molecular parameters used in the RRKM/ME computations can be

8

found in Tables 3 and 4 with the corresponding transition states given in Table 5. The values were used in the calculation of thermodynamic data from the partition function and, in particular, vibrational frequencies were used in the calculation of the contribution from vibrational motion. The symmetry numbers and moments of inertia were used in calculating the contribution from the rotational motion and the molecular mass the translation contribution. The density and sum of states in the RRKM calculation were obtained using either the direct count algorithm of Beyer and Swinehart [53] or the Whitten–Rabinovitch [54] approximation with vibrational frequencies and moments of inertia used as input parameters.

Molecular properties of the transition state are required for the RRKM/ME analysis and barrierless reactions were dealt via the estimation of transition states using the enthalpy of formation and vibrational frequencies determined from the properties of both reactants and products [19]. The applied rotational data was evaluated from the external rotors of the active component and Benson correction parameters were taken into account, including the vibrational frequency of the bond to be broken. Due to the inherent assumptions of the method, it needs to be applied with caution and was mainly used for the determination of the less sensitive oxidation channels. However, the method was also applied to the hydrogen expulsion from cyclopentadiene in an effort to explore how pressure fall-off would affect the calculated rate constants and to permit further comparisons with literature values. The values of rate parameters obtained after fitting the results to the modified three–parameter form of the Arrhenius equation are shown in Table 6.

4. Rate Constant Analysis

4.1. Reactions with oxygen molecules

Zhong and Bozzelli [4] considered the reaction of cyclopentadienyl with molecular oxygen in detail and examined multiple pathways, including the possibility of the second oxygen atom attaching to the five membered ring forming

9

bicyclic species, notably the cyclopentene-3,4-cycloperoxy-5-yl (BICYC5.O2) and bicyclo[2,2,1]hexene peroxy (C2O2H221) radicals. The latter route leads to the formation of vinyl ketene and the formyl radical. Both paths were considered here with energies computed using the G4MP2 methodology and considerable differences in the heats of formation were found for the transition states leading from the bicyclic species as compared to the earlier study [4]. The G4MP2 energies for the transition states to and from BICYC5.O2 were found to be 316 kJ mol^{-1} and 351 kJ mol^{-1} resulting in barriers of 111 kJ mol^{-1} and 126 kJ mol^{-1}. By contrast, Zhong and Bozzelli [4] calculated a barrier of 73.6 kJ mol^{-1} to BICYC5.O2 from C_5H_5OO for the first transition state and estimated a barrier of 41.8 kJ mol^{-1} from BICYC5.O2 to the second transition state. The route passing through C2O2H221 was assigned [4] an activation energy of 126 kJ mol^{-1} due to the significant rotation of the double bond required in order to allow peroxy radical attack on the π bond. The corresponding G4MP2 energy for the transition state is again significantly higher with the determined heat of formation of 368 kJ mol^{-1} leading to a barrier of 163 kJ mol^{-1}. The larger barriers calculated using the G4MP2 method suggest that these routes are likely to be of secondary importance.

The multiple pathways considered here include the direct formation of oxygen atoms via reaction (1) and the PES for the channels selected for further study are shown in Fig. 2 with the subsequent fate of C_5H_5O discussed in Section 4.2 below.

$$C_5H_5 + O_2 \rightleftharpoons C_5H_5O + O \tag{1}$$

If channel (1) is treated as a strictly uphill bimolecular reaction then an energy change of 202 kJ mol^{-1} is implied and a comparison of the determined rate with the suggestions from Zhong and Bozzelli [4] and Murakami et al. [7] is shown in Fig. 3. The current rate is considerably slower despite a similar barrier to the 190 kJ mol^{-1} proposed by Zhong and Bozzelli [4]. Murakami et al. [7] investigated the oxidation of cyclopentadienyl experimentally by monitoring O atom and CO formation behind the reflected shock in $C_5H_6/O_2/Ar$ and $C_6H_5OCH_3/O_2/Ar$

10

mixtures and the temporal evolution of oxygen atoms was used to estimate the rate constant. There are inevitably contributions from other channels and the determination provides an upper limit estimate with a barrier of 117 kJ mol^{-1}.

The oxidation of cyclopentadienyl also leads to the formation of the chemically activated cyclopentadienyl-peroxy adduct (C_5H_5OO) via reaction (2) followed by possible stabilisation.

$$C_5H_5 + O_2 \rightleftharpoons C_5H_5OO \qquad (2)$$

DFT calculations at the B3LYP/6-31G(d) level show the presence of a transition state (TS1) as the oxygen molecule approaches the five membered ring. The resonance stability is disrupted as the radical form is localised. However, the calculated barrier is small $\simeq 13.8$ kJ mol^{-1} at 298 K. The current RRKM/ME rates, as well as the high and low pressure rates from Zhong and Bozzelli [4] are shown in Fig. 4. Both studies have an overall enthalpy change of approximately 60 kJ mol^{-1}. However, the inclusion of a transition state in the present work, absent in the study performed by Zhong and Bozzelli [4], leads to an increased temperature dependence for the high pressure limit. The corresponding [4] atmospheric pressure rate is close to the current 10 atmosphere determination at high temperatures and somewhat faster at temperatures below 1200 K.

A hydrogen re-arrangement leading to the expulsion of hydroxyl (3) and peroxy bond cleavage in the activated adduct (4) was also considered for completeness. However, dissociation back to reactants is strongly favoured as can be seen from the PES shown in Fig. 2, where energies obtained with the G4/G4MP2 methods are shown as discussed below.

$$C_5H_5OO \rightleftharpoons C_5H_4O + OH \qquad (3)$$

$$C_5H_5OO \rightleftharpoons C_5H_5O + O \qquad (4)$$

Results obtained with the G4MP2 method suggest an energy barrier to TS15 of 201 kJ mol^{-1} for reaction (3) and 253 kJ mol^{-1} to products for reaction (4). The channels are therefore likely to be important only at higher temperatures. For reaction (3), the rate determining step was found to be the hydrogen transfer

11

from the ring to the oxygen chain and the G4MP2 method produces a higher energy for TS15 ($\triangle_f H^{298K} \simeq 406$ kJ mol^{-1}) as compared to the G3B3 value ($\triangle_f H^{298K} \simeq 370$ kJ mol^{-1}). The energy difference of 35 kJ mol^{-1} between the two methodologies is a cause for concern and calculations were therefore also performed at the more accurate G4 level resulting in a value of 365 kJ mol^{-1} for $\triangle_f H^{298K}$ of TS15. The corresponding barrier height is 159 kJ mol^{-1} – close to the 156 kJ mol^{-1} suggested by Zhong and Bozzelli [4]. The current rate parameters for reaction (3) were determined using the G4 data for TS15 as indicated in Table 2.

Eckart quantum tunnelling corrections were applied to the H transfer and IRC calculations were carried out from TS15 (see Fig. (2)) following the reaction path coordinate in both directions. The barrier width was determined to be 4.76 Å and this value was used in the computation of the tunnelling corrections. With tunnelling taken into account, the calculated rate for reaction (3) is consistently faster than the previous suggestion [4] as shown in Fig. 5. For reaction (4) the energy barrier around 253 kJ mol^{-1} is again similar to previous studies and the high pressure rate determined by Zhong and Bozzelli [4] falls between the current 10 atm and high pressure limits at higher temperatures as shown in Fig. 6. The 2,4-cyclopentadienoxy radical can lead to the 1,3-butadienyl radical and cyclopentadienone via reactions (5) and (6) following the PES (see Fig. 7) from C_5H_5O onwards.

$$C_5H_5O \rightleftharpoons C = CC = C. + CO \tag{5}$$

$$C_5H_5O \rightleftharpoons C_5H_4O + H \tag{6}$$
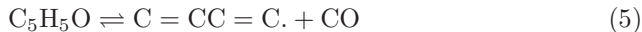
The determined rates for the above reactions are compared with alternative suggestions in Figs. 8 and 9 respectively. The rate used by Alzueta et al. [56] was obtained using QRRK methods while the rate by Emdee et al. [3] was estimated from the decomposition of C_6H_5O to CO and C_5H_5. The previous estimates for reaction (5) suggest an activation energy around 184 kJ mol^{-1} [3, 55, 56] though sequential increases in the frequency factor were applied from $2.51 \cdot 10^{11}$ s^{-1} [3] via $4.5 \cdot 10^{11}$ s^{-1} [57] to $7.5 \cdot 10^{11}$ s^{-1} [56]. The barrier for the initial step via

12

TS3, see Fig. 7, is much lower at 21.9 kJ mol^{-1} suggesting stabilisation at some point. The largest energy well found was for CYC5ODE requiring a climb of 199 kJ mol^{-1} to TS5 according to the G4MP2 method with the G3B3 result somewhat higher. Assuming this to be the rate determining step results in the rates shown in Fig. 8. It is possible that further stabilisation may occur at O=C=CC.C=C leading to the need to treat the reaction as a multi-step process.

Significant pressure fall-off is predicted for reaction (6), even at lower temperatures, though the current rate is faster than that proposed by Zhong and Bozzelli [4]. The computed enthalpy of reaction was 62.7 kJ mol^{-1}, compared to 69.5 kJ mol^{-1} with the proposed transition state raising the barrier to 79.9 kJ mol^{-1} [4]. The absence of a transition state in the current calculations was investigated using the B3LYP/6-31G DFT functional via a scan of the energy surface as the hydrogen is extracted. Starting from C_5H_5O, the relevant C-H bond distance was increased in steps of 0.1 Å for 50 steps and the energy of the structure calculated at each stage. A slight energy maximum of approximately 0.001 Hartrees (2.6 kJ mol^{-1}) was observed before complete separation to C_5H_4O + H. A further optimisation was started from the observed maximum and no transition state was found. We expect the small barrier to be a discrepancy that would disappear if higher level methods (e.g. [23]) were applied.

4.2. Reactions with oxygen atoms

The reaction between C_5H_5 + O can proceed through pathways that may lead straight to products or stabilisation depending on conditions. The PES for the reaction rate channels selected for further study are shown in Fig. 7. Possible products include 1,3-butadienyl radical and carbon monoxide via reaction (7) and cyclopentadienone and hydrogen via reaction (8).

$$C_5H_5 + O \rightleftharpoons C = CC = C. + CO \tag{7}$$

$$C_5H_5 + O \rightleftharpoons C_5H_4O + H \tag{8}$$
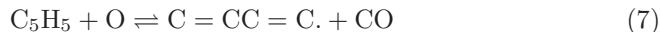
The corresponding energy data is shown in Table 2. For both channels the initial formation of 2,4-cyclopentadienoxy (C_5H_5O) is exothermic and the energies

13

of the transition states and intermediates are considerably lower than the reactants. The initial addition reaction can be expected to be rate determining if the reaction proceeds without stabilisation. The branching ratio for the two channels was estimated proceeding from C_5H_5O and found to be almost exclusively in favour of reaction (7). The result is consistent with the experimental findings of Butler and Glassman [2] who did not detect cyclopentadienone (C_5H_4O) experimentally. Accordingly, reaction (8) has been omitted. The rate constants determined for the reaction $C_5H_5 + O$ are shown in Fig. 10. The current rate is in good agreement with the suggestion of 10^{11} m^3 kmol^{-1} s^{-1} by Emdee et al. [3] for temperatures up to 1200 K. The rate was suggested on the basis that the activated adduct decomposes to products through the exothermic channel much faster than the return to reactants. The corresponding QRRK suggestion of Zhong and Bozzelli [4] for reaction (7) intersects the current 1 and 10 atm rates at temperatures in excess of 1650 K.

The case of stabilisation of intermediate products via (9) and subsequent reaction channels was also considered. Stabilisation may occur at C_5H_5O with further reaction via (5,6) as outlined above. The possibility of the reaction progressing to CYC5ODE, the deepest well in the PES, with subsequent product formation via (10) and (11) was also considered with the rate limiting step for the formation of C=CC=C. + CO passing via TS5.

$$C_5H_5 + O \rightleftharpoons \text{products} \tag{9}$$

$$\text{CYC5ODE} \rightleftharpoons C = CC = C. + CO \tag{10}$$

$$\text{CYC5ODE} \rightleftharpoons C_5H_4O + H \tag{11}$$
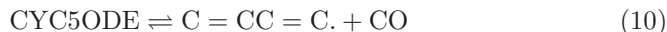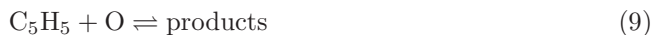
Under circumstances where stabilisation occurs the resulting conversion to the 1,3-butadienyl radical (C=CC=C$\cdot$) or cyclopentadienone (C_5H_4O) will be considerably slower as several significant energy barriers must be overcome. The point of stabilisation along the PES also has an impact. For example, the formation of cyclopentadienone via reaction (11) is substantially slower than via (6). The rates for both reactions are given in Table 6. Bittker [58] assumed stabilisation to C_5H_5O and suggested a rate of 10^{10} m^3 kmol^{-1} s^{-1} for reaction (9),

14

while Zhong and Bozzelli [4] considered a range of stabilisation products and typically computed much slower rates as exemplified in Fig. 10. Two possible pathways to the 1,3-butadienyl radical are shown in Fig. 11. The first route passes through cyclopenten-3,4-epoxy-5-yl radical ($BICYC_5H_5O$) as described by Zhong and Bozzelli [4]. We also considered a more direct route with immediate cleavage of the carbon ring. Although the overall energy maxima are very similar for both routes, the conversion via the bicyclic species has a much more favourable initial step.

4.3. Reactions with the hydroxyl radical

Zhong and Bozzelli [4] also studied the C_5H_5 + OH reaction and identified cyclopentadienol (12) as the major initial product with cyclopentadien-1-ol and cyclopentadien-2-ol favoured subsequent outcomes.

$$C_5H_5 + OH \rightleftharpoons C_5H_5OH \qquad (12)$$

The PES for the reaction rate channels selected for further study are shown in Fig. 12 and the computed rates for reaction (12) are compared with the QRRK determinations by Zhong and Bozzelli [4] in Fig. 13. The decomposition of C_5H_5OH leads to either C_5H_4OH (13) or C_5H_5O (14) with the former leading to C_5H_4O via reaction (15).

$$C_5H_5OH \rightleftharpoons C_5H_4OH + H \qquad (13)$$

$$C_5H_5OH \rightleftharpoons C_5H_5O + H \qquad (14)$$

$$C_5H_4OH \rightleftharpoons C_5H_4O + H \qquad (15)$$

The current rate for the formation of C_5H_4OH via reaction (13) is compared with the QRRK determination of Zhong and Bozzelli [4] in Fig. 14. The current rate determination is substantially faster. The rate for the less significant channel (not shown) featuring the conversion of cyclopentadienol to the 2,4-cyclopentadieneoxy radical via reaction (14) is similar to that of Zhong and Bozzelli [4] with the current high pressure rate between 1 to 3 times faster for the temperature range 800 – 1400 K. The rate for reaction (15), see Fig. 15,

15

was estimated by Emdee et al. [3] using Benson's method in a study of toluene oxidation at 1200 K.

Direct product dissociation channels were also suggested by Zhong and Bozzelli [4] and proposed to predominantly lead to H expulsion via reaction (16) with reaction (17) a comparatively minor contributor. The channels were considered in the present work and, analogous to reaction (7) ($C_5H_5 + O \rightleftharpoons C{=}CC{=}C.$ $+ CO$), the possibility that the cyclopentadienyl and hydroxyl radicals may react and re–arrange to form 1,3-butadiene ($C{=}CC{=}C$) and CO was also considered.

$$C_5H_5 + OH \rightleftharpoons C_5H_4OH + H \tag{16}$$

$$C_5H_5 + OH \rightleftharpoons C_5H_5O + H \tag{17}$$

$$C_5H_5 + OH \rightleftharpoons C = CC = C + CO \tag{18}$$

Two routes were investigated for reaction (18). The first pathway passing via the bicyclic C_5H_6O species with the second proceeding via an initially energetically favourable hydrogen transfer leading to C_5H_5-1-OH and C_5H_5-1-O. The G4MP2 calculation suggests that both products are lower in energy than C_5H_5OH and C_5H_5O and that it may be more favourable for $C_5H_5 + OH$ to pass via these channels. However, the further breakdown of C_5H_5-1-O requires a rearrangement passing via a number of energy barriers and the channel was not considered further in the current work. Two alternative routes and structures leading from C_5H_5-1-OH are shown in Fig. 16. The first route provided the lower energy pathway with intermediates and transition states (TS9, TS10 and TS11) all having a lower enthalpy of formation than the reactants. Accordingly, under conditions where stabilisation does not occur it is likely that $C_5H_5 + OH$ $\rightleftharpoons C_5H_5OH$ (12) is rate controlling. For the second route, the energy of TS14 is considerably higher than the initial reactants and contributions from this route are likely to be correspondingly reduced.

4.4. Reactions with hydroperoxyl radicals

The current study also considers lower temperatures where reactions with HO_2 may exert an influence. The PES for the reaction rate channels selected

16

for further study are shown in Fig. 17. Zhong and Bozzelli [4] also considered the reaction and identified dissociation to cyclopentadienoxy + OH (19) and cyclopentadienone and H_2O (20) as likely product channels. The same reactions are also considered in the current study.

$$C_5H_5 + HO_2 \rightleftharpoons C_5H_5O + OH \tag{19}$$

$$C_5H_5 + HO_2 \rightleftharpoons C_5H_4O + H_2O \tag{20}$$
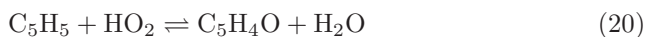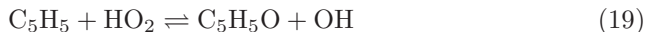
The formation of 2,4-cylopentadienoxy (19) is particularly important as it converts resonance stabilised radicals into the more reactive species. The rate determining step for both reactions is likely to be the initial formation of the cyclopentadienyl-hydroperoxide (C_5H_5OOH) adduct as all intermediates and transition states are downhill from the energy of the reactants. However, TS2 can be expected to have an impact on the branching ratio between the two channels and an estimate proceeding from C_5H_5OOH suggests that reaction (20) is insignificant at 1200 K. The estimated rate is in excess of 3 orders of magnitude slower than reaction (19) as also suggested by Zhong and Bozzelli [4]. A comparison of the estimated rate for reaction (19) with previous studies is shown in Fig. 18. The current estimated bimolecular rate is in comparatively good agreement with the suggestion by Emdee et al. [3] at temperatures around 1000 K. The high pressure rate of Zhong and Bozzelli '[4] leading to C_5H_5OOH and the corresponding bimolecular rate are also shown.

4.5. Decomposition channels

The decomposition reactions involving cyclopentadiene (CPD) and cyclopentadienyl (CPDyl) have received a comparatively large amount of attention. The reaction channels discussed below include the thermal decomposition of CPD, the H abstraction from CPD and the thermal decomposition of CPDyl. The reactions are considered for two primary reasons: (i) To provide extended comparisons of the current methodology with alternative approaches and (ii) to select alternative rates for use in a sensitivity analysis.

17

Roy et al. [20] experimentally determined rate constants for the thermal decomposition of CPD (21) from H-absorption profiles measured during CPD pyrolysis in the temperature window 1250 - 1666 K.

$$C_5H_6 \rightleftharpoons C_5H_5 + H \tag{21}$$

Kern et al. [21] produced rate constants using RRKM theory with vibrational frequencies calculated at the B3LYP/6-311G(d,p) level for radicals and the B3LYP/6-31G(d,p) level for the transition state. Tokmakov et al. [48] calculated energies and vibrational frequencies using a variety of computational methods including G2M combined with RRKM/ME and canonical variational transition state theory (CVTST) to derive rate constants. Harding et al. [23] performed CASPT2/cc-pvdz calculations and used variable reaction coordinate transition state theory to deduce reaction rate data. Rates were produced for both CPD symmetries ($^2A_2$ and $^2B_1$) although the values differed by less than 10%. The current high pressure (HP) limit rate is a factor of 1.9 faster than that obtained for the $^2A_2$ symmetry by Harding et al. [23] at 1200 K (3.4 times faster at 2000 K). However, the current 1 atm rate is a factor of 2.2 slower at 1200 K and 16 times slower at 2000 K than the alternative HP limit [23], which suggests that neglecting fall-off effects may have a potentially dominant influence on uncertainties for the current reaction. A comparison of the rate determinations is shown in Fig. 19.

The second routes feature hydrogen abstraction via H (22) and OH attack (23) with the former dominant and discussed in some detail below.

$$C_5H_6 + H \rightleftharpoons C_5H_5 + H_2 \tag{22}$$

$$C_5H_6 + OH \rightleftharpoons C_5H_5 + H_2O \tag{23}$$

Emdee et al. [3] provided an estimate for reaction (22) based on similarity with H abstraction from formaldehyde that was revised by Roy et al. [20]. Bacskay and Mackie [26] carried out a more detailed study using a combination of CASSCF/CASPT2 and RRKM theory. Moskaleva and Lin [27] characterised the PES of the reaction at the G2M level and applied multichannel variational

18

Rice-Ramsperger-Kassel-Marcus theory (VRRKM) to obtain rate data. The current determination is in good agreement with the latter study, in particular at higher temperatures as shown in Fig. 20, with overall differences less than a factor of 2. The barrier height for the abstraction reaction obtained with the G4 method is 14.4 kJ mol^{-1} compared to 26.4 kJ mol^{-1} computed by Moskaleva and Lin [27] at the G2M(RCC,MP2) level. The H addition route via reaction (24) leading to the allyl radical and acetylene provides a tertiary path and the rate parameters were obtained from the study by Zhong and Bozzelli [4].

$$C_5H_6 + H \rightleftharpoons C_3H_5(A) + C_2H_2 \tag{24}$$

The decomposition of the cyclopentadienyl radical is of key importance to predictions of acetylene and benzene levels in the current system [8] and may proceed via a direct route through reaction (25)

$$C_5H_5 \rightleftharpoons C_3H_3 + C_2H_2 \tag{25}$$

or a corresponding two-step sequence via reactions (26) and (27).
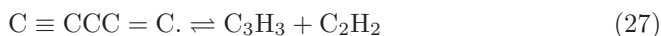
$$C_5H_5 \rightleftharpoons C \equiv CCC = C. \tag{26}$$

$$C \equiv CCC = C. \rightleftharpoons C_3H_3 + C_2H_2 \tag{27}$$

Kern et al. [21] produced rate constants using RRKM theory with vibrational frequencies calculated at the B3LYP/6-311G(d,p) level for radicals and the B3LYP/6-31G(d,p) level for the transition state resulting in a barrier of 259 kJ mol^{-1}. The high pressure limit rate was investigated by Roy et al. [20] using transition state theory with data from *ab initio* calculations at the PUMP2 level and a barrier height of 230 kJ mol^{-1} was found. Moskaleva and Lin [22] used a combination of methods, including CASTP2 and G2M, to calculate energies and other molecular properties and used multichannel RRKM calculations to derive reaction rate data. The inherent complexities of the system were also outlined and it was suggested that the first transition state (TS17), shown in the simplified potential energy diagram in Fig. 21, is rate controlling. The latter

19

finding, also proposed by Kern et al. [21], is perhaps surprising given the additional energy required to reach the final products. It may also be noted that energies for TS17, TS18 and TS19 computed at the G4 level suggest that rearrangements back to reactants, e.g. from $CHCCH_2CHCH$ to C_5H_5-1 via TS18, are consistently energetically favoured over further forward reaction progress. The computed energy for TS17 relative to CPD was 275 kJ mol^{-1}[22] as compared to the current G4 value of 253 kJ mol^{-1}. The corresponding G3B3 value is somewhat higher at 257 kJ mol^{-1}. Moskaleva and Lin [22] further considered several pathways leading to propargyl and acetylene. However, the energy barriers for the dominant channels differed by less than 4 kJ mol^{-1} – similar to the uncertainty of the method. The current corresponding values for TS18 and TS19 are 318 kJ mol^{-1} and 372 kJ mol^{-1} compared to 317 kJ mol^{-1} and 383 kJ mol^{-1} [22] and hence the major difference is in the proposed rate controlling TS17 [21, 22]. The different determinations (e.g. [20–22]) for reaction (25) differ by more than two orders of magnitude at 1200 K. Moskaleva and Lin [22] also performed RRKM calculations for the reverse reaction (28) and computed pressure dependent rate constants based on the microscopic reversibility principle. Given the uncertainties associated with the decomposition rate and the rate controlling step, the reverse rate (28) computed by Moskaleva and Lin [22], as applied for example in the JetSurf mechanism [59], is in the current work combined with the Jahn-Teller corrected G4 thermodynamics for C_5H_5.

$$C_3H_3 + C_2H_2 \rightleftharpoons C_5H_5 \tag{28}$$

The significant differences for the thermal decomposition of C_5H_5 can only partly be explained through updates in the thermochemistry and the sensitivity of predictions to alternative rate determinations is discussed below.

5. Evaluation Framework

The revised thermochemistry outlined above was combined with an updated version of the mechanism applied by Lindstedt and Rizos [6] to study the oxidation of cyclopentene and related species. Key reaction rates and changes are

20

shown in Table 7. Furthermore, thermodynamic data was updated to include determinations at the G4, G4MP2 and G3B3 levels as shown in Table 1. The resulting reaction mechanism was applied to study the oxidation of cyclopentadiene under conditions corresponding to the experimental studies of Butler [1] and Butler and Glassman [2] as shown in Table 8.

The propargyl radical has a central role in the chemistry of CPD. The direct route from cyclopentadienyl to the propargyl radical via reactions (25)–(27) emphasises the importance of propargyl radical re-combination as a route to C_6 species such as phenyl (29) and 2-ethynyl-1,2-butadiene (30). Past work has also considered additional pathways leading via adducts such as 1,5-hexadiyne [6, 60] following the seminal work of Miller and Melius [61].

$$C_3H_3 + C_3H_3 \rightleftharpoons C_6H_5 + H \tag{29}$$

$$C_3H_3 + C_3H_3 \rightleftharpoons C_4H_5C_2H \tag{30}$$
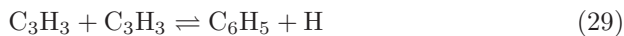
Direct routes leading to fulvene and benzene (31) and (32) have also been extensively studied by Miller et al. [50].

$$C_3H_3 + C_3H_3 \rightleftharpoons \text{fulvene} \tag{31}$$

$$C_3H_3 + C_3H_3 \rightleftharpoons C_6H_6 \tag{32}$$

The above routes also provide the dominant pyrolytic propagyl removal mechanism and hence computed benzene levels can provide an indicator of the amount of propargyl formed. The subsequent rearrangements of 2-ethynyl-1,2-butadiene lead to fulvene, benzene and the phenyl radical via cyclization

$$C_4H_5C_2H \rightleftharpoons \text{fulvene} \tag{33}$$

$$C_4H_5C_2H \rightleftharpoons C_6H_6 \tag{34}$$

$$C_4H_5C_2H \rightleftharpoons C_6H_5 + H \tag{35}$$

followed by fulvene isomerization.

$$\text{fulvene} \rightleftharpoons C_6H_6 \tag{36}$$

$$\text{fulvene} \rightleftharpoons C_6H_5 + H \tag{37}$$

21

The above reactions have recently been studied by Georgievskii et al. [62] and evaluated in the context of the isomer specific combustion chemistry in allene and propyne flames [63]. The sequences are applied in the current work with the rate parameters shown in Table 7. The benzene decomposition reaction was also updated for reasons of consistency.

$$C_6H_6 \rightleftharpoons C_6H_5 + H \tag{38}$$

The dominant ($\geq 95\%$) channel for propargyl formation is via reaction (22) and the formation of benzene provides some indication of the accuracy of the rate determination for this reaction. Further reactions for the propargyl radical were also added as shown.

$$C_3H_3 + OH \rightleftharpoons C_2H_3 + HCO \tag{39}$$

$$C_3H_3 + OH \rightleftharpoons C_2H_4 + CO \tag{40}$$

The reaction sequence $C_3H_5(A) \longrightarrow C_3H_4(A) \longrightarrow C_3H_4(P)$ is important and, depending on conditions, the allyl radical ($C_3H_5(A)$) is partly produced via reaction (24) as discussed above. The chemistry of the allyl radical has been studied experimentally by Fernandes et al. [64] and computationally by Miller et al. [49]. The rate determinations are in good agreement and the parameters proposed in the latter study have been adopted for reactions (41) and (42).

$$C_3H_5(A) \rightleftharpoons C_3H_4(A) + H \tag{41}$$

$$C_3H_4(P) + H \rightleftharpoons C_2H_2 + CH_3 \tag{42}$$

Harding and Klippenstein [65] studied the $C_3H_5(A) + H$ (43) reaction and proposed an upper limit value. The product distribution was not explored and propene has here tentatively been assigned. However, propene is mainly formed via H abstraction from CPD (44).

$$C_3H_5(A) + H \rightleftharpoons C_3H_6 \tag{43}$$

$$C_5H_6 + C_3H_5(A) \rightleftharpoons C_5H_5 + C_3H_6 \tag{44}$$

22
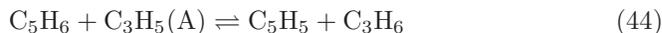
The abstraction reactions from CPD (e.g. (44)) use the functional form of Zhong and Bozzelli [4] with adjustments to the frequency factor. A similar approach was used by Alzueta et al. [9] among others. The above steps have an impact on the formation of ethylene [8] through reaction (45).

$$C_3H_6 + H \rightleftharpoons C_2H_4 + CH_3 \tag{45}$$
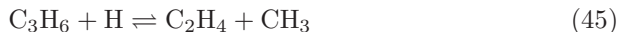
Key isomeric C_3H_4 reaction channels have been discussed by Hansen et al. [63] and steps adopted as shown in Table 7.

Benzene formation via the CH_3 addition sequence proposed by Moskaleva et al. [31], passing via $C_5H_5CH_3$ (47) and fulvene (48), was evaluated for cyclopentene and methyl-CPD mixtures by Lindstedt and Rizos [6].

$$C_5H_5 + CH_3 \rightleftharpoons C_5H_4CH_3 + H \tag{46}$$

$$C_5H_4CH_3 \rightleftharpoons \text{fulvene} + H \tag{47}$$

$$\text{fulvene} + H \rightleftharpoons C_6H_6 + H \tag{48}$$
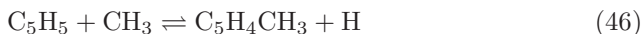
The hydrogen assisted isomerization reaction (48) provides the dominant route from fulvene to benzene under the current conditions. The channel has been explored further by Sharma and Green [32] using RRKM theory with the challenges caused by loose transition states and chemically activated products channels clearly outlined. The route is of typically of secondary importance under flame conditions [6] and the above sequence has been retained.

The reaction channels leading to naphthalene via cyclopentadienyl radical recombination have received much attention. A reaction path to naphthalene passing via 1,10-dihydrofulvalene and the C_5H_5–C_5H_4 moiety was evaluated by Lindstedt et al. [5] on the basis of the PES computed by Melius et al. [34]. The proposed two-step sequence was found to reproduce naphthalene levels well in a number of systems with aromatic fuel components [5, 6].

$$C_5H_5 + C_5H_5 \rightleftharpoons C_5H_5 - C_5H_4 + H \tag{49}$$

$$C_5H_5 - C_5H_4 \rightleftharpoons C_{10}H_8 + H \tag{50}$$

23

A related pathway proceeding via 9,10-dihydrofulvalene has been studied by Mebel and Kislov [37] and Kislov and Mebel [66]. The stabilisation of 9,10-dihydrofulvalene was considered highly unlikely with the subsequent product specified as 9-H-fulvalenyl leading to either fulvalene or naphthalene.

$$C_5H_5 + C_5H_5 \rightleftharpoons 9 - H - \text{fulvalenyl} + H \tag{51}$$

$$9 - H - \text{fulvalenyl} \rightleftharpoons C_{10}H_8 + H \tag{52}$$
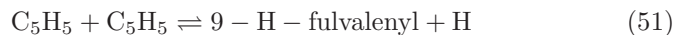
The rate for the initiating step (51) was not determined and tentative computations featuring estimates based on a barrier height of of 96 kJ mol^{-1} [66] suggest that an accurate rate determination is required. Accordingly, the sequence could not be considered further at this stage. The frequently used step $C_5H_5 + C_5H_5 = C_{10}H_8 + H + H$ (k(T) = 2×10^{10}exp(-2013/T) m^3 kmol^{-1} s^{-1}) has been excluded as it leads to significant excess formation of naphthalene in related systems (c.f. [6, 8]).

Reaction channels leading to naphthalene and indene from CPD and CPDyl have also been proposed. Wang et al. [28] performed a DFT study of the reaction pathways leading to indene from $C_5H_5 + C_5H_6$ and Butler [1] provided an estimated global rate ((k$_{53}$(T) = 9.63×10^{10} T$^{1.63}$exp(-29972/T) m^3 kmol^{-1} s^{-1}) based on temperature variation experiments.

$$C_5H_5 + C_5H_6 \rightleftharpoons C_9H_8 + CH_3$$
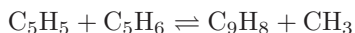
The suggested rate is around one order of magnitude larger at 1200 K than the initiating step ((k$_{53}$(T) = 3.55×10^{-3} T$^{2.75}$exp(-4982/T) m^3 kmol^{-1} s^{-1}) suggested by Wang et al. [28]. The latter rate is an upper limit as it does not account for subsequent energy barriers and any additional rate limiting steps. The investigation by Kislov and Mebel [30], using the B3LYP method with the 6-311G** basis set and with rate constants determined using RRKM and TST theories, indicates that the rates determined by Wang et al. [28] are indeed slow. However, the proposed rate remains much less significant than the global estimate of Butler [1]. Nevertheless, the current system does produce significant amounts of indene and a global step was used for the exclusive purpose of

estimating the formation under the current conditions.

$$C_5H_5 + C_5H_5 \rightleftharpoons C_9H_7 + CH_3 \tag{53}$$

$$C_5H_5 + C_3H_3 \rightleftharpoons C_8H_8 \tag{54}$$
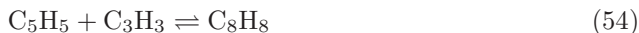
The same frequency factor as used for the formation of 1,10-dihydrofulvalene via reaction (49) was applied along with a barrier of 40 kJ mol^{-1}. The same approach was used to estimate the potential impact of a pathway leading via CPDyl and propargyl to styrene (54). The formation of methyl through the above step is also significant with methane formation proceeding via H abstraction from CPD (55).

$$C_5H_6 + CH_3 \rightleftharpoons C_5H_5 + CH_4 \tag{55}$$

Lindstedt et al. [5] and Colket et al. [67] discussed the potential importance of alternative indene formation via allene and propargyl addition to the phenyl radical and acetylene addition to the benzyl and methylphenyl radicals. However, the sequences do not contribute significantly under the current conditions. A related formation path leading to toluene via the norbornadienyl radical was proposed by Colket and Seery [68] and pathways leading from CPD to indene via successive acetylene addition reactions have been further studied by Cavallotti et al. [33] and Fascella et al. [69] with the cycloheptatrienyl (c–C_7H_7) radical proposed as a key intermediate.

$$C_5H_5 + C_2H_2 \rightleftharpoons c - C_7H_7 \tag{56}$$

$$c - C_7H_7 + C_2H_2 \rightleftharpoons C_9H_8 + H \tag{57}$$
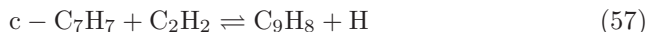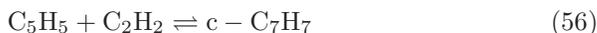
Side channels leading to toluene and subsequent products via cycloheptatriene (CHT) and norcoradiene (NCD) were identified as competing pathways. In the current work, steps leading to benzyl (58) and phenyl (59) have been included.

$$c - C_7H_7 + H \rightleftharpoons C_7H_7 + H \tag{58}$$

$$c - C_7H_7 + H \rightleftharpoons C_6H_5 + CH_3 \tag{59}$$

25

Rates for the above reactions were obtained using QRRK theory with structures computed using DFT at the B3LYP/6-31+G(d,p) level with energies evaluated using the G2MP2 approach [33, 69].

The thermal decomposition of CPDone remains subject to uncertainties. Wang and Brezinsky [11] suggest that the formation of cyclobutadiene and, in particular, decomposition pathways leading to acetylene are favoured. By contrast, studies of benzene oxidation performed by Alzueta et al. [9], Di-Naro et al. [12], Ristori et al. [13] and Tan et al. [70] favour the formation of vinylacetylene. In the current work, both paths have been tentatively included using the rates of Ristori et al. [13] and Wang and Brezinsky [11] for reactions (60,61).

$$C_5H_4O \rightleftharpoons C_4H_4 + CO \tag{60}$$

$$C_5H_4O \rightleftharpoons C_2H_2 + C_2H_2 + CO \tag{61}$$
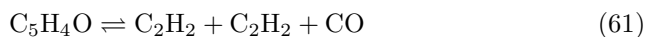
The above reactions have been included with the thermochemistry of the relevant species determined at the G4MP2 level as shown in Table 1.

6. Computational Results and Path Analysis

Computations corresponding to the experimental data sets reported in Table 8 were performed both as isothermal, with the temperature fixed to the initial experimental value, and as adiabatic [55]. The differences in results are small apart from for Cases 1 and 4, which yield significant heat release both experimentally and computationally. For reasons of consistency all reported results were obtained using the adiabatic assumption. The percentages quoted below refer to Case 2 and cover the initial fuel consumption period with averages computed over a time window from 20 to 30 ms. The choice was made to remove the impact of ignition upon the reported path analysis. The computational profiles were shifted by 20 ms towards the origin for Cases 1 to 3 and by 30 ms for Case 4 due to greater initial reactivity [1].

The dominant fuel consumption channels feature hydrogen abstraction via H (29%) and OH (21%) radical attack leading to the formation of CPDyl via

26

reactions (22) and (23). The thermal decomposition of CPD (21) accounts for around 24% and the hydrogen abstraction via the methyl radical 6% (55). The dominant CPDyl removal paths are oxidative via HO_2 attack (52%) through reaction (19), OH attack (7%) via (16) and O attack (4%) via (7). The thermal decomposition via reaction (28) accounts for 4%, while the CPDyl recombination to naphthalene via (49) accounts for around 11% with the corresponding reaction (53) to the indenyl radical contributing around 6%. The generation of the hydrogen radical is dominated (67%) by the thermal decomposition of CPD, the thermal decomposition of C_5H_4OH (15) contributes 6% and reaction (16) 5%. The CPDyl recombination sequence (49,50) to naphthalene provides a further 8%. The heat release is strongly dependent upon reaction (19) and the dynamics of the system are comparatively well reproduced for Cases 1 and 2 as shown in Fig. 22 with the influence of heterogeneous reactions, as outlined by Butler [1], a likely cause of early CO_2 formation. However, the overall impact of the latter appears modest.

Reaction (19) is also the dominant (90%) path leading to the 1,3-butadienyl radical following the thermal decomposition of C_5H_5O through reaction (5). The butadiene system has been studied by Lindstedt and Skevis [71], Laskin et al. [72] and Hansen et al. [73] among others. In the current system, the balance between molecular oxygen attack on 1,3-butadienyl leading to C–C bond breakage and competing pathways exert a strong influence on computed species concentrations. The critical sequence, also responsible for the majority (68%) of allyl radical formation, passes via $C \cdot H_2 - CH = CH - CHO$ as suggested by Laskin et al. [72]. The rate is an estimate based on similarity with the $C_2H_3 + O_2$ reaction and the proposed rate was reduced by a factor of 2 and it is likely that further adjustments will improve the agreement with the current data sets. However, despite the uncertainties, the computed levels of allene ($C_3H_4(A)$), propyne ($C_3H_4(P)$) and propene (C_3H_6) are comparatively well reproduced as shown in Fig. 23. The ratio of allene and propyne is sensitive to the thermodynamics and it was found that an update to G4MP2 determinations improved agreement with measurements. The main (94%) pathway to 1,3-butadiene is

27

also oxidative via reaction (18) and the overall levels are comparatively well reproduced along with the dependency on temperature. The introduction of pressure fall-off effects for reaction (18) reduces 1,3-butadiene levels by around a factor of two.

The overall distribution of C_1-C_2 hydrocarbons is shown in Fig. 24 with the heat release at the higher temperature causing a qualitatively different profile shape. The dominant reaction sequence for methane formation is via reaction (55) with the methyl radical formed via an oxidation sequence initiated by the reaction of the 1,3-butadienyl radical with O_2 (85%) passing through CH_3CO [74] and (14%) via CPDyl recombination (53). The rate expression used for the abstraction reaction from CPD (55) provides a value of $2 \cdot 10^8 m^3$ $kmol^{-1}$ s^{-1} at 1200 K compared to the value of $3.6 \cdot 10^8$ m^3 $kmol^{-1}$ s^{-1} used by Alzueta et al. [9] and $3 \cdot 10^7 m^3$ $kmol^{-1}$ s^{-1} used by Ristori et al. [13]. The formation of acetylene is essentially controlled by reactions (24) and (28) which contribute 54% and 29% respectively. The challenges associated with the CPDyl decomposition reaction have been outlined above and use of the alternative rate suggestion of Kern et al. [21] leads to significant overpredictions of acetylene. While acetylene and ethane levels are arguably reasonably well reproduced, including the 10-fold increase caused by an initial temperature difference of 50 K, the computed levels of ethylene are less satisfactory and indicate a systematic underprediction. Hansen et al. [73] suggest that 1,3-butadiene decomposition to vinylidene and ethylene, followed by isomerization of vinylidene to acetylene, plays a significant role under flame conditions and the impact of the sequence was investigated. However, as suggested [73] higher temperatures are required. Markaki [8] also observed persistent issues for pyrolytic cases and it appears likely that additional non-oxidative pathways need to be introduced. The focus of the current work is on the less studied oxidation reactions. However, it appears possible that some pyrolytic pathways, including the PES for the $H + C_5H_6$ reaction studied by Moskaleva and Lin [27], merit further investigation. The alternative pyrolysis steps shown in Table 7 for reactions (21), (22) and (26,27) do not cause significant changes in results. In particular, the rate

28

determination by Harding et al. [23] is compatible with the current mechanism.

The computed vinylacetylene (C_4H_4) levels are well reproduced as shown in Fig. 25. The key paths progress via oxidation (60%) and thermal decomposition (10%) of the 1,3-butadienyl radical formed predominantly through reaction (5). The sequence $C_5H_4OH \longrightarrow C_5H_4O \longrightarrow C_4H_4 + CO$ contributes 29% when the rate of Ristori et al. [13] is applied to reaction (60). However, the comparatively fast rate to vinylacetylene is conjectural. The pathway via CPDone is also interesting in the sense that the species could not be detected experimentally [1, 2], while persistent accumulation has been noted in computational studies (e.g. [9]). The above reaction sequence results in peak concentrations ≤ 10 ppm for the rich and stoichiometric cases and $\simeq 20$ ppm for the fuel lean case. Accordingly, some uncertainties remain, particularly under fuel lean conditions and further investigations of the CPDone decomposition pathways are desirable.

The principal reaction channels leading to naphthalene ($C_{10}H_8$) and benzene (C_6H_6) result in good agreement as shown in Fig. 25. The thermal decomposition of CPDyl is responsible ($\simeq 99\%$) for the production of propargyl and at this low temperature the propargyl radical contributes only 5% of the formation of benzene, while at the higher temperature of 1200 K (Case 1) the proportion increases to around 19%. The dominant channel is via the reaction sequence $C_5H_5 + CH_3 \longrightarrow C_5H_4CH_3 + H \longrightarrow$ fulvene $\longrightarrow$ benzene via reactions (46, 47, 48). The balance between the pathway and the propargyl recombination route is strongly dependent upon the rate of the thermal decomposition of CPDyl and hence subject to the uncertainties outlined above. The dominant reaction ($\geq 95\%$) leading to naphthalene is via cyclopentadienyl radical recombination and the simple two-step sequence provides reasonable agreement following adjustments to the frequency factor to account for the slower thermal decomposition of CPDyl, as compared to earlier studies (e.g. [5]), applied in the current work. Finally, the impact of temperature on toluene (C_7H_8) formation is well reproduced with the dominant (97%) pathway via C_9H_7 oxidation through $C_9H_7 + O_2 \longrightarrow C_7H_7 \longrightarrow C_7H_8$ using the rates determined by Lindstedt et al. [79] using a RRKM/ME approach.

29

The impact of changes in the stoichiometry of the mixture to 0.6 and 1.6 is shown in Figs. 26 to 28. The major species are arguably reasonably well reproduced though there is a consistent underprediction of benzene coupled with an underprediction of acetylene. As outlined above, both effects can be directly related to the reduced rate for the thermal decomposition of CPDyl. The dominant (72%) balancing oxidation path from the propargyl radical under stoichiometric conditions is via $C_3H_3 + O_2$ with the rate and product channel adopted from Slagle and Gutman [75] and it is also possible that uncertainties may exert an influence. However, Hahn et al. [76] performed a comprehensive theoretical analysis of the reaction and presented good agreement with the earlier suggestion. At the current conditions the rates differ by less than a factor of 2 with the earlier determination [75] somewhat slower.

Encouragingly, the distribution of secondary products such as methane, indene (C_9H_8), styrene (C_8H_8) and toluene are reproduced with reasonable accuracy as shown in Fig. 27. The result suggests that the rate for the global indene formation step (53) has some validity for a reasonably wide range of stoichiometries in a narrow temperature range around 1200 K. The main (86%) formation path for styrene (C_8H_8) is via the estimated $C_5H_5 + C_3H_3$ reaction (54) (c.f. [5]). The result for toluene is interesting and shows that the barriers for pathways passing via $C_5H_5 + C_2H_2$ pathways, e.g. via the cycloheptatriene [33] and fulveneallene C_7H_6 [77, 78] intermediates, are associated with significant barriers. Finally, computed levels of C_3 species and 1,3-butadiene are arguably in reasonable agreement with measurements. The dominant formation path (93%) for the latter species is via $C_5H_5 + OH$ through reaction (18).

7. Conclusions

The current study has applied G4/G4MP2 methods coupled with RRKM/ME calculations to determine rate parameters for selected oxidation paths featuring the cyclopentadienyl radical. The approach has been further assessed through the consideration of selected cyclopentadiene pyrolysis reactions. Comparisons

30

for the latter, comparatively well investigated pathways, suggest that the approach provides a useful methodology for estimating rate constants though caution is required, for example, when dealing with barrierless reactions. However, it has been shown by comparisons with the experimental data of Butler and Glassman [1, 2] that application of the determined rate parameters can lead to good agreement for the reaction dynamics and directly affected reaction products as well as providing an estimate of pressure fall-off. A major remaining issue affecting the chemistry of CPD under the current conditions has been shown to be the thermal decomposition of the CPDyl radical and, possibly, the $C_5H_5 + H$ addition reaction. Comparisons suggests that the current approach is arguably accurate to around a factor of two for cases where comparisons with recent studies could be made and that the neglect of fall-off effects can be expected to introduce significant errors for some reactions. However, there are additional factors, such as rates and product distributions of secondary reactions that may also impact results strongly, though an effort has been made to minimise such effects through the application of recent accurate chemical kinetic data where possible. Overall, comparisons with experimental data suggests good qualitative agreements with stoichiometric and temperature trends and, in most cases, reasonable quantitative agreement. However, the difficulties associated CPDyl and/or CPDyl/CPD pathways to indene have also been outlined and it is suggested that further work is required. Finally, the 1,3-butadiene subsystem exerts a significant influence on results and merits further investigation.

Acknowledgements

References

[1] R. G. Butler, *Combustion Chemistry of 1-3 Cyclopentadiene*, Ph.D. thesis, Princeton University, Princeton NJ (2001).

[2] R. G. Butler, I. Glassman, *Proc. Combust. Inst.* 32 (2009) 395–402.

[3] J. L. Emdee, K. Brezinsky, I. Glassman, *J. Phys. Chem. A* 96 (1992) 2151–2161.

[4] X. Zhong, J. W. Bozzelli, *J. Phys. Chem. A* 102 (1998) 3537–3555.

[5] R. P. Lindstedt, L. Q. Maurice, M. P. Meyer, *Faraday Discuss.* 119 (2001) 409–432.

[6] R. P. Lindstedt, K. A. Rizos, *Proc. Combust. Inst.* 29 (2002) 2291–2298.

[7] Y. Murakami, K. Mitsui, K. Naito, T. Itoh, T. Kobayashi, N. Fujii, *Shock Waves* 13 (2003) 149–154.

[8] V. Markaki, *Detailed and Simplified Chemical Kinetics of Aviation Fuels and Surrogates*, Ph.D. thesis, Imperial College, London (2010).

[9] M. U. Alzueta, P. Glarborg, K. Dam-Johansen, *Int. J. Chem. Kinet. (8)* 32 (2000) 498–522.

[10] H. Richter, J. B. Howard, *Phys. Chem. Chem. Phys.* 4 (2002) 2038–2055.

[11] H. Wang, K. Brezinsky, *J. Phys. Chem. A* 102 (1998) 1503–1541.

[12] J. L. DiNaro, J. B. Howard, W. H. Green, J. W. Tester, J. W. Bozzelli, *J. Phys. Chem.* 104 (2000) 10576–10586.

[13] A. Ristori, P. Dagaut, A. E. Bakali, G. Pengloan, M. Cathonnet, *Combust. Sci. Technol.* 167 (2001) 223–256.

[14] M. J. Frisch, G. W. Trucks, H. B. Schlegel, G. E. Scuseria, M. A. Robb, J. R. Cheeseman, G. Scalmani, V. Barone, B. Mennucci, G. A. Petersson, H. Nakatsuji, M. Caricato, X. Li, H. P. Hratchian, A. F. Izmaylov, J. Bloino, G. Zheng, J. L. Sonnenberg, M. Hada, M. Ehara, K. Toyota, R. Fukuda, J. Hasegawa, M. Ishida, T. Nakajima, Y. Honda, O. Kitao, H. Nakai, T. Vreven, J. A. Montgomery, Jr., J. E. Peralta, F. Ogliaro, M. Bearpark, J. J. Heyd, E. Brothers, K. N. Kudin,

V. N. Staroverov, R. Kobayashi, J. Normand, K. Raghavachari, A. Rendell, J. C. Burant, S. S. Iyengar, J. Tomasi, M. Cossi, N. Rega, J. M. Millam, M. Klene, J. E. Knox, J. B. Cross, V. Bakken, C. Adamo, J. Jaramillo, R. Gomperts, R. E. Stratmann, O. Yazyev, A. J. Austin, R. Cammi, C. Pomelli, J. W. Ochterski, R. L. Martin, K. Morokuma, V. G. Zakrzewski, G. A. Voth, P. Salvador, J. J. Dannenberg, S. Dapprich, A. D. Daniels, O. Farkas, J. B. Foresman, J. V. Ortiz, J. Cioslowski, D. J. Fox, *Gaussian 09 Revision A.1*, Gaussian Inc. Wallingford CT 2009.

[15] A. D. Becke, *J. Chem. Phys.* 98 (1993) 5648–5652.

[16] C. Lee, W. Yang, R. G. Parr, *J. Phys. Rev.* B41 (1988) 785–789.

[17] L. A. Curtiss, P. C. Redfern, K. Raghavachari, *J. Chem. Phys.* 126 (2007) 084108.

[18] L. A. Curtiss, P. C. Redfern, K. Raghavachari, J. A. Pople, *J. Chem. Phys.* 114 (2001) 108–117.

[19] V. Mokrushin, V. Bedanov, W. Tsang, M. Zachariah, V. Knyazev, *CHEMRATE version 1.5.8*, National Institute of Standardds and Technology, Gaithersburg, MD (2006).

[20] K. Roy, C. Horn, P. Frank, V. G. Slutsky, T. Just, *Proc. Combust. Inst.* 27 (1998) 329–336.

[21] R. D. Kern, Q. Zhang, J. Yao, B. S. Jursic, R. S. Tranter, M. A. Greybill, J. H. Kiefer, *Proc. Combust. Inst.* (1998) 143–150.

[22] L. V. Moskaleva, M. C. Lin, *J. Comp. Chem.* 21 (2000) 415–425.

[23] L. Harding, S. Klippenstein, Y. Georgievskii, *J. Phys. Chem. A* 111 (2007) 3789–3801.

[24] V. D. Knyazev, I. R. Slage, *J. Chem. Phys. A* 106 (2002) 5613–5617.

[25] K. Roy, P. Frank, *21st International Symposium on Shock Waves* (1997).

[26] G. B. Bacskay, J. C. Mackie, *Phys. Chem. Chem. Phys.* 3 (2001) 2467–2473.

[27] L. V. Moskaleva, M. C. Lin, *Proc. Combust. Inst.* 29 (2002) 1319–1327.

33

[28] D. Wang, A. Violi, D. H. Kim, J. A. Mullholland, *J. Phys. Chem. A* 110 (2006) 4719–4725.

[29] N. Hansen, T. Kasper, S. J. Klippenstein, P. R. Westmoreland, M. E. Law, C. A. Taatjes, K. Kohse-Höinghaus, J. Wang, T. A. Cool, *J. Phys. Chem. A* 111 (2007) 4081–4092.

[30] V. V. Kislov, A. M. Mebel, *J. Phys. Chem. A* 112 (2008) 700–716.

[31] L. V. Moskaleva, A. M. Mebel, M. C. Lin, *Proc. Combust. Inst.* 26 (1996) 521–526.

[32] S. Sharma, W. H. Green, *J. Phys. Chem. A* 113 (2009) 8871–8882.

[33] C. Cavallotti, S. Mancarella, R. Rota, S. Carra, *J. Phys. Chem. A* 111 (2007) 3959–3969.

[34] C. F. Melius, M. E. Colvin, N. M. Marinov, W. J. Pitz, S. M. Senkan, *Proc. Combust. Inst.* 26 (1996) 685–692.

[35] N. M. Marinov, W. J. Pitz, C. K. Westbrook, M. J. Castaldi, S. M. Senkan, *Combust. Sci. Technol.* 116 (1996) 211–287.

[36] N. M. Marinov, M. J. Castaldi, C. F. Melius, W. Tsang, *Combust. Sci. Technol.* 128 (1997) 295–342.

[37] A. M. Mebel, V. V. Kislov, *J. Phys. Chem. A* 113 (2009) 9825–9833.

[38] J. L. Durant, C. M. Rohlfing, *J. Chem. Phys. A* 98 (1993) 8031–8036.

[39] B. J. McBride, S. Gordon, *Computer Program for Calculating and Fitting Thermodynamic Functions*, NASA RP 1271, (1998).

[40] P. Bishof, *J. Phys. Chem. A* 99 (1977) 8145–8149.

[41] M. Karni, I. Oref, A. Burcat, *J. Phys. Chem. Ref. Data* 20 (1991) 665–683.

[42] H. Wang, K. Brezinsky, *J. Phys. Chem. A* 102 (1998) 1530–1541.

[43] D. J. DeFrees, R. T. McIver, W. J. Hehre, *J. Phys. Chem. A* 102 (1980) 3334–3338.

[44] J. Puttemans, J. P. Smith, D. M. Golden, *J. Phys. Chem. A* 90 (1990) 3226–3227.

34

[45] G. Katzer, A. F. Sax, *J. Chem. Phys.* 117 (2002) 8219–8228.

[46] A. Burcat, B. Ruscic, *Third Millennium Ideal Gas and Condensed Phase Thermochemical Database for Combustion with updates from Active Thermochemical Tables*, Tech. rep., Technion-IIT, Aerospace Engineering and Argonne National Laboratory (2005).

[47] D. Ben-Amotz, D. Herschbach, *J. Phys. Chem. A* 94 (1990) 1038–1047.

[48] I. V. Tokmakov, L. V. Moskaleva, M. C. Lin, *Int. J. Chem. Kin.* 36 (2004) 139–151.

[49] J. A. Miller, J. P. Senosiaian, S. J. Klippenstein, Y. Georgievskii, *J. Phys. Chem. A* 112 (2008) 9429–9438.

[50] J. A. Miller, S. J. Klippenstein, *J. Phys. Chem. A* 107 (2003) 7783–7799.

[51] B. S. Rabinovitch, D. C. Tardy, *J. Chem. Phys.* 45 (1966) 3720–3730.

[52] C. Eckart, *Phys. Rev.* 35 (1930) 1303–1309.

[53] T. Beyer, D. F. Swinehart, *Commun. ACM* 16 (1973) 379.

[54] G. Z. Whitten, B. S. Rabinovitch, *J. Chem. Phys. A* 38 (1963) 2466–2473.

[55] R. P. Lindstedt, L. Q. Maurice, *Comb. Sci. Tech.* 120 (1996) 119 – 167.

[56] M. U. Alzueta, M. Oliva, P. Glarborg, *Int. J. Chem. Kinet.* 30 (1998) 683–697.

[57] R. P. Lindstedt, G. Skevis, *Combust. Sci. Technol.* 125 (1997) 73–137.

[58] D. A. Bittker, *Combust. Sci. Technol.* 79 (1991) 49–72.

[59] B. Sirjean, E. Dames, D. Sheen, F. Egolfopoulos, H. Wang, D. Davidson, R. Hanson, H. Pitsch, C. Bowman, C. Law, W. Tsang, N. Cernansky, D. Miller, A. Violi, R. Lindstedt, *A high-temperature chemical kinetic model of n-alkane, cyclohexane, and methyl-, ethyl-, n-propyl- and n-butyl-cyclohexane oxidation at high temperatures*, Ph.D. thesis, JetSurF version 1.1, September 15, 2009 ((http://melchior.usc.edu/JetSurF/JetSurF1.1)).

[60] K. M. Leung, R. P. Lindstedt, *Comb. Flame* 102 (1995) 129–160.

35

[61] J. A. Miller, C. F. Melius, *Combust. Flame* 91 (1992) 21–39.

[62] Y. Georgievskii, S. J. Klippenstein, J. A. Miller, *Phys. Chem. Chem. Phys.* 112 (2007) 4259–4268.

[63] N. Hansen, J. A. Miller, P. R. Westmoreland, T. Kasper, M. E. Law, K. Kohse-Höinghaus, J. Wang, T. A. Cool, *Combust. Flame.* 156 (2009) 2153–2164.

[64] R. X. Fernandes, B. R. Giri, H. Hippler, C. Kachiani, F. Striebel, *J. Phys. Chem. A* 109 (2005) 1063–1070.

[65] L. B. Harding, S. J. Klippenstein, *Proc. Combust. Inst.* 28 (2000) 1503–1509.

[66] V. V. Kislov, A. M. Mebel, *J. Phys. Chem. A* 111 (2007) 9532–9543.

[67] M. B. Colket, R. J. Hall, M. D. Smooke, *Mechanistic Models of Soot Formation*, Tech. Rep. F49620-91-C-0056, AFOSR Contract (1994).

[68] M. B. Colket, D. J. Seery, *Proc. Combust. Inst.* 25 (1994) 883–891.

[69] S. Fascella, C. Cavallotti, R. Rota, S. Carra, *J. Phys. Chem. A* 109 (2005) 7546–7457.

[70] Y. Tan, P. Frank, *Proc. Combust. Inst.* 26 (1996) 677–684.

[71] R. P. Lindstedt, G. Skevis, *Proc. Combust. Inst.* 26 (1996) 703–709.

[72] A. Laskin, H. Wang, C. Law, *Int. J. Chem. Kin.* 32 (2000) 589–614.

[73] N. Hansen, J. A. Miller, T. Kasper, K. Kohse-Höinghaus, P. R. Westmoreland, J. Wang, T. A. Cool, *Proc. Combust. Inst.* 32 (2009) 623–630.

[74] R. P. Lindstedt, G. Skevis, *Proc. Combust. Inst.* 28 (2000) 1801-1807.

[75] I. R. Slagle, D. Gutman, *Proc. Combust. Inst.* 21 (1986) 875–883.

[76] D. K. Hahn, S. J. Klippenstein, J. A. Miller, *Faraday Discuss.* 119 (2001) 79–100.

[77] V. Detilleux, J. Vandooren, *J. Phys. Chem. A* 113 (2009) 10913–10922.

[78] G. de Silva, J. W. Bozzelli, *J. Phys. Chem. A Letters* 113 (2009) 12045 – 12048.

[79] R. P. Lindstedt, V. Markaki, R. K. Robinson, *Oxidation of two-ringed aromatic species as models for soot surface reactions*, in Combustion Generated Fine Carbonaceous Particles, (Eds.) H. Bockhorn and A. D'Anna and A. F. Sarofim and H. Wang, Karlsruhe University Press, New York, 2009.

[80] Y. Hidaka, T. Nakamura, H. Tanaka, A. Jinno, H. Kawano, *Int. J. Chem. Kinet. (9)* 24 (1992) 761–780.

[81] K. Roy, M. Braun-Unkhoff, P. Frank, T. Just, *Int. J. Chem. Kin.* 33 (2001) 821–833.

List of Tables

List of Figures

Table 1: Thermochemical data for species featuring in the chemical kinetic modelling.

Species Acronym	Species Name	$\triangle_f H^{298K}$ kJ mol^{-1}	S^{298K} J K^{-1} mol^{-1}	C_p^{298K} J K^{-1} mol^{-1}	$\triangle_f H^{1000K}$ kJ mol^{-1}	Ref.[a]
H$_2$	—	0.000	130.671	28.834	20.685	[46]
O$_2$	—	0.000	205.137	29.377	22.706	[46]
H	—	217.985	114.711	20.785	232.573	[46]
OH	—	37.298	183.727	29.884	58.215	[46]
O	—	249.185	160.937	21.898	264.045	[46]
H$_2$O	—	-241.811	188.818	33.586	-215.81	[46]
HO$_2$	—	12.551	229.092	34.891	42.103	[46]
C=CC=C	1,3-Butadiene	107.535	290.176	81.462	201.075	pw
C=CC=C.	1,3-Butadiene-1-yl radical	357.497	295.933	76.183	444.977	pw
C$_5$H$_6$	Cyclopentadiene (CPD)	136.388	275.050	76.695	239.516	pw
C$_5$H$_5$	Cyclopentadienyl (CPDyl) radical	257.804	271.300	74.574	352.527	pw
C$_5$H$_5$O	2,4-Cyclopentadieneoxy radical	210.042	309.878	87.327	319.356	pw
C$_5$H$_5$OO	Cyclopentadienyl-peroxy radical	205.312	342.239	103.124	326.722	pw
C$_5$H$_5$OOH	Cyclopentadienylicperoxide (CPDOOH)	70.620	346.974	115.702	202.453	pw
C$_5$H$_5$OH	Cyclopentadienol	-10.164	308.306	98.182	109.348	pw
C$_5$H$_4$OH	Cyclopentadienol-1-yl radical	59.471	301.984	89.765	170.233	pw
C$_5$H$_4$O	Cyclopentadienone (CPDone)	53.335	289.926	82.141	153.603	pw
CYC5ODE	Pyran-1-yl radical	79.757	295.996	86.239	188.407	pw
CHT	Cycloheptatriene	178.964	316.787	105.776	320.316	pw
c-C$_7$H$_7$	Cycloheptatrienyl radical	272.199	321.646	110.573	409.829	pw
NCD	Norcoradiene	204.661	310.967	103.499	346.354	pw

[a]pw: present work, see text

Table 2: Heats of formation in kJ mol^{-1} for studied reactions determined using the G4, G4MP2 and G3B3 methods

Species	G4MP2	G3B3	Species	G4MP2	G3B3	Species	G4MP2	G3B3
Reaction 1			Reaction 8			Reaction 18 (R1)		
$C_5H_5 + O_2$	257.80	261.54	$C_5H_5 + O$	506.45	510.84	$C_5H_5 + OH$	293.63	296.55
$C_5H_5O + O$	458.72	467.71	C_5H_5O	210.07	218.41	C_5H_5OH	-10.15	-8.16
			$C_5H_4O + H$	272.74	272.75	TS9	265.02	278.32
Reaction 2						$BICYC_5H_6O$	37.67	38.13
$C_5H_5 + O2$	257.80	261.54	Reaction 9			TS10	197.25	210.41
TS1	275.31	282.86	$C_5H_5 + O$	506.45	510.84	$O=CC=CC=C$	8.94	9.61
C_5H_5OO	205.33	215.60	C_5H_5O	210.07	218.41	Int Rot	22.12	22.97
			TS3	231.95	235.89	TS11	297.57	305.10
Reaction 3			$BICYC_5H_5O$	177.03	182.96	$C=CC=C + CO$	-10.17	-2.27
C_5H_5OO	205.33	215.60	TS4	262.61	268.59			
TS15	364.78^a	369.56	CYC5ODE	79.78	83.66	Reaction 18 (R2)		
C_5H_4OOH	149.40	157.05				C5H5 + OH	293.63	296.55
$C_5H_4O + OH$	90.58	89.76	Reaction 10			C_5H_5OH	-10.15	-8.16
			CYC5ODE	79.78	83.66	TS12	92.07	96.51
Reaction 4			TS4	262.61	268.59	C_5H_5-1-OH	-34.36	-32.63
C_5H_5OO	205.33	215.60	$BICYC_5H_5O$	177.03	182.96	TS13	212.42	214.75
$C_5H_5O + O$	458.72	467.71	TS3	231.95	235.89	$HOC.C=CC=C$	210.89	219.12
			C_5H_5O	210.07	218.41	Int Rot	224.62	228.90
Reaction 5 (R1)			$C_5H_4O + H$	272.74	272.75	TS14	418.96	426.05
C_5H_5O	210.07	218.41				$C=CC=C + CO$	-10.17	-2.27
TS3	231.95	235.89	Reaction 11					
$BICYC_5H_5O$	177.03	182.96	CYC5ODE	79.78	83.66	Reaction 19		
TS4	262.61	268.59	TS5	278.53	284.66	$C_5H_5 + HO_2$	270.83	274.39
CYC5ODE	79.78	83.66	$O=CC=CC=C.$	259.63	267.89	C_5H_5OOH	70.62	67.11
TS5	278.53	284.66	TS6	276.06	281.69	$C_5H_5O + OH$	245.89	253.41
$O=CC=CC=C.$	259.63	267.89	$O=C=CC.C=C$	126.63	129.66			
TS6	276.06	281.69	TS7	263.06	273.68	Reaction 20		
$O=C=CC.C=C$	126.63	129.66	$C=CC=C. + CO$	239.80	250.22	$C_5H_5 + HO_2$	270.83	274.39
TS7	263.06	273.68				C_5H_5OOH	70.62	67.11
$C=CC=C. + CO$	239.80	250.22	Reaction 12			TS2	249.72	248.25
			$C_5H_5 + OH$	293.63	296.55	$C_5H_4O + H_2O$	-186.04	-186.37
Reaction 5 (R2)			C_5H_5OH	-10.15	-8.16			
C_5H_5O	210.07	218.41				**Species**	**G4**	**G3B3**
TS8	280.62	286.44	Reaction 13			Reaction 21		
$O=CC=CC=C.$	259.63	267.89	C_5H_5OH	-10.15	-8.16	C_5H_6	135.35	136.40
TS6	276.06	281.69	$C_5H_4OH + H$	277.48	285.31	$C_5H_5 + H$	475.80	479.54
$O=C=CC.C=C$	126.63	129.66						
TS7	263.06	273.68	Reaction 14			Reaction 22		
$C=CC=C. + CO$	239.80	250.22	C_5H_5OH	-10.15	-8.16	$C_5H_6 + H$	353.35	354.40
			$C_5H_5O + H$	428.06	436.41	TS16	367.73	373.56
Reaction 6						$C_5H_5 + H_2$	257.80	261.54
C_5H_5O	210.07	218.41	Reaction 15					
$C_5H_4O + H$	272.74	272.75	C_5H_4OH	59.49	67.31	Reaction 25		
			$C_5H_4O + H$	272.74	272.75	C_5H_5	257.80	261.54
Reaction 7						TS17	511.26	518.84
$C_5H_5 + O$	506.45	510.84	Reaction 16			C_5H_5-1	398.16	407.49
C_5H_5O	210.07	218.41	$C_5H_5 + OH$	293.63	296.55	TS18	575.74	576.70
TS8	280.62	286.44	C_5H_5OH	-10.15	-8.16	$CHCCH_2CHCH$	519.47	522.55
$O=CC=CC=C.$	259.63	267.89	$C_5H_4OH + H$	277.48	285.31	TS19	630.83	629.83
TS6	276.06	281.69				$C_3H_3 + C_2H_2$	573.32	572.63
$O=C=CC.C=C$	126.63	129.66	Reaction 17					
TS7	263.06	273.68	$C_5H_5 + OH$	293.63	296.55			
$C=CC=C. + CO$	239.80	250.22	C_5H_5OH	-10.15	-8.16			
			$C_5H_5O + H$	428.06	436.41			

^{a} determined from G4 composite method.

41

Table 3: Molecular Parameters used in RRRKM/ME calculations.

Species Name	Sym. No.	Moments of Inertia[a] 10^{-39} g cm^2	Vibrational Frequencies[b,c] cm^{-1}
C_5H_5	10	9.02; 9.85; 18.87	(i30), 496, 510, 686, 718, 813, 828, 878, 887, 915, 934, 1047, 1065, 1128, 1195, 1276, 1370, 1471, 1516, 3163, 3168, 3180, 3198, 3206
C_5H_5O	1	11.57; 20.82; 29.23	129, 256, 514, 519, 692, 726, 781, 793, 874, 931, 943, 971, 995, 1078, 1093, 1117, 1193, 1260, 1277, 1363, 1512, 1607, 2858, 3152, 3164, 3193, 3210
C_5H_4O	2	10.28; 21.27; 31.55	210, 450, 453, 648, 649, 715, 741, 837, 849, 944, 954, 960, 1081, 1084, 1114, 1285, 1332, 1569, 1639, 1792, 3164, 3174, 3208, 3211
BICYC$_5$H$_5$O	1	11.82; 17.21; 24.60	358, 375, 539, 670, 682, 713, 786, 810, 823, 915, 919, 969, 1002, 1042, 1079, 1084, 1220, 1267, 1284, 1338, 1377, 1444, 3113, 3123, 3155, 3182, 3190
BICYC$_5$H$_6$O	1	12.77; 17.54; 25.38	301, 376, 504, 697, 722, 778, 826, 841, 906, 916, 940, 957, 1000, 1021, 1088, 1115, 1167, 1235, 1279, 1287, 1354, 1389, 1437, 1636, 2983, 3019, 3100, 3120, 3144, 3174
CYC5ODE	2	14.28; 15.07; 29.35	228, 402, 533, 582, 595, 633, 677, 708, 880, 884, 885, 965, 970, 1000, 1055, 1180, 1216, 1287, 1329, 1407, 1490, 1594, 3076, 3078, 3111, 3129, 3133
O=C=CC.C=C	1	12.71; 31.24; 43.95	90, 145, 275, 322, 462, 530, 564, 594, 732, 766, 793, 875, 975, 1035, 1090, 1177, 1257, 1371, 1425, 1442, 1538, 2160, 3100, 3117, 3118, 3150, 3200
C_5H_5-1	1	8.87; 10.34; 18.69	343, 514, 652, 695, 772, 776, 891, 893, 934, 955, 1019, 1092, 1102, 1187, 1225, 1336, 1385, 1528, 1586, 2972, 3003, 3162, 3193, 3199
C_5H_6	2	9.91; 10.19; 19.58	344, 516, 680, 709, 799, 800, 909, 913, 940, 947, 957, 1001, 1100, 1101, 1116, 1244, 1296, 1377, 1392, 1537, 1621, 2971, 2994, 3152, 3162, 3182, 3188

[a] determined from B3LYP/6-31G(2df,p) geometries.
[b] calculated at the B3LYP/6-31G(2df,p) level with a correction factor of 0.9854.
[c] vibrations modelled as psuedo rotations in brackets.

42

Table 4: Molecular parameters used for RRRKM/ME calculations with hindered internal rotations. All symmetry numbers are unity.

Species Name	Moments of Inertia[a] 10^{-39} g cm^2	Hindered Internal Rotors[b] Barrier[c]; Moment of Inertia kJ mol^{-1}; 10^{-39} g cm^2	Vibrational Frequencies[d,e] cm^{-1}
C_5H_5OOH	16.01; 37.05; 41.43	C_5H_5-OOH=20.92; 4.86 C_5H_5O-OH=19.64; 1.58	(129), (211), 134, 346, 359, 538, 633, 683, 718, 779, 846, 869, 913, 946, 950, 971, 1027, 1041, 1092, 1125, 1199, 1291, 1293, 1369, 1372, 1560, 1636, 2943, 3154, 3166, 3184, 3197, 3687
C_5H_5OH	11.37; 23.33; 32.01	C_5H_5-OH=17.10; 0.143	174, 293, (363) , 546, 554, 692, 727, 780, 827, 864, 948, 949, 971, 1027, 1052, 1091, 1134, 1216, 1223, 1291, 1366, 1387, 1558, 1633, 2954, 3150, 3161, 3185, 3189, 3748
C_5H_5-1-OH	8.26; 3.42; 2.45	C_5H_5-OH=20.67; 0.139	(245), 258, 388, 411, 508, 621, 672, 795, 836, 885, 904, 942, 947, 1000, 1106, 1113, 1163, 1215, 1275, 1322, 1382, 1406, 1574, 1669, 2969, 2999, 3156, 3188, 3195, 3780
C_5H_4OH	9.96; 22.88; 32.84	C_5H_4-OH=32.04; 0.13	(261), 396, 450, 541, 636, 644, 671, 686, 727, 827, 865, 917, 1004, 1026, 1077, 1103, 1267, 1298, 1338, 1416, 1532, 1539, 3168, 3179, 3191, 3209, 3747
O=CC=CC=C	10.65; 38.47; 47.67	$OCH-CHCHCH_2$=32.21; 2.61 $CHCHCH-CHCH_2$=28.66; 3.27	(108), (155), 224, 293, 372, 510, 569, 738, 814, 896, 955, 1009, 1016, 1032, 1070, 1088, 1216, 1308, 1365, 1420, 1441, 1637, 1661, 1751, 2886, 3080, 3094, 3111, 3129, 3194
O=CC=CC=C.	10.29; 36.68; 46.97	$OCH-CHCHCHCH$=34.81; 2.62 $OCHCHCH-CHCH$=27.40; 2.60	(27), (144), 151, 333, 387, 483, 600, 685, 764, 822, 867, 964, 1012, 1023, 1089, 1219, 1262, 1360, 1417, 1600, 1649, 1754, 2806, 2993, 3109, 3135, 3208
HOC.C=CC=C	10.16; 38.91; 48.59	$HOC-CHCHCHCH_2$=10.0; 3.38 $HOCCHCH-CHCH_2$=43.28; 3.26	(51), (125), 211, 320, 374, 480, 527, 739, 761, 860, 891, 957, 1005, 1024, 1042, 1083, 1184, 1259, 1323, 1332, 1413, 1439, 1597, 1654, 3032, 3083, 3098, 3110, 3207, 3715
C=CC=C	1.97; 18.95; 20.93	$CH_2CH-CHCH_2$=31.15; 1.74	(175), 291, 507, 535, 776, 887, 923, 927, 985, 995, 1052, 1209, 1298, 1300, 1399, 1455, 1637, 1688, 3088, 3098, 3103, 3104, 3187, 3187
C=CC=C.	1.69; 18.32; 20.01	$CH_2CH-CHCH$=30.22; 1.53	(180), 291, 501, 561, 722, 784, 850, 925, 934, 1026, 1158, 1231, 1299, 1425, 1618, 1667, 2983, 3102, 3120, 3189, 3213
$CHCCH_2CHCH$	7.12; 22.67; 29.27	$CHCCH_2-CHCH$=9.61; 2.66	(136), 153, 328, 348, 574, 606, 628, 635, 827, 839, 867, 951, 997, 1199, 1216, 1316, 1435, 1660, 2210, 2962, 2985, 3067, 3219, 3455

[a] determined from B3LYP/6-31G(2df,p) geometries.

[b] dashed line - denotes internal rotor.

[c] determined from maximum and minimum energies at the B3LYP/6-31G(d) level.

[d] calculated at the B3LYP/6-31G(2df,p) level with a correction factor of 0.9854.

[e] vibrations modelled as internal rotors in brackets.

Table 5: Transition state parameters for RRRKM/ME calculations.

Species Name	Moments of Inertia[a] 10^{-39} g cm^2	Vibrational Frequencies[b] cm^{-1}
TS1	19.64; 32.90; 33.13	i289, 102, 134, 208, 406, 522, 551, 727, 735, 755, 828, 898, 917, 919, 938, 987, 1034, 1090, 1131, 1273, 1292, 1367, 1418, 1525, 1567, 3170, 3170, 3182, 3202, 3209
TS2	13.63; 43.68; 50.35	i2211, 144, 162, 356, 417, 431, 490, 571, 599, 710, 722, 772, 784, 811, 881, 906, 920, 997, 1069, 1083, 1130, 1165, 1276, 1288, 1384, 1482, 1588, 1663, 3161, 3173, 3198, 3204, 3664
TS3	12.17; 18.31; 25.60	i428, 298, 431, 548, 722, 752, 761, 801, 840, 924, 942, 957, 1020, 1077, 1086, 1093, 1210, 1275, 1292, 1339, 1384, 1514, 2990, 3157, 3176, 3188, 3226
TS4	12.64; 16.30; 25.83	i864, 375, 420, 536, 569, 671, 702, 717, 815, 863, 893, 918, 983, 1019, 1092, 1146, 1169, 1282, 1367, 1369, 1420, 1550, 3107, 3143, 3150, 3161, 3174
TS5	14.70; 19.10; 33.42	i342, 175, 291, 355, 517, 564, 632, 752, 821, 876, 912, 960, 977, 994, 1048, 1198, 1236, 1372, 1400, 1442, 1588, 1641, 2912, 3028, 3108, 3143, 3175
TS6	11.26; 30.76; 42.02	i1064, 151, 202, 363, 424, 500, 538, 546, 737, 766, 873, 914, 1006, 1012, 1077, 1082, 1172, 1268, 1381, 1553, 1607, 1675, 1824, 3049, 3116, 3138, 3150
TS7	16.81; 31.31; 45.66	i208, 49, 92, 128, 195, 209, 309, 520, 608, 736, 837, 849, 939, 981, 1018, 1066, 1246, 1315, 1429, 1619, 1663, 2084, 2983, 3102, 3117, 3200, 3216
TS8	12.02; 24.27; 34.76	i340, 183, 286, 369, 470, 549, 638, 683, 727, 835, 841, 881, 957, 983, 996, 1124, 1206, 1318, 1363, 1547, 1569, 1635, 2740, 3070, 3144, 3166, 3248
TS9	12.19; 20.42; 27.78	i1585, 209, 352, 504, 627, 715, 778, 799, 817, 854, 929, 958, 1002, 1011, 1064, 1087, 1096, 1214, 1245, 1264, 1283, 1396, 1430, 1501, 1840, 2961, 3128, 3147, 3170, 3189
TS10	11.72; 22.38; 31.06	i526, 256, 353, 435, 485, 562, 767, 803, 814, 909, 954, 996, 1007, 1071, 1088, 1098, 1125, 1207, 1257, 1328, 1344, 1436, 1454, 1482, 2763, 3038, 3104, 3123, 3159, 3186
TS11	15.86; 22.39; 35.33	i1388, 145, 184, 316, 330, 442, 552, 649, 696, 706, 827, 857, 945, 1003, 1011, 1062, 1176, 1232, 1302, 1350, 1418, 1461, 1582, 1817, 1921, 3084, 3109, 3117, 3131, 3222
TS12	10.03; 24.15; 33.59	i1197, 298, 324, 386, 596, 624, 679, 726, 756, 832, 896, 915, 926, 1051, 1069, 1089, 1140, 1231, 1274, 1310, 1397, 1446, 1484, 1492, 1989, 3160, 3183, 3191, 3207, 3761
TS13	11.58; 32.14; 42.32	i99, 174, 270, 371, 377, 520, 596, 740, 768, 811, 881, 937, 961, 970, 1010, 1068, 1145, 1227, 1278, 1332, 1399, 1453, 1537, 1616, 3065, 3098, 3114, 3124, 3203, 3707
TS14	9.65; 41.64; 49.05	i2340, 103, 146, 199, 277, 359, 499, 561, 604, 706, 830, 922, 947, 980, 1030, 1071, 1139, 1234, 1298, 1307, 1408, 1442, 1505, 1643, 1802, 3071, 3104, 3113, 3127, 3194
TS15	12.68; 39.46; 46.99	i1593, 17, 184, 353, 466, 519, 581, 719, 745, 746, 805, 838, 865, 886, 924, 933, 971, 1069, 1086, 1121, 1236, 1275, 1370, 1514, 1582, 1963, 3167, 3179, 3212, 3215
TS16	10.78; 11.56; 20.64	i934, 221, 251, 498, 528, 699, 714, 791, 800, 924, 926, 932, 940, 961, 1004, 1074, 1100, 1114, 1246, 1272, 1292, 1378, 1513, 1546, 1601, 3036, 3157, 3168, 3189, 3194
TS17	8.69; 9.94; 18.24	i1355, 536, 574, 713, 720, 793, 811, 837, 916, 976, 1042, 1081, 1103, 1149, 1214, 1314, 1354, 1411, 1470, 2048, 3152, 3182, 3204, 3210
TS18	9.54; 13.44; 22.46	i465, 305, 318, 502, 618, 636, 673, 730, 814, 842, 920, 947, 982, 1161, 1184, 1271, 1436, 1632, 1965, 2984, 3006, 3076, 3196, 3408
TS19	8.26; 27.32; 35.02	i572, 43, 106, 271, 339, 452, 523, 525, 556, 602, 648, 736, 782, 897, 1035, 1055, 1435, 1842, 2105, 3081, 3162, 3322, 3425, 3452

[a] determined from B3LYP/6-31G(2df,p) geometries.
[b] B3LYP/6-31G(2df,p) frequencies multiplied by a correction factor of 0.9854.

44

Table 6: Rate constants calculated in the present work (pw) with rate coefficients in the form $k = AT^n exp(-E/RT)$. Units are kmol, m^3, s, K and kJ mol^{-1}

No.	Reaction	A	n	E	Ref.
1	$C_5H_5 + O_2 \rightleftharpoons C_5H_5O + O$	4.367E+00	2.399	211.5	pw
2	$C_5H_5 + O_2 \rightleftharpoons C_5H_5OO$				
	k(1 Atm)	9.108E+12	-2.211	10.2	pw
	k(10 Atm)	1.456E+17	-3.106	26.1	pw
	k$_\infty$	7.983E-01	2.773	13.7	pw
3	$C_5H_5OO \rightleftharpoons C_5H_4O + OH$				
	k(1 Atm)	7.527E+50	-11.443	226.6	pw
	k(10 Atm)	2.566E+43	-9.027	218.1	pw
	k$_\infty$	3.199E+10	0.949	159.4	pw
4	$C_5H_5OO \rightleftharpoons C_5H_5O + O$				
	k(1 Atm)	3.605E+63	-14.526	348.4	pw
	k(10 Atm)	5.665E+53	-11.456	334.0	pw
	k$_\infty$	2.597E+19	-1.074	271.0	pw
5	$C_5H_5O \rightleftharpoons C=CC=C. + CO$				
	k(1 Atm)	2.149E+64	-15.141	278.0	pw
	k(10 Atm)	3.784E+60	-13.746	278.9	pw
	k$_\infty$	2.820E+14	0.434	202.6	pw
6	$C_5H_5O \rightleftharpoons C_5H_4O + H$				
	k(1 Atm)	8.183E+16	-2.319	36.5	pw
	k(10 Atm)	5.064E+18	-2.543	39.8	pw
	k$_\infty$	9.101E+19	-0.957	77.2	pw
7	$C_5H_5 + O \rightleftharpoons C=CC=C. + CO$	1.274E+11	0.260	16.5	pw[a]
9	$C_5H_5 + O \rightleftharpoons products$				
	k(1 Atm)	8.583E+56	-13.625	99.9	pw
	k(10 Atm)	2.696E+46	-10.370	83.5	pw
	k$_\infty$	1.274E+11	0.260	16.5	pw
10	$CYC5ODE \rightleftharpoons C_5H_4O + H$				
	k(1 Atm)	2.655E+49	-10.931	250.1	pw
	k(10 Atm)	1.250E+40	-8.012	236.5	pw
	k$_\infty$	5.255E+12	0.233	185.7	pw
11	$CYC5ODE \rightleftharpoons C=CC=C. + CO$				
	k(1 Atm)	2.149E+64	-15.141	278.0	pw
	k(10 Atm)	3.784E+60	-13.746	278.9	pw
	k$_\infty$	2.820E+14	0.434	202.6	pw
12	$C_5H_5 + OH \rightleftharpoons C_5H_5OH$				
	k(1 Atm)	2.724E+50	-11.703	90.2	pw
	k(10 Atm)	2.046E+39	-8.290	71.7	pw
	k$_\infty$	8.530E+10	0.246	18.2	pw
13	$C_5H_5OH \rightleftharpoons C_5H_4OH + H$				
	k(1 Atm)	8.506E+70	-16.413	395.7	pw
	k(10 Atm)	1.180E+62	-13.596	384.0	pw
	k$_\infty$	2.047E+18	-0.337	304.7	pw
14	$C_5H_5OH \rightleftharpoons C_5H_5O + H$				
	k(1 Atm)	6.539E+48	-9.478	512.7	pw
	k(10 Atm)	9.714E+37	-6.213	492.8	pw
	k$_\infty$	1.933E+18	-0.318	454.3	pw
15	$C_5H_4OH \rightleftharpoons C_5H_4O + H$				
	k(1 Atm)	2.345E+69	-16.568	295.0	pw
	k(10 Atm)	3.755E+68	-16.003	302.4	pw
	k$_\infty$	9.543E+19	-0.842	227.6	pw
16	$C_5H_5 + OH \rightleftharpoons C_5H_4OH + H$	8.530E+10	0.246	18.2	pw[a]
17	$C_5H_5 + OH \rightleftharpoons C_5H_5O + H$	1.114E+02	1.902	138.6	pw
18	$C_5H_5 + OH \rightleftharpoons C=CC=C + CO$	8.530E+10	0.246	18.2	pw[a]
19	$C_5H_5 + HO_2 \rightleftharpoons C_5H_5O + OH$	6.858E+10	0.252	21.3	pw
21	$C_5H_6 \rightleftharpoons C_5H_5 + H$				
	k(1 Atm)	3.236E+49	-10.009	423.4	pw
	k(10 Atm)	1.358E+38	-6.536	398.7	pw
	k$_\infty$	3.031E+18	-0.532	361.1	pw
22	$C_5H_6 + H \rightleftharpoons C_5H_5 + H_2$	8.587E+04	1.847	13.96	pw

[a] Estimated bimolecular rate.

Table 7: Selected updated, alternative or discussed rate parameters used in the modelling of cyclopentadiene oxidation. Rate coefficients in the form $k = AT^n exp(-E/RT)$. Units are kmol, m^3, s, K and kJ mol^{-1}

No.	Reaction	A	n	E	Ref.
	Alternative Pyrolysis and Abstraction Steps				
21	$C_5H_6 \rightleftharpoons C_5H_5 + H$	k_∞ 1.61E+13	0.86	374.8	[23]
22	$C_5H_6 + H \rightleftharpoons C_5H_5 + H_2$	3.03E+05	1.71	11.77	[27]
23	$C_5H_6 + OH \rightleftharpoons C_5H_5 + H_2O$	1.14E+06	1.18	-1.87	[3, 6][a]
24	$C_5H_6 + H \rightleftharpoons C_3H_5(A) + C_2H_2$	7.74E+33	-6.81	137.6	[4][b]
26	$C_5H_5 \rightleftharpoons CH_2CCHCHCH$	1.21E+109	-28.1	545.7	[22][b]
27	$CH_2CCHCHCH \rightleftharpoons C_3H_3 + C_2H_2$	1.95E+83	-20.6	288.7	[22][b]
28	$C_3H_3 + C_2H_2 \rightleftharpoons C_5H_5$	6.87E+52	-12.5	175.8	[22][b]
	Propargyl Recombination and Subsequent Steps				
29	$C_3H_3 + C_3H_3 \rightleftharpoons C_6H_5 + H$	2.02E+30	-6.0	66.70	[63]
30	$C_3H_3 + C_3H_3 \rightleftharpoons C_4H_5C_2H$	6.48E+65	-16.7	120.2	[63]
	$C_3H_3 + C_3H_3 \rightleftharpoons C_4H_5C_2H$	1.54E+33	-7.8	23.35	[63]
31	$C_3H_3 + C_3H_3 \rightleftharpoons$ fulvene	7.25E+62	-16.0	104.8	[63]
	$C_3H_3 + C_3H_3 \rightleftharpoons$ fulvene	4.19E+39	-9.0	25.5	[63]
32	$C_3H_3 + C_3H_3 \rightleftharpoons C_6H_6$	1.64E+63	-15.9	115.2	[63]
	$C_3H_3 + C_3H_3 \rightleftharpoons C_6H_6$	1.20E+32	-7.4	21.2	[63]
33	$C_4H_5C_2H \rightleftharpoons$ fulvene	2.34E+56	-12.6	361.5	[63][b]
34	$C_4H_5C_2H \rightleftharpoons C_6H_6$	1.62E+53	-11.3	419.3	[63][b]
35	$C_4H_5C_2H \rightleftharpoons C_6H_5 + H$	4.17E+77	-17.7	558.7	[63][b]
36	fulvene $\rightleftharpoons C_6H_6$	1.45E+45	-8.9	405.9	[63][b]
37	fulvene $\rightleftharpoons C_6H_5 + H$	2.24E+68	-14.7	596.5	[63][b]
38	$C_6H_6 \rightleftharpoons C_6H_5 + H$	6.31E+60	-12.4	619.5	[63][b]
	Updated C$_3$ Chemistry				
39	$C_3H_3 + OH \rightleftharpoons C_2H_3 + HCO$	5.00E+10	0.0	0.0	[63]
40	$C_3H_3 + OH \rightleftharpoons C_2H_4 + CO$	3.00E+10	0.0	0.0	[63]
41	$C_3H_4(A) + H \rightleftharpoons C_3H_5(A)$	4.67E+48	-11.5	89.3	[63][b]
41	$C_3H_4(A) + H \rightleftharpoons C_3H_5(A)$	3.32E+30	-5.8	89.3	[63][b]
42	$C_3H_4(P) + H \rightleftharpoons C_2H_2 + CH_3$	4.26E+07	1.0	28.9	[63]
43	$C_3H_5(A) + H \rightleftharpoons C_3H_6$	2.29E+10	0	0.20	[65]
44	$C_5H_6 + C_3H_5(A) \rightleftharpoons C_5H_5 + C_3H_6$	1.00E-05	4.0	0	[4][a]
45	$C_3H_6 + H \rightleftharpoons C_2H_4 + CH_3$	2.60E+05	1.50	8.36	[80]
	Linkage of C$_5$ and C$_6$ Rings				
46	$C_5H_5 + CH_3 \rightleftharpoons C_5H_4CH_3 + H$	2.00E+10	0	26.0	[6, 31]
47	$C_5H_4CH_3 \rightleftharpoons$ fulvene + H	1.00E+14	0	217	[6, 31]
48	fulvene + H $\rightleftharpoons C_6H_6 + H$	3.00E+09	0.50	8.37	[36]
	MSA and PAH Formation Steps				
49	$C_5H_5 + C_5H_5 \rightleftharpoons C_5H_5\text{-}C_5H_4 + H$	2.50E+09	0	34.7	[5][a]
50	$C_5H_5\text{-}C_5H_4 \rightleftharpoons C_{10}H_8 + H$	3.00E+13	0	197.0	[5]
51	$C_5H_5 + C_5H_5 \rightleftharpoons$ 9-H-fulvalenyl + H	—	—	—	[37][c]
52	9-H-fulvalenyl $\rightleftharpoons C_{10}H_8 + H$	4.53E+05	1.83	150.1	[37]
53	$C_5H_5 + C_5H_5 \rightleftharpoons C_9H_7 + CH_3$	2.50E+09	0	40.0	est.[d]
54	$C_5H_5 + C_3H_3 \rightleftharpoons C_8H_8$	1.00E+10	0	34.7	est.
55	$C_5H_6 + CH_3 \rightleftharpoons C_5H_5 + CH_4$	1.00E-04	4.0	0	[4][a]
56	$C_5H_5 + C_2H_2 \rightleftharpoons$ c-C_7H_7	2.20E+08	0	53.54	[33]
57	c-$C_7H_7 + C_2H_2 \rightleftharpoons C_9H_8 + H$	6.60E+08	0	83.81	[33]
58	c-$C_7H_7 + H \rightleftharpoons C_7H_7 + H$	2.20E+60	-13.0	245.3	[33]
59	c-$C_7H_7 + H \rightleftharpoons C_6H_5 + CH_3$	1.20E+58	-12.4	238.5	[33]
	Cyclopentadienone Decomposition Steps				
60	$C_5H_4O \rightleftharpoons C_4H_4 + CO$	1.00E+12	0	221.8	[13]
61	$C_5H_4O \rightleftharpoons C_2H_2 + C_2H_2 + CO$	6.20E+41	-7.87	413.0	[11][b]

[a]Value adjusted as part of previous (23) or current work (44, 49, 55).

[b]Value at 1 atm.

[c]Reaction step outlined [37] with rate determination in progress.

[d]Estimated global step providing a pathway to the indene/indenyl system.

46

Table 8: Experimental and modelling conditions for cyclopentadiene oxidation [1, 2]. Fuel and oxygen refer to the initial fuel concentration and ϕ the stoichiometry of the mixture.

Case	ϕ	T (K)	Fuel (ppm)	Oxygen (ppm)
1	1.03	1198	2243	14128
2	1.03	1148	1051	6618
3	1.61	1153	2070	8263
4	0.60	1150	2200	22793
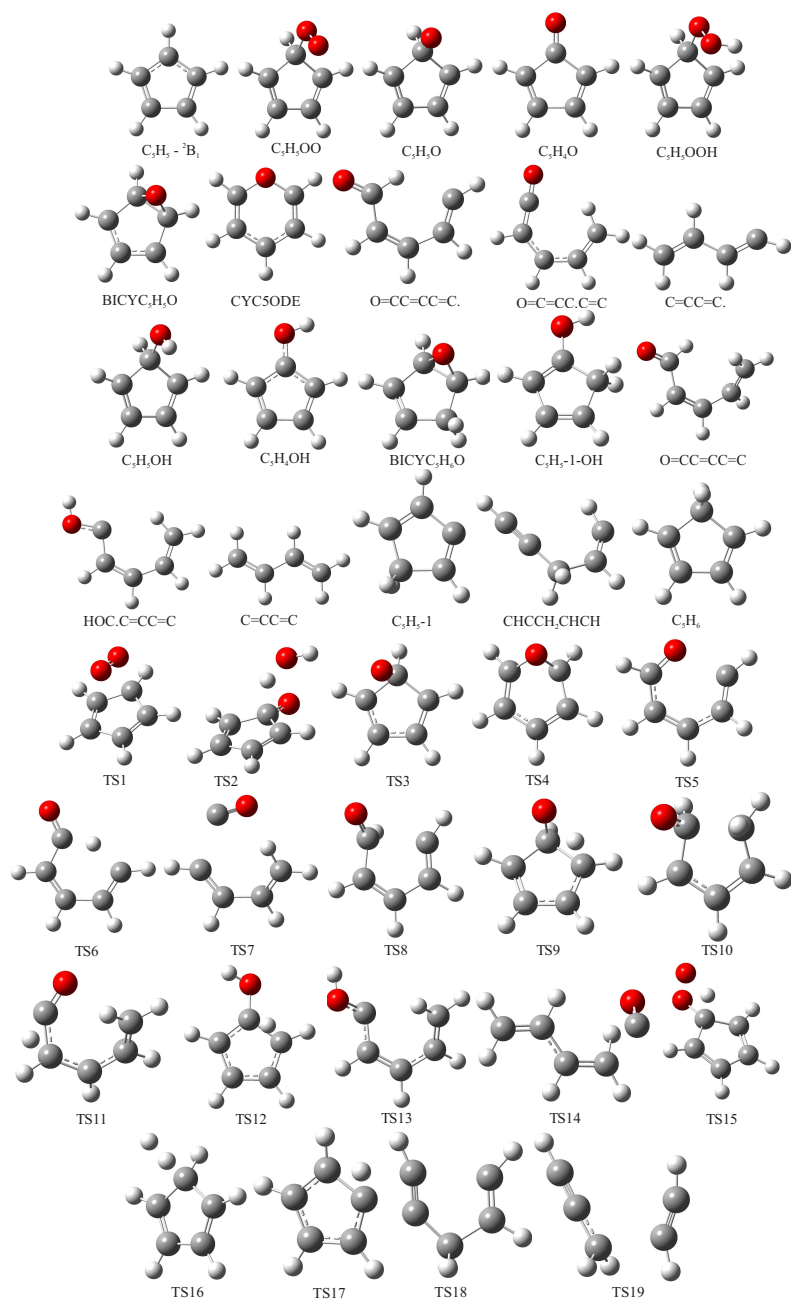
Figure 1: Molecular structures determined at the B3LYP/6-31(2df,p) level.
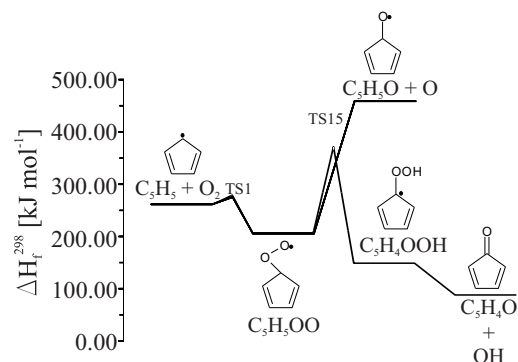
Figure 2: The potential energy surface for the reaction $C_5H_5 + O_2$ determined at the G4MP2 level with TS15 determined at the G4 level.
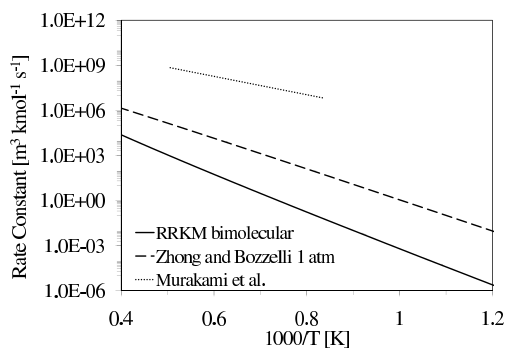
Figure 3: Rates for the bimolecular reaction (1) $C_5H_5 + O_2 \rightleftharpoons C_5H_5O + O$ calculated over the range $833 \leq T \ [K] \leq 2500$. The rate determinations by Zhong and Bozzelli [4] and Murakami et al. [7] are also shown.

49
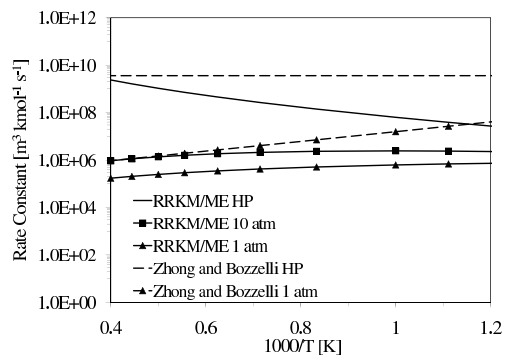
Figure 4: Rates for the reaction (2) $C_5H_5 + O_2 \rightleftharpoons C_5H_5OO$ calculated at P = 1 atm, 10 atm and the high pressure limit over the range $833 \leq T$ [K] ≤ 2500. The rate determinations by Zhong and Bozzelli [4] are also shown.
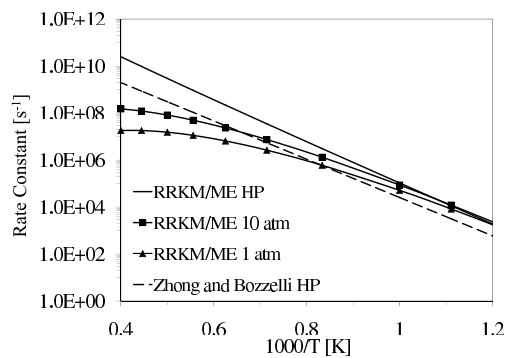
Figure 5: Rates for the reaction (3) $C_5H_5OO \rightleftharpoons C_5H_4O + OH$ calculated at P = 1 atm, 10 atm and the high pressure limit over the range $833 \leq T$ [K] ≤ 2500. The high pressure rate determination by Zhong and Bozzelli [4] is also shown.
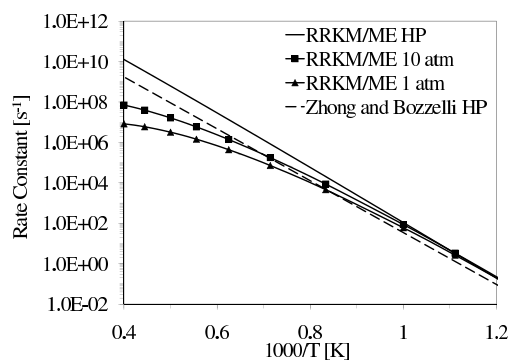
Figure 6: Rates for the reaction (4) $C_5H_5OO \rightleftharpoons C_5H_5O + O$ calculated at P = 1 atm, 10 atm and the high pressure limit over the range $833 \leq T$ [K] ≤ 2500. The high pressure rate determination by Zhong and Bozzelli [4] is also shown.
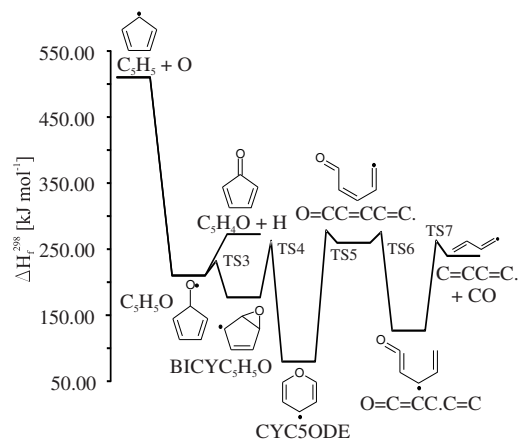
Figure 7: The potential energy surface for the reaction $C_5H_5 + O$ determined at the G4MP2 level.

51
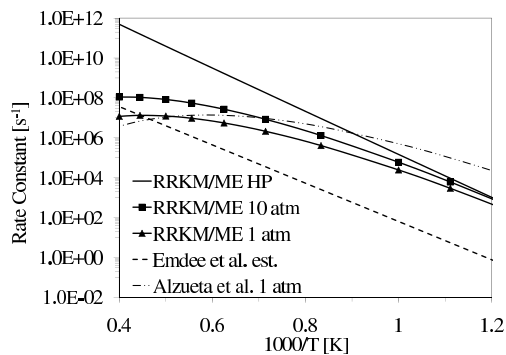
Figure 8: Rates for the reaction (5) $C_5H_5O \rightleftharpoons$ C=CC=C. + CO calculated at P = 1 atm, 10 atm and the high pressure limit over the range $833 \leq$ T [K] ≤ 2500. The rate estimations by Emdee et al. [3] and Alzueta et al. [9] are also shown.
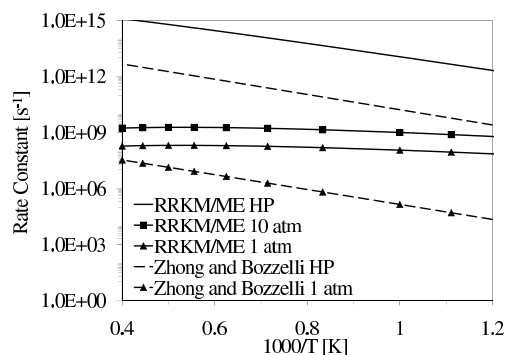
Figure 9: Rates for reaction (6) $C_5H_5O \rightleftharpoons C_5H_4O$ + H calculated at P = 1 atm, 10 atm and the high pressure limit over the range $833 \leq$ T [K] ≤ 2500. The high and low pressure rates from Zhong and Bozzelli [4] are also shown.

52
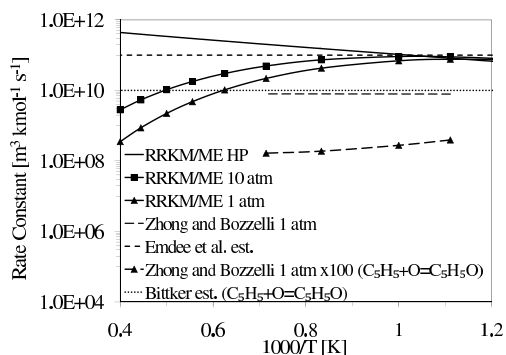
Figure 10: Rates for the reaction (7) $C_5H_5 + O \rightleftharpoons$ products calculated at P = 1 atm, 10 atm and the high pressure limit over the range $833 \leq T [K] \leq 2500$. The rate determinations by Emdee et al. [3] and Zhong and Bozzelli [4] for the formation of $C=CC=C. + CO$ are shown along with the rates of Zhong and Bozzelli [4] and Bittker [58] leading to stabilisation.
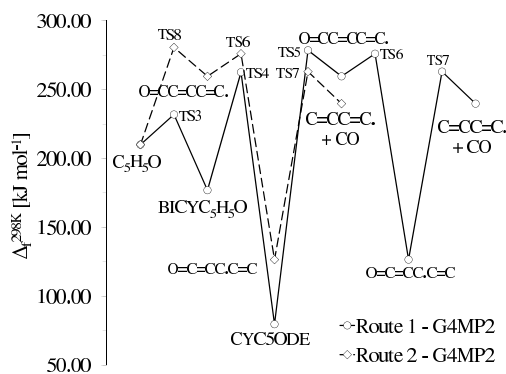
Figure 11: Possible pathways for reaction (10), $C_5H_5O \rightleftharpoons C=CC=C. + CO$.

53
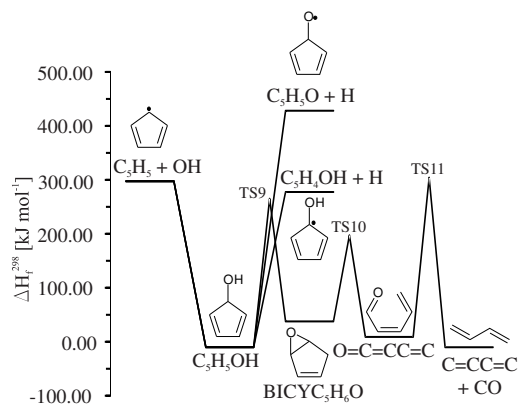
Figure 12: The potential energy surface for the reaction $C_5H_5 + OH$ determined at the G4MP2 level.
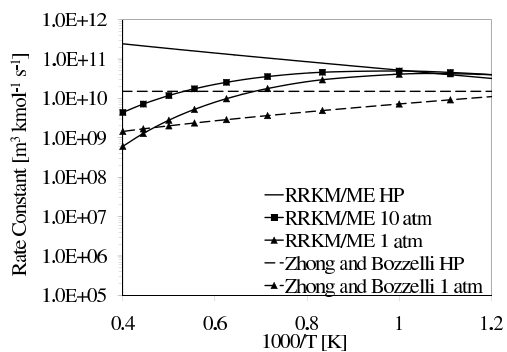
Figure 13: Rates for the reaction (12) $C_5H_5 + OH \rightleftharpoons C_5H_5OH$ calculated at P = 1 atm, 10 atm and the high pressure limit over the range $833 \leq T \text{ [K]} \leq 2500$. The rate determinations by Zhong and Bozzelli [4] are also shown.

54
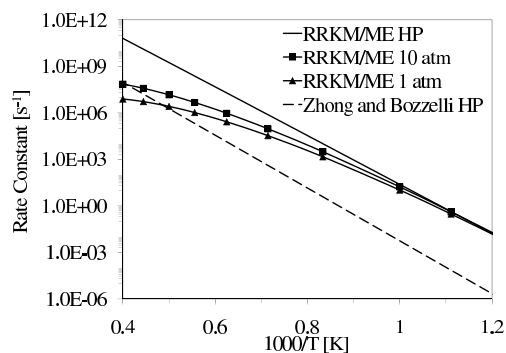
Figure 14: Rates for the reaction (13) $C_5H_5OH \rightleftharpoons C_5H_4OH + H$ calculated at P = 1 atm, 10 atm and the high pressure limit over the range $833 \leq T [K] \leq 2500$. The high pressure rate determination by Zhong and Bozzelli [4] is also shown.
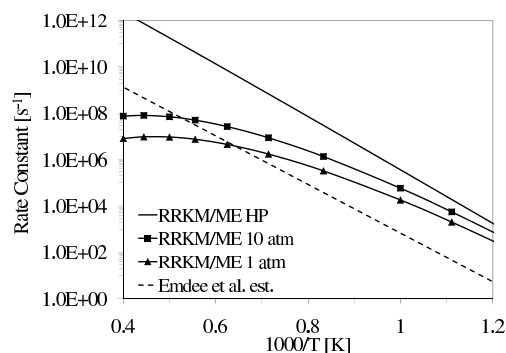
Figure 15: Rates for the reaction (15) $C_5H_4OH \rightleftharpoons C_5H_4O + H$ calculated at P = 1 atm, 10 atm and the high pressure limit over the range $833 \leq T [K] \leq 2500$. The rate determination by Emdee et al. [3] is also shown.
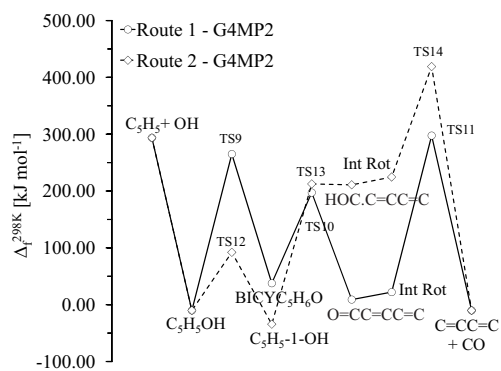
Figure 16: Possible pathways for reaction (18), $C_5H_5 + OH \rightleftharpoons C=CC=C + CO$.
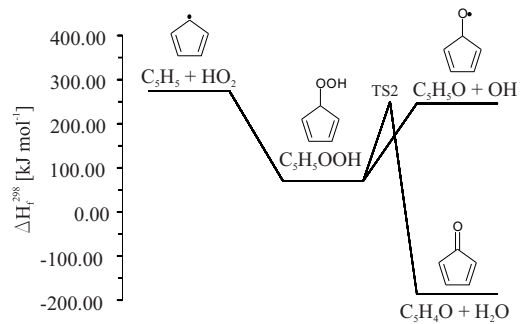
Figure 17: The potential energy surface for the reaction $C_5H_5 + HO_2$ determined at the G4MP2 level.
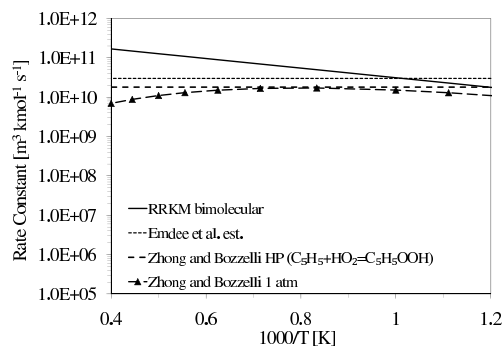
Figure 18: Rates for the bimolecular reaction (19) $C_5H_5 + HO_2 \rightleftharpoons C_5H_5O + OH$ calculated at the high pressure limit over the range $833 \leq T \ [K] \leq 2500$. The rate determinations by Zhong and Bozzelli [4] and Emdee et al. [3] are also shown.
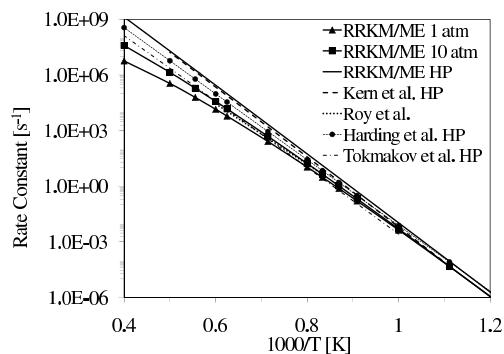
Figure 19: Rates for the reaction (21) $C_5H_6 \rightleftharpoons C_5H_5 + H$ calculated over the range $833 \leq T \ [K] \leq 2500$. The rate determinations by Kern et al. [21], Roy et al. [20], Harding et al. [23] for the $^2A_2$ symmetry and Tokmakov et al. [48] are compared with the current results.
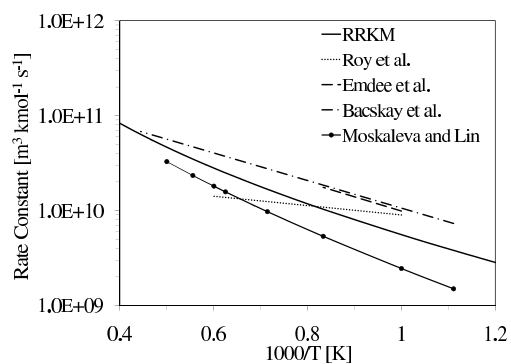
Figure 20: Rates for the bimolecular reaction (22) $C_5H_6 + H \rightleftharpoons C_5H_5 + H_2$ calculated at the high pressure limit over the range $833 \leq T$ [K] ≤ 2500. The rate determinations by Roy et al. [81], Emdee et al. [3], Bacskay et al. [26] and Moskaleva and Lin [27] are compared with the current results.
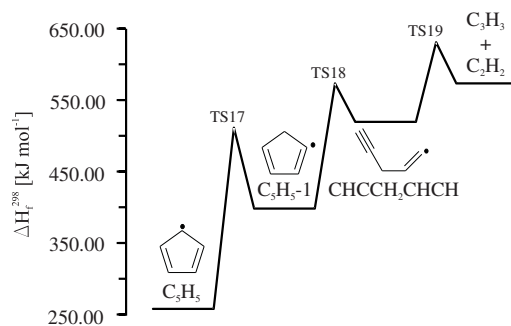
Figure 21: Simplified PES for reaction (25) $C_5H_5 \rightleftharpoons C_3H_3 + C_2H_2$ with energies determined at the G4 level.

58
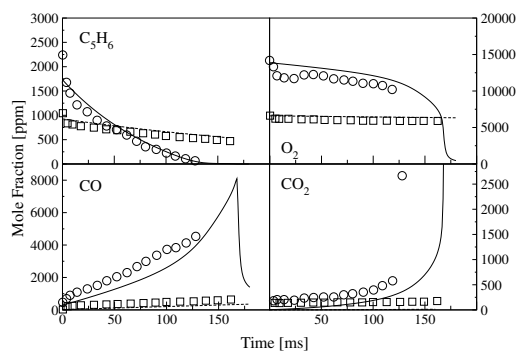
Figure 22: Concentration profiles during cyclopentadiene oxidation in a plug flow reactor at atmospheric pressure: Case 1, see Table 8, shown with solid line and open circles; Case 2 shown with dashed line and open squares. All computations time-shifted by 20 ms. Symbols are measurements from Butler [1] and Butler and Glassman [2].
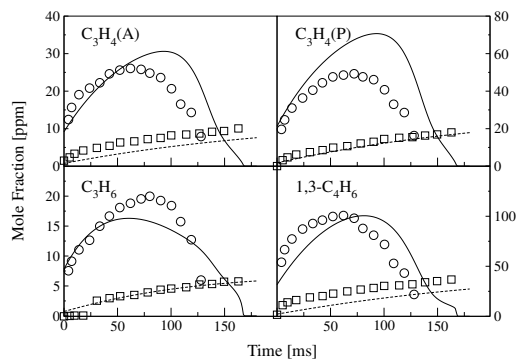
Figure 23: Concentration profiles during cyclopentadiene oxidation in a plug flow reactor at atmospheric pressure: Case 1, see Table 8, shown with solid line and open circles; Case 2 shown with dashed line and open squares. All computations time-shifted by 20 ms. Symbols are measurements from Butler [1] and Butler and Glassman [2].

59
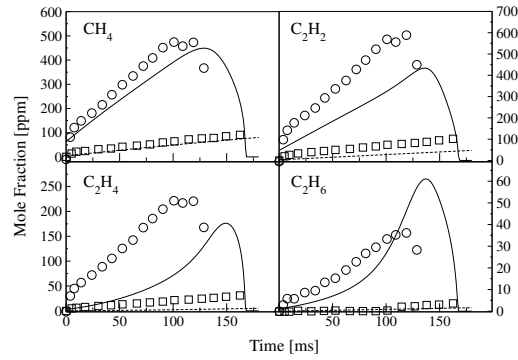
Figure 24: Concentration profiles during cyclopentadiene oxidation in a plug flow reactor at atmospheric pressure: Case 1, see Table 8, shown with solid line and open circles; Case 2 shown with dashed line and open squares. All computations time-shifted by 20 ms. Symbols are measurements from Butler [1] and Butler and Glassman [2].
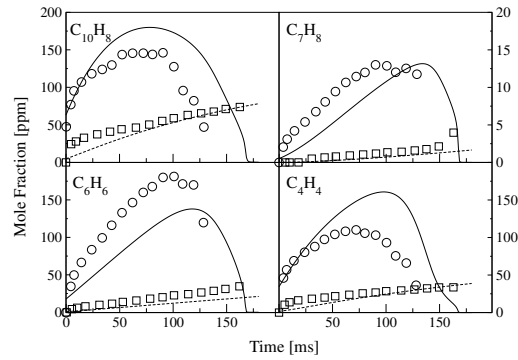
Figure 25: Concentration profiles during cyclopentadiene oxidation in a plug flow reactor at atmospheric pressure: Case 1, see Table 8, shown with solid line and open circles; Case 2 shown with dashed line and open squares. All computations time-shifted by 20 ms. Symbols are measurements from Butler [1] and Butler and Glassman [2].

60
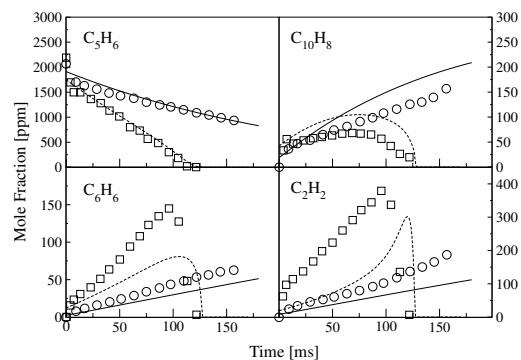
Figure 26: Concentration profiles during lean and rich cyclopentadiene oxidation in a plug flow reactor at atmospheric pressure: Case 3, see Table 8, shown with solid line and open circles; Case 4 is shown with dashed line and open squares. The computations for Case 3 time-shifted by 20 ms and Case 4 by 30 ms. Symbols are measurements from Butler [1] and Butler and Glassman [2].
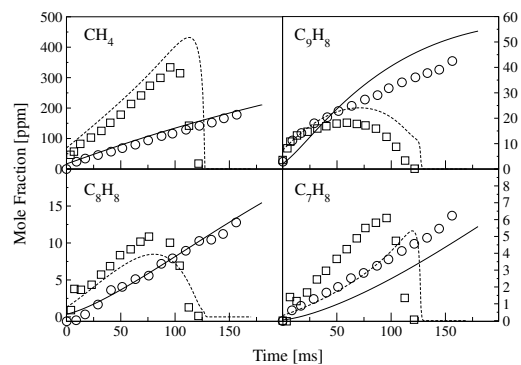
Figure 27: Concentration profiles during lean and rich cyclopentadiene oxidation in a plug flow reactor at atmospheric pressure: Case 3, see Table 8, shown with solid line and open circles; Case 4 shown with dashed line and open squares. The computations for Case 3 time-shifted by 20 ms and Case 4 by 30 ms. Symbols are measurements from Butler [1] and Butler and Glassman [2].

61
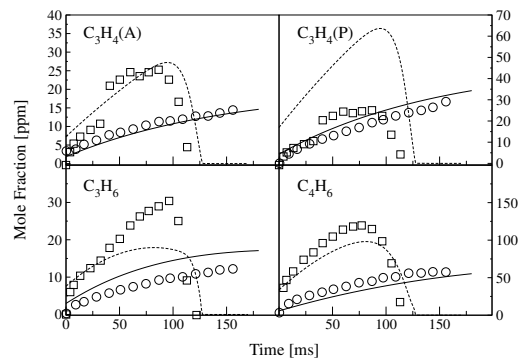
Figure 28: Concentration profiles during lean and rich cyclopentadiene oxidation in a plug flow reactor at atmospheric pressure: Case 3, see Table 8, shown with solid line and open circles; Case 4 shown with dashed line and open squares. The computations for Case 3 time-shifted by 20 ms and Case 4 by 30 ms. Symbols are measurements from Butler [1] and Butler and Glassman [2].

62

Appendix 2: Summary of Work on the n-Propyl Benzene System

Hydrogen abstraction reactions from n-propyl benzene

R.K. Robinson[a], R. P. Lindstedt[a,*]

[a]*Department of Mechanical Engineering, Imperial College London, South Kensington Campus, London, SW7 2BX, UK*

Abstract

Aromatics form an integral part of typical aviation fuels with n-propyl benzene (nPB) selected as a representative molecule for inclusion in EU and US surrogate blends. Despite the practical relevance of such fuel molecules, kinetic and thermodynamic data, obtained using comparatively accurate *ab initio* methods (e.g. quantum mechanical methods combined with transition state theory), have not to date been compared with currently used reaction class based estimates. The use of *ab initio* methods for comparatively complex molecules also requires an assessment of the relative benefits of higher levels of theory as it is typically necessary to balance a desire to understand individual reactions with the need to consider more complete reaction sequences. The current study explores the issue by examining six hydrogen extractions via the hydrogen or methyl radicals from the n-propyl side chain. Potential energy surfaces (PES) were determined using 10 different approaches, including state-of-the-art DFT (M06, M06-2X and M08-SO) and contemporary composite methods (G4, G4MP2, CBS-QB3 and CBS-4M). Results are presented relative to data obtained using the coupled cluster CCSD(T)/aug-cc-pVDZ//M06-2X/6-311++G(3df,3pd) method. Rate parameters were determined using transition state theory (TST) with small curvature tunnelling (SCT) combined with energetics obtained at (i) the M06-2X/6-31G(2df,p) and (ii) the CCSD(T)/aug-cc-pVDZ levels. Results were found to agree comparatively well with differences in barrier heights less than 8 kJ/mol, resulting in comparatively modest differences in reaction rates. By contrast, substantial deviations can arise with respect to reaction class based estimation techniques.

1. Introduction

Aromatics can be found in most petroleum based fuels and their kinetics need to be understood due to performance and toxicity considerations. The wide variety of side-chains necessitates the use of model fuel components that

---

*Corresponding author. Fax: +44 20 7589 3905.
  Email address: `p.lindstedt@imperial.ac.uk` (R. P. Lindstedt)

are capable of reproducing selected aspects of the performance of the real fuel, as outlined by Colket *et al.* [1, 2], with n-propyl benzene (nPB) selected as a target compound by several working groups. Dagaut *et al.* [3] addressed the kinetics of nPB combustion following a similar EU based evaluation with more recent studies presented by Wang *et al.* [4] and Brezinsky and Gudiyella [5]. The study by Dagaut *et al.* [3] featured an experimental investigation using a jet-stirred reactor with temperatures in the range 900 – 1250 K and concentration profiles of 23 species were measured by probe sampling. A detailed kinetic model for the oxidation of nPB was developed using estimates based on (i) the rules of Dean *et al.* [6], (ii) the corresponding reactions for toluene/propane/alkyl radicals and (iii) the rules proposed by Walker [7]. Brezinsky *et al.* [5] studied the high pressure oxidation of nPB in a shock tube and constructed a detailed chemical mechanism based on the work by Dagaut *et al.* [3], while noting the scarcity of detailed studies of the chemistry of nPB. The current study accordingly considers six hydrogen extractions from nPB initiated via hydrogen or methyl radicals.

$$C_9H_{12} + H \rightleftharpoons C_9H_{11} - 1 + H_2 \tag{1}$$

$$C_9H_{12} + H \rightleftharpoons C_9H_{11} - 2 + H_2 \tag{2}$$

$$C_9H_{12} + H \rightleftharpoons C_9H_{11} - 3 + H_2 \tag{3}$$

$$C_9H_{12} + CH_3 \rightleftharpoons C_9H_{11} - 1 + CH_4 \tag{4}$$

$$C_9H_{12} + CH_3 \rightleftharpoons C_9H_{11} - 2 + CH_4 \tag{5}$$

$$C_9H_{12} + CH_3 \rightleftharpoons C_9H_{11} - 3 + CH_4 \tag{6}$$
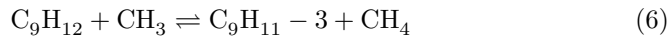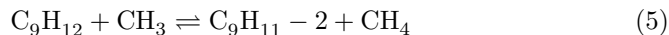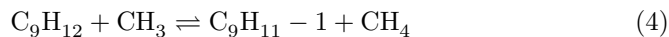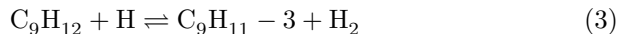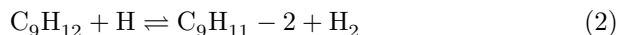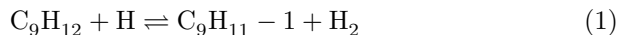
All six reactions have a clear transition state and provide a suitable basis for exploring the relative accuracy of different *ab initio* methods for a more complex fuel molecule of practical relevance. Zheng *et al.* [8] highlighted inaccuracies in calculated transition state energies associated with older G2/G3 based composite methods and found a tendency to underestimate barrier heights. However, recent studies [9] have suggested that the G4 methodology estimates barrier

2

heights with greater accuracy than the earlier composite methods. The matter is further explored here by computing barrier heights using a wide variety of composite, Density Functional Theory (DFT) and coupled cluster (CC) methods. The M05, M06, M08 line of DFT functionals produce improved barrier heights compared with older DFT methods [10–16]. The functionals were developed and designed such that they are broadly applicable to organometallic, inorganometallic and nonmetallic bonding, as well as thermochemistry, thermochemical kinetics and non-covalent interactions [10]. Previous studies have assessed barrier heights determined from various quantum mechanical methods and hence their applicability to reaction kinetics. It has been suggested that the M08 functionals [14] are particularly favoured. Zhao and Truhlar [15] found M08-SO to be the best performing DFT functional for organic hydrogen transfer isomerisations and Zhao et al. [16], covering 21 rearrangement reaction energies and 13 dissociation/association energies, found M08-SO to be the best performing DFT functional of the 30 tested.

The M05 [11, 12] functional is based on a parameter optimisation using a genetic algorithm to minimize the error of 35 data in the training function. Atomisation energies, ionisation potentials, electron affinities, forward and reverse barrier heights and energies of reaction of both organics and organometallics were included. The functional was assessed on a larger test set of 231 data points covering the above categories with particular emphasis on 38 chemical barrier heights that included hydrogen atom transfers. The functional performed well across the four categories of interactions listed above, but did not stand out from other functionals in any individual category. The M05-2X [11, 12] functional was only parametrized for non-metals using a training set of 34 data with 9 databases used as test sets. Thermochemical kinetics were tested on 19 reactions of which 18 involved radicals given that reactions with an odd number of electrons form an important test for DFT. It has been shown that functionals that correctly estimate energetics for hydrogen transfers also work well for other reaction families [17]. The observation suggests increasing confidence in the general applicability of the method. For the thermochemical test set, M05-

3

2X gave an average mean unsigned error (AMUE) of 4.1 kJ mol^{-1} compared to 4.7 kJ mol^{-1} for BMK and 12.9 kJ mol^{-1} for B3LYP.

The subsequent series includes the M06, M06-L, M06-HX [13] and M06-2X [13] functionals. The M06 functional is recommended for applications in organometallic and inorganometallic chemistry with M06-2X is recommended for systems involving main-group thermochemistry and kinetics. The combined tests gave an AMUE of 4.4 kJ mol^{-1} for the M06-2X functional compared to 5.4 kJ mol^{-1} for BMK, 5.6 kJ mol^{-1} for M05-2X and 12.9 kJ mol^{-1} for B3LYP. The reported values suggest that the M06-2X functional calculates reaction barriers for hydrogen exchange reactions with comparatively good accuracy while retaining the computational efficiency of DFT. The M08 functionals were trained with a larger set of 267 data, while the test set consisted of another 250 values. Overall the M08-HX [14] was deemed to be the most accurate functional from this generation and was found to perform well for main-group atomization energies, large-molecule atomization energies, electron affinities, hydrogen-transfer barrier heights and heavy-atom transfer barrier heights. However, it was also concluded that M08-SO [14] is more accurate for main-group thermochemistry.

The current work investigates hydrogen transfers in the nPB system using the modern DFT functionals M06, M06-2X, M08-SO and B3LYP [18, 19], the latest composite methods including G4 [20], G4MP2 [21], CBS-4M [22] along with CBS-QB3 [23] and, finally, a high level coupled cluster CCSD(T) [24] calculation. Selected basis sets include 6-31G(2df,p), 6-311++G(3df,3dp) and the augmented double zeta basis set (aug-cc-pVDZ). Coupled cluster (CC) calculations were carried out with the largest basis set (aug-cc-pVDZ) currently achievable for a molecule of this size. Comparisons [25] suggest that the larger augmented triple zeta basis set (aug-cc-pVTZ) would require approximately 42 times the computational effort and the non-augmented basis set (cc-pVTZ) 5 times. Such timings and the size of the resulting I/O requirements moved these calculations beyond current computational resources. Results were therefore subsequently compared relative to the CCSD(T)/aug-cc-pVDZ//M06-2X/6-311++G(3df,3pd) values with the geometries and Zero Point

4

Energy (ZPE) taken from the M06-2X functional to define the most accurate methodology applied. From the resulting findings, representative approaches for the determination of the potential energy surfaces (PES) were selected. The procedure outlined by Robinson and Lindstedt [26] was used for calculating thermochemistry with energetics determined from the composite G4 method [20]. Transition State Theory (TST) and Canonical Variational Transition State Theory (CVT) [27], incorporating small curvature tunnelling (SCT) [28, 29], were also applied via approach of Zheng *et al.* [30] using the most appropriate DFT approach given the calculated barrier heights. The selected reactions are bimolecular with a pronounced barrier, it is expected that the variational character will be minimal and the CVT calculations were performed to confirm the non-variational result. The current work extends past studies of the chemistry of substituted aromatics by (i) considering six hydrogen abstraction reactions from nPB, (ii) comparing the reaction energetics obtained using a wide variety of computational methods and (iii) by computing reaction rate parameters using TST based methods.

2. Computational Methods

Calculations were performed using Gaussian 09 [31] and prior to the main computations molecules were subjected to a lower level minimisation to determine basic configurations. If a molecule was found to have many torsion angles, or if the structure appeared to be strained, a conformational analysis was performed. Subsequently, DFT calculations, with the B3LYP functional and 6-31G(2df,p) basis set were used to locate stationary points along the PES. Vibrational frequency calculations were performed at the same level of theory to identify the latter as either transition states, having one imaginary frequency, or minima with no imaginary frequencies. For the energy comparisons, geometries were further optimised at the relevant level of theory and M06-2X/6-311++G(3df,3pd) geometries used for higher level calculations.

Two possible nPB geometries (C_9H_{12} and $C_9H_{12}b$) were considered as shown

in Fig. 1. Both geometries were optimised and local minima found. Energies for the structures were calculated at several levels, including G4, and in each instance the C_9H_{12} geometry proved to be the global minimum. However, the energies were very similar. For example, at the G4 level, heats of formation at 0 K were 40.16 kJ mol^{-1} for C_9H_{12} and 40.25 kJ mol^{-1} for C_9H_{12}b. Similar geometries can also be expected for some of the radical species, e.g. C_9H_{11} and C_9H_{11}b, as also shown. Optimisations were started from both geometries and no local minimum was found for C_9H_{11}b with the calculation proceeding straight to the C_9H_{11}-1 geometry. For C_9H_{11}-2 it was found, as expected, that an out of plane geometry is favoured, while for C_9H_{11}-3 an in–plane geometry was observed. The M08-SO calculations were carried using the August 2011 release of General Atomic and Molecular Electronic Structure System (GAMESS) [32, 33]. The default integration grid for Gaussian 09 has 75 radial shells and 302 angular points per shell, resulting in about 7000 points per atom [34]. Therefore for each GAMESS calculation the grid was set up in the same manner to produce consistent results. This version of GAMESS does not include the case of one-electron systems for the Minnesota functionals and this was corrected prior to the the energy calculation of the hydrogen radical.

Intrinsic reaction coordinate (IRC) calculations were carried out starting from each transition state in order to link reactants and products. The calculations were allowed to follow the energy profile in both directions from the maxima, the number/size of steps were optimized for each calculation to allow enough movement to identify the reactants and products and to confirm that the correct transition state had been located. The resulting structures were then used as the basis for higher accuracy calculations to provide more precise energy data. The transition state structures are shown in Fig. 1.

2.1. Thermochemistry of Stable Species and Radicals

Thermochemical data was also produced alongside the kinetic parameters. G4 energetics were used as this method has an agreeable record for calculat-

6

ing accurate energies for non-transition state species [20]. Included for completeness is a short description of the G4 composite method. Starting with a geometry optimisation at the B3LYP/6-31G(2df,p) level to obtain the equilibrium structure, the harmonic frequencies are scaled by a correction factor of 0.9854 to account for known deficiencies [35]. Durant and Rohlfing [36] reported that B3LYP density functional methods provide improved geometries and vibrational frequencies in comparison to MP2 and Hartree-Fock *ab initio* used in older composite methods such as G1, G2 and G3. The frequencies are then used to calculate the ZPE. Also in contrast to previous G series composite methods, the Hartree–Fock energy limit is calculated and a series of single point energy calculations are carried out at various levels of theory (MP2/6-31G(d), MP2/6-31G(2df,p) and MP2(full)/G3MP2LargeXP, MP4/6-31G(d), MP4/6-31G(2df,p) and CCSD(T)/6-31G(d)). The resulting energies are combined and a higher-level correction obtained by taking into account remaining deficiencies. The total energy is obtained by adding the previously calculated ZPE.

The calculation of the contributions to the thermochemistry from hindered internal rotors using vibrational frequencies can lead to considerable inaccuracies. Therefore rotors were investigated in more detail for the relevant species. Each molecule underwent a series of scans in which internal rotors were rotated though $360\,^\circ$ in $15\,^\circ$ steps. At each step, the molecular structure was optimised and the energy of the molecule calculated at the B3LYP/6-31G(2df,p) level. The final potential was fitted to a six term series (see below). The method for treating (hindered) internal rotations is based on the diagonalization of the one-dimensional Hamiltonian and has been described by Lewis *et al.* [37]. The method features the summation of energy levels for each rotor using a six term (n = 6) expansion of the type $V = \frac{1}{2}\Sigma V_n(1 - cos(n\Theta))$. The technique is consistent with the active thermodynamic tables of Argonne National Laboratory (e.g. Burcat and Rusic [38]) and is also used in the the NIST–JANAF Thermochemical Tables (e.g. Dorofeeva et al. [39]). Vibrational frequencies, enthalpies of formation, moments of inertia and molecular symmetry numbers were extracted

7

and, if required, data for low frequency vibrations were omitted and modelled as hindered internal rotors. The NASA statistical mechanics program Properties and Coefficients (PAC) 99 [40] was then used with the rigid rotor harmonic oscillator approximation to calculate thermodynamic data for enthalpy, heat capacity, entropy and Gibbs free energy. The resulting data was fitted to the standard 7 term JANAF polynomial form covering the range 200 K to 6000 K with the enthalpy at 298 K anchored to the G4 value. Thermochemical data for selected species are shown in Table 1 with molecular properties of the species and transition states at the M06-2X level given in Tables 2 and 3.

2.2. Thermochemistry of Reaction Barriers

The fundamental importance of correctly estimating the barrier height in determining kinetic parameters is well known. Past studies have highlighted [8] the inaccuracies of older composite methods, such as G2 and G3, in calculating barrier heights. Errors similar to some DFT based calculations can be found with a tendency to underestimate barrier heights. In order to explore the matter further for the current practical surrogate fuel molecule (nPB), energies were calculated using a wide variety of quantum mechanical methods and basis sets. Forward and reverse barrier heights for all six reactions are shown in Tables 4 to 9 with energies compared to the CCSD(T)/aug-cc-pVDZ//M06-2X/6-311++G(3df,3pd) (CC) method. For each nPB hydrogen extraction reaction, the deviations of the methods were compared to the CC calculation with results found to differ somewhat. However, some general trends can be observed. As expected, the B3LYP functional, used to find the initial geometries, consistently produced lower barrier heights. The M06-2X functional was arguably the best performing DFT method and provided the closest match to the CC result for five of the six reactions. Generally, the composite methods returned values somewhere between the extremes of B3LYP and M06-2X, with G4MP2 generally providing comparatively low forward barriers with the CBS methodologies (CBS-4M and CBS-QB3) giving more consistent results.

For reaction (1) the CCSD(T)/aug-cc-pVDZ//M06-2X/6-311++G(3df,3pd) level of theory calculated a forward barrier height of 43.1 kJ mol^{-1}. The latest composite method (G4) gave a value of 36.2 kJ mol^{-1}. Also, the composite methods are incompatible with several methods for calculating variational TST (VTST) based rates, necessary for more complicated PES, and CC methods are computationally very demanding for molecules the size of nPB. Among the DFT calculations, the M06-2X/6-31G(2df,p) method resulted in a barrier of 45.1 kJ mol^{-1} – similar to the CC method. The more general method, M06/6-31G(2df,p), gave a barrier of 39.6 kJ mol^{-1}, as shown in Table 4, with the M08-SO functional suggesting a barriers more distant from the CC method than the M06 values. Reaction (2) showed a similar trend with CCSD(T)/aug-cc-pVDZ//M06-2X/6-311++G(3df,3pd) producing a barrier of 34.0 kJ mol^{-1}, while the G4 method resulted in a barrier of 25.1 kJ mol^{-1}. The M06-2X functional with the 6-31G(2df,p) basis set gave an almost exact match for the CC calculation at 33.9 kJ mol^{-1}. Again the M08-SO functional showed a larger deviation with a forward barrier of 35.9 kJ mol^{-1}. For reaction (3) the M08-SO functional showed a deviation of only 1.3 kJ mol^{-1} from the CC findings with the M06-2X functional also close.

Reactions (4), (5) and (6) (see Tables 7, 8 and 9) considered H extraction via the methyl radical. For reaction (4) the CCSD(T)/aug-cc-pVDZ//M06-2X/6-311++G(3df,3pd) and G4 methods resulted in forward barriers of 58.3 kJ mol^{-1} and 52.6 kJ mol^{-1} respectively. For this case, the M06-2X/6-31G(2df,p) level of theory produced a barrier 52.0 kJ mol^{-1}. For all the methyl reactions the M08-SO functional produced forward barriers very close to the CC method. However, the reverse barriers were found to be less well correlated. For reaction (6) the M06-2X functional with the 6-311++G(3df,3pd) basis set gave the best overall match for the forward and reverse barriers. The M06-2X/6-31G(2df,p) method was hence considered a potentially good compromise between speed and accuracy for the kinetics calculations. Barriers for all six reactions at the M08-SO/6-31G(2df,p) and M06-2X/6-31G(2df,p) levels are compared to the CC calculations in Table 10. The DFT functionals provide a similar overall accuracy

9

for the forward barriers with the M06-2X functional arguably more consisted for the reverse barriers. For the CH_3 reactions (3), (5) and (6) the M06-2X forward barriers deviated by -6.3 kJ mol^{-1}, -3.8 kJ mol^{-1} and -6.9 kJ mol^{-1} from the CCSD(T)/aug-cc-pVDZ//M06-2X/6-311++G(3df,3pd) values. The deviation of -6.9 kJ mol^{-1} for reaction (6) is of particular concern with the barrier obtained by the M08-SO functional 2.8 kJ mol^{-1} closer to the CC value.

2.3. Reaction Kinetics

The equivalent nature of the hydrogen atoms sited on the nPB propyl side chain leads to easier handling of the transition states than for completely asymmetric molecules. Three transition states TS1, TS1-b and TS1-c, shown Fig. 1, are all capable of extracting a hydrogen to proceed to C_9H_{11}-1. At 0 K, TS1 has an enthalpy of formation of 292.3 kJ mol^{-1}, TS1b 291.2 kJ mol^{-1} and TS1c 291.2 kJ mol^{-1}. The transition states are similar enough to be treated as effectively identical. Therefore the extraction of a hydrogen from the terminal carbon via reactions (1) and (4) were considered to have a reaction degeneracy of 3. Likewise reactions (2), (3), (5) and (6) will each have 2 equivalent transition states and therefore were treated with a reaction degeneracy of 2. For the methyl extractions, it was assumed that the CH_3 group can rotate freely perpendicular to the axis of the reaction coordinate. Therefore it was deemed these reactions would have a further degeneracy of 2 as opposed to the methyl symmetry number of 6, as all angles of rotation in this direction were considered equivalent. The resulting total reaction degeneracy is 6 for reaction (4) and 4 for reactions (5) and (6).

It is often found that for reactions with larger barrier heights and larger imaginary frequencies tunnelling effects play a significant role. Several of the current reactions fall into this category and SCT corrections were applied where possible. For conventional TST, data is only required at the stationary points. However, the calculation of the SCT corrections requires information on the curvature. Hence, rates with the tunnelling correction were produced using the

10

M06-2X/6-31G(2df,p) level of theory and with TST rates also determined using CC stationary point energetics without tunnelling corrections.

The current reactions are expected to show little or no variational character and CVT was mainly applied to evaluate the suitability of the M06-2X functional. In the CVT calculations, data is required on the curvature of the barrier and therefore the minimum energy path (MEP) is examined in detail for many steps on each side of the stationary point. The GAUSSRATE interface [41] was used to provide direct dynamics calculations of energies, gradients and Hessians on the reaction path at the M06-2X/6-31G(2d,f) level as discussed above. The CVT rate for temperature T is expressed as,

$$k^{CVT}(T,s) = min \ k^{GT}(T,s) \tag{2}$$

where $k^{GT}(T,s)$ is the rate constant in generalised transition state theory at the dividing surface s. Calculations along the MEP were carried in both directions along the reaction coordinate (s). Steps of 0.01 Å were used and the ratio of gradients to Hessians was set to 10. To correctly calculate tunnelling corrections, data was calculated to approximately ±1.5 Å in each direction. The value was varied as required for each reaction until all turning points had been identified for the studied temperatures. All rate constants were fitted to the modified three–parameter form of the Arrhenius equation (see Eq. (3)).

$$k(T) = AT^n exp(\frac{-Ea}{RT}) \tag{3}$$

The TST/SCT and CVT/SCT results for reaction (1) are, as expected, very similar as shown in Fig. 2. A more detailed analysis shows that a 3 point fit identified the generalised transition state (TS) as located between 0.0018 and 0.0002 Å, while the 5 point fit identified the TS between 0.0015 and 0.0001 Å. Both are very close to the conventional transition state (at 0.0 Å) showing a minimal variational character. Accordingly, only TST and TST/SCT rates are discussed below.

11

3. Discussion

The results obtained for all six reactions are given in Table 11 and also shown in Figs. 3 to 8. The calculated rates obtained using TST and TST/SCT with M06-2X/6-31G(2df,p) and TST with CCSD(T)/aug-cc-pVDZ energies at stationary points are discussed below and comparisons made with alternative determinations.

Tunnelling corrections were found to be of importance especially for reactions with large barrier heights and at low temperatures. For reactions (1) and (2) the rate constants accounting for tunnelling are approximately 3.5 times quicker at 500 K, 1.5 times quicker at 900 K and the effect is not negligible until well after 1500 K. The smaller barrier height (26.7 kJ mol^{-1}) for reaction (3) limits the importance of tunnelling, but rates over 2 times greater were still found at 500 K. The effect was again noticeable for the methyl reactions, although somewhat smaller. For reactions (4) and (5) the rates accounting for tunneling were 3.5 and 2.5 times quicker. However, the effect was less than double at 700 K and of little importance after 1400 K. For reaction (6) tunnelling effects were again seen using the M06-2X functional. As outlined above, this method calculates a barrier of 32.6 kJ mol^{-1} and at the CC barrier of 40.0 kJ mol^{-1} it can be expected that tunnelling would be of somewhat greater importance.

The above determinations have been compared to the values used by Dagaut *et al.* [3] and Brezinsky and Gudiyella [5]. There are similarities between the current findings and the earlier suggestions for some of the reactions. In particular, the hydrogen extractions, reactions (1–3), show good agreement between our calculated rates and the estimates of Dagaut *et al.* [3]. For the methyl extractions, reactions (4–6), there is a much greater disparity between the three studies. Some similarity is seen between our values and Brezinsky and Gudiyella [5] at the mid to lower range of combustion temperatures (800–1200 K). Overall, it is expected that the methods used in the current study will lead to increased accuracy and confidence in kinetic models. For use in kinetic models we recommend that the TST/SCT rate constants are used. Tunnelling

12

corrections appear important and may not have been taken into account in previous studies. For reaction (6) the M06-2X functional gives a barrier considerably lower than the CC calculations. The TST rates at the CC level were determined without tunnelling corrections. However, the M06-2X results suggest that such effects can be expected to be of less importance and that more accurate kinetics for this reaction will be found by using the TST/CCSD(T)/aug-cc-pVDZ determination.

4. Conclusions

We have explored the geometries and energetics of a group of bimolecular hydrogen exchange reactions involved in the combustion of nPB. Energies from a wide selection of methods were compared with the CCSD(T)/aug-cc-pVDZ//M06-2X/6-311++G(3df,3pd) level of theory, the most accurate achievable for molecules the size of nPB. It was established that the energies produced at M06-2X/6-31G(2df,p) level provide a comparatively good match. Thermodynamic data, based on the G4 calculations, was also produced in the form of JANAF polynomials for the compounds involved. Kinetic rate data was determined for a range of temperatures using TST and TST/SCT. For the current bimolecular reactions no variational character was found and we recommend the use of the TST/SCT determination obtained at the M06-2X/6-31G(2df,p) level. However, for reaction (6), a disagreement of -6.9 kJ mol^{-1} in the barrier height, as compared to the CC calculation, has been highlighted and we therefore recommend the rate based on TST using CCSD(T)/aug-cc-pVDZ energies. Some agreement was found between our calculations and older reaction class based determinations. However, for the CH_3 based extractions significant deviations were noted. Finally, the current exercise has allowed the identification of candidate functionals and basis sets that describe the nPB system with sufficient accuracy.

13

Acknowledgements

References

[1] M. Colket, T. Edwards, S. William, N. Cernansky, D. Miller, F. Egolfopoulos, R. Lindstedt, K. Seshadri, F. Dryer, C. Law, D. Friend, D. Lenhert, H. Pitsch, A. Sarofim, M. Smooke, W. Tsang, *Development of an Experimental Database and Kinetic Models for Surrogate Jet Fuels* (2007).

[2] M. Colket, T. Edwards, S. William, N. Cernansky, D. Miller, F. Egolfopoulos, R. Lindstedt, K. Seshadri, F. Dryer, C. Law, D. Friend, D. Lenhert, H. Pitsch, A. Sarofim, M. Smooke, W. Tsang, *Identification of Target Validation Data for Development of Surrogate Jet Fuels* (2008).

[3] P. Dagaut, A. Ristori, A. E. Bakali, M. Cathonnet, *Fuel* 81 (2002) 173–184.

[4] H. Wang, M. Oehlschlaeger, S. Dooley, F. Dryer, *7th US National Technical Meeting of the Combustion Institute* (2011).

[5] S. Gudiyella, K. Brezinsky, *Combustion and Flame* 159 (2012) 940–958.

[6] A. M. Dean, *J. Phys. Chem.* 89 (1985) 4600–4620.

[7] R. W. Walker, in: R. Compton, G. Hancock (Eds.), Research in Chemical Kinetics, Blackwell Science Ltd, 2002, pp. 1–68.

[8] J. Zheng, Y. Zhao, D. G. Truhlar, *J. Chem. Theory Comput.* 77 (2009) 145 – 170.

[9] S. E. Wheeler, D. H. Ess, K. N. Houk, *J. Phys. Chem. A* 112 (2008) 1798–1807.

[10] Y. Zhao, N. E. Schultz, D. G. Truhlar, *J. Chem. Phys.* 123 (2005) 161103.

[11] Y. Zhao, N. E. Schultz, D. G. Truhlar, *J. Chem. Theory Comput.* 2 (2006) 364–382.

[12] Y. Zhao, D. G. Truhlar, *Acc. Chem. Res.* 41 (2008) 157–167.

[13] Y. Zhao, D. G. Truhlar, *Theor. Chem.* 120 (2008) 215–241.

[14] Y. Zhao, D. Truhlar, *J. Chem. Theory Comput.* 4 (2008) 1849–1868.

[15] J. Zheng, D. G. Truhlar, *Physical Chemistry Chemical Physics* 12 (2010) 7782–7793.

[16] Y. Zhao, D. G. Truhlar, *Journal of Chemical Theory and Computation* 7 (2011) 669–676.

[17] Y. Zhao, N. Gonzalez-Garcia, D. G. J. Truhlar, *J. Chem. Phys.* 109 (2005) 2012–2018.

[18] A. D. Becke, *J. Chem. Phys.* 98 (1993) 5648–5652.

[19] C. Lee, W. Yang, R. G. Parr, *J. Phys. Rev.* B41 (1988) 785–789.

[20] L. A. Curtiss, P. C. Redfern, K. Raghavachari, *J. Chem. Phys.* 126 (2007) 084108–12.

[21] L. A. Curtiss, P. C. Redfern, K. Raghavachari, *J. Chem. Phys.* 127 (2007) 124105–1.

[22] J. A. Montgomery-Jr, M. J. Frisch, J. W. Ochterski, G. A. Petersson, *J. Chem. Phys.* 112 (2000) 6532–6542.

[23] G. P. F. Wood, L. Radom, G. A. Petersson, E. C. Barnes, M. J. Frisch, , J. A. M. Jr., *J. Chem. Phys.* 125 (2006) 1–16.

[24] K. Raghavachari, G. W. Trucks, J. A. Pople, M. Head-Gordon, *Chem. Phys. Lett.* 157 (1989) 479–483.

[25] *Computational Chemistry Comparison and Benchmark DataBase* (2010). URL http://cccbdb.nist.gov/timings.asp

[26] R. K. Robinson, R. P. Lindstedt, *Combustion and Flame* 158 (2011) 666–686.

[27] B. C. Garrett, D. G. Truhlar, *J. Chem. Phys.* 70 (1979) 1593–1598.

[28] D. H. Lu, T. N. Truong, V. S. Melissas, C. G. Lynch, Y. P. Liu, B. C. Garrett, R. Steckler, A. D. Issacson, S. N. Rai, G. C. Hancock, J. G. Lauderdale, T. Joseph, D. G. Truhlar, *Comput. Phys. Commun.* 71 (1992) 235–262.

[29] Y. P. Liu, C. G. Lynch, T. N. Truong, D. Lu, D. G. Truhlar, B. C. Garrett, *J. Am. Chem. Soc.* 115 (1993) 2408–2415.

[30] J. Zheng, S. Zhang, B. J. Lynch, J. C. Corchado, Y.-Y. Chuang, P. L. Fast, W.-P. Hu, Y.-P. Liu, G. C. Lynch, K. A. Nguyen, C. F. Jackels, A. F. Ramos, B. A. Ellingson, V. S. Melissas, J. Vill, I. Rossi, E. L. Coitio, J. Pu, T. V. Albu, R. Steckler, B. C. Garrett, A. D. Isaacson, D. G. Truhlar., *POLYRATE version 2010-A*, Department of Chemistry and Supercomputer Institute, University of Minnesota (2010).

[31] M. J. Frisch, G. W. Trucks, H. B. Schlegel, G. E. Scuseria, M. A. Robb, J. R. Cheeseman, G. Scalmani, V. Barone, B. Mennucci, G. A. Petersson, H. Nakatsuji, M. Caricato, X. Li, H. P. Hratchian, A. F. Izmaylov, J. Bloino, G. Zheng, J. L. Sonnenberg, M. Hada, M. Ehara, K. Toyota, R. Fukuda, J. Hasegawa, M. Ishida, T. Nakajima, Y. Honda, O. Kitao, H. Nakai, T. Vreven, J. A. Montgomery, Jr., J. E. Peralta, F. Ogliaro, M. Bearpark, J. J. Heyd, E. Brothers, K. N. Kudin, V. N. Staroverov, R. Kobayashi, J. Normand, K. Raghavachari, A. Rendell, J. C. Burant, S. S. Iyengar, J. Tomasi, M. Cossi, N. Rega, J. M. Millam, M. Klene,

J. E. Knox, J. B. Cross, V. Bakken, C. Adamo, J. Jaramillo, R. Gomperts, R. E. Stratmann, O. Yazyev, A. J. Austin, R. Cammi, C. Pomelli, J. W. Ochterski, R. L. Martin, K. Morokuma, V. G. Zakrzewski, G. A. Voth, P. Salvador, J. J. Dannenberg, S. Dapprich, A. D. Daniels, O. Farkas, J. B. Foresman, J. V. Ortiz, J. Cioslowski, D. J. Fox, *Gaussian 09 Revision A.1*, Gaussian Inc. Wallingford CT (2009).

[32] M. W. Schmidt, K. K. Baldridge, J. A. Boatz, S. T. Elbert, M. S. Gordon, J. H. Jensen, S. Koseki, K. A. N. N. Matsunaga, S. Su, T. L. Windus, M. upuis, J. A. Montgomery, *J. Comput. Chem.* 14 (1993) 1347–1363.

[33] M. S. Gordon, M. W. Schmidt, in: C.E.Dykstra, G.Frenking, K.S.Kim, G.E.Scuseria (Eds.), Theory and Applications of Computational Chemistry: the first forty years, Elsevier, Amsterdam, 2005, pp. 1167–1189.

[34] *Gaussian Manual* (2009).
URL http://www.gaussian.com/g_tech/g_ur/k_integral.htm

[35] L. A. Curtiss, P. C. Redfern, K. Raghavachari, J. A. Pople, *J. Chem. Phys.* 114 (2001) 108–117.

[36] J. L. Durant, C. M. Rohlfing, *J. Chem. Phys. A* 98 (1993) 8031–8036.

[37] J. D. Lewis, T. B. M. Jr., T. H. Chao, J. Laane, *J. Mol. Structure* 12 (1972) 427–449.

[38] A. Burcat, B. Rusic, *Third Millenium Ideal Gas and Condensed Phase Thermochemical ANL-05/20 and TAE 960* (2005).

[39] O. V. Dorofeeva, V. S. Iorish, V. P. Novikov, D. B. Neumann, *J. Phys. Chem. Ref. Data* 32 (2003) 879–901.

[40] B. J. McBride, S. Gordon, *Computer Program for Calculating and Fitting Thermodynamic Functions*, NASA RP 1271 (1998).

17

[41] J. Zheng, S. Zhang, J. C. Corchado, Y.-Y. Chuang, E. L. Coitino, B. A. Ellingson, D. G. Truhlar., *GAUSSRATE version 2009-A*, Department of Chemistry and Supercomputer Institute, University of Minnesota (2009).

Tables

Table 1: *Thermochemical data for species determined at the G4 level.*

Species Structure	$\triangle_f H^{298K}$ kJ mol^{-1}	S^{298K} J K^{-1} mol^{-1}	C_p^{298K} J K^{-1} mol^{-1}	$\triangle_f H^{1000K}$ kJ mol^{-1}
C_9H_{12}	5.6	412.1	154.9	200.6
C_9H_{11}-1	203.7	413.8	156.3	395.6
C_9H_{11}-2	193.8	413.7	160.7	387.7
C_9H_{11}-3	155.0	395.3	155.4	352.5

Table 2: *Molecular parameters used in rate reterminations established from M06-2X/6-31G(2df,p) geometries.*

Species Name	Sym. No.	Moments of Inertia (10^{-39} g cm^2)	Vibrational Frequencies[a] (cm^{-1})
C_9H_{12}	1	19.2; 97.3; 108.7	33, 90, 98, 236, 266, 296, 330, 393, 484, 564, 595, 688, 703, 738, 789, 827, 836, 862, 896, 932, 961, 963, 1007, 1013, 1015, 1060, 1065, 1111, 1137, 1173, 1180, 1237, 1244, 1265, 1275, 1308, 1336, 1404, 1413, 1415, 1422, 1429, 1458, 1571, 1592, 2888, 2897, 2900, 2924, 2944, 2971, 2980, 3017, 3018, 3035, 3043, 3056,
C_9H_{11}-1	1	19.1; 93.8; 105.3	23, 76, 99, 101, 263, 286, 331, 393, 451, 493, 568, 595, 688, 698, 740, 794, 811, 835, 889, 932, 945, 961, 964, 1007, 1009, 1033, 1062, 1111, 1137, 1167, 1170, 1204, 1241, 1264, 1274, 1275, 1386, 1405, 1413, 1417, 1457, 1571, 1591, 2889, 2905, 2932, 2955, 3009, 3017, 3018, 3035, 3043, 3057, 3109,
C_9H_{11}-2	1	18.2; 95.6; 110.1	40, 66, 105, 148, 238, 305, 341, 394, 434, 470, 562, 594, 687, 724, 778, 834, 837, 874, 899, 935, 944, 961, 964, 1008, 1048, 1059, 1095, 1111, 1129, 1136, 1164, 1225, 1263, 1272, 1324, 1345, 1382, 1399, 1409, 1414, 1457, 1570, 1592, 2824, 2843, 2872, 2918, 2974, 3021, 3023, 3028, 3036, 3044, 3056
C_9H_{11}-3	1	17.4; 97.2; 113.6	35, 108, 134, 206, 259, 298, 383, 391, 455, 566, 567, 588, 667, 728, 749, 793, 811, 867, 899, 926, 943, 954, 999, 1007, 1023, 1040, 1085, 1106, 1123, 1176, 1203, 1240, 1263, 1269, 1334, 1358, 1393, 1413, 1421, 1427, 1431, 1530, 1547, 2851, 2875, 2904, 2977, 2987, 3014, 3024, 3031, 3041, 3047, 3058
H_2	1	1.871	4320
CH_3	1	0.3; 0.3; 0.6	330, 1339, 1339, 2991, 3167, 3167
CH_4	1	0.5; 0.5; 0.5	1271, 1271, 1271, 1486, 1486, 2902, 3023, 3023, 3023

[a] calculated at the M06-2X/6-31G(2df,p) level with a correction factor of 0.947.

21

Distribution A: Approved for public release; distribution is unlimited.

Table 3: *Transition state parameters for rate determinations established from M06-2X/6-31G(2df,p) geometries.*

Species Name	Moments of Inertia 10^{-39} g cm^2	Vibrational Frequencies[a] (cm^{-1})
TS1	20.2; 101.9; 112.4	i1363, 32, 89, 91, 120, 216, 285, 330, 331, 392, 488, 536, 562, 595, 687, 704, 739, 790, 828, 834, 884, 900, 930, 961, 962, 1006, 1009, 1014, 1017, 1064, 1112, 1136, 1145, 1147, 1171, 1187, 1216, 1242, 1264, 1275, 1289, 1384, 1403, 1413, 1418, 1457, 1542, 1571, 1591, 2893, 2903, 2933, 2944, 2953, 3018, 3019, 3024, 3037, 3045, 3058
TS2	20.3; 98.2; 109.9	i1292, 40, 73, 97, 183, 254, 280, 292, 308, 328, 393, 482, 565, 595, 688, 736, 769, 789, 833, 841, 865, 897, 932, 961, 963, 999, 1007, 1031, 1053, 1064, 1111, 1127, 1137, 1164, 1170, 1183, 1231, 1262, 1273, 1308, 1331, 1396, 1406, 1412, 1413, 1457, 1458, 1572, 1592, 2866, 2884, 2917, 2948, 2958, 2983, 3018, 3024, 3037, 3045, 3057
TS3	19.0; 100.0; 115.0	i1475, 42, 85, 138, 181, 229, 274, 305, 315, 377, 392, 487, 563, 592, 682, 724, 735, 778, 828, 853, 888, 896, 931, 959, 963, 1008, 1019, 1030, 1040, 1079, 1111, 1138, 1144, 1176, 1227, 1237, 1253, 1265, 1272, 1288, 1333, 1337, 1406, 1412, 1421, 1426, 1456, 1564, 1586, 2886, 2901, 2924, 2937, 2974, 2985, 3022, 3032, 3042, 3050, 3058
TS4	29.4; 168.4; 170.5	i1376, 22, 48, 74, 92, 95, 117, 253, 276, 330, 345, 392, 473, 484, 539, 577, 595, 653, 687, 711, 739, 794, 831, 845, 890, 930, 945, 962, 962, 1009, 1018, 1020, 1047, 1066, 1102, 1114, 1137, 1174, 1184, 1231, 1246, 1273, 1276, 1296, 1307, 1311, 1376, 1380, 1387, 1401, 1416, 1418, 1460, 1577, 1597, 2887, 2898, 2926, 2931, 2933, 2949, 3005, 3006, 3008, 3023, 3031, 3044, 3065, 3075
TS5	37.2; 110.6; 130.7	i1453, 29, 57, 81, 92, 115, 127, 197, 262, 293, 325, 394, 460, 486, 501, 510, 567, 595, 689, 736, 788, 805, 835, 848, 873, 899, 934, 961, 963, 1007, 1015, 1039, 1062, 1073, 1076, 1111, 1135, 1164, 1170, 1232, 1261, 1269, 1282, 1316, 1320, 1332, 1371, 1373, 1399, 1410, 1413, 1415, 1456, 1571, 1591, 2865, 2881, 2914, 2930, 2936, 2948, 2974, 3018, 3022, 3035, 3045, 3056, 3063, 3073
TS6	37.2; 118.3; 132.7	i1436, 27, 50, 59, 87, 118, 143, 208, 242, 303, 359, 393, 428, 467, 493, 559, 575, 593, 685, 738, 743, 784, 831, 860, 889, 899, 931, 958, 962, 1008, 1019, 1039, 1045, 1067, 1081, 1111, 1139, 1168, 1212, 1233, 1260, 1267, 1276, 1317, 1333, 1337, 1357, 1358, 1408, 1411, 1420, 1427, 1456, 1563, 1586, 2879, 2899, 2914, 2928, 2937, 2971, 2982, 3019, 3031, 3040, 3049, 3058, 3081, 3085

[a] M06-2X/6-31G(2df,p) frequencies multiplied by a correction factor of 0.947.

Table 4: *Calculated barrier heights for Reaction 1. Results arranged relative to CCSD(T)/aug-cc-pVDZ//M06-2X/6-311++G(3df,3pd). $V_f^{\#}$ and $V_r^{\#}$ are the forward and reverse barriers, $\Delta V_f^{\#}$ and $\Delta V_r^{\#}$ show the forward and reverse deviation from the CCSD(T) values, $|\Delta|$ is the absolute average deviation. Units in kJ mol^{-1}.*

Method and Basis Set	$V_f^{\#}$	$V_r^{\#}$	$\Delta V_f^{\#}$	$\Delta V_r^{\#}$	$|\Delta|$
CCSD(T)/aug-cc-VDZ//M06-2X/6-311++G(3df,3pd)	43.1	50.2	0.0	0.0	0.0
M06-2X/6-31G(2df,p)	45.1	52.4	2.0	2.2	2.1
M06/6-31G(2df,p)	39.6	51.5	-3.5	1.3	2.4
M08-SO/6-31g(2df,p)	46.9	55.1	3.8	4.9	4.3
CBS-QB3	42.7	59.4	-0.4	9.2	4.8
M06-2X/6-311++G(3df,3pd)	46.7	58.5	3.6	8.3	5.9
CBS-4M	46.8	60.8	3.7	10.5	7.1
G4	36.2	61.0	-6.9	10.8	8.9
G4MP2	19.2	37.3	-14.9	-9.6	12.3
B3LYP/6-31G(2df,p)	20.0	45.9	-23.1	-4.4	13.7

Table 5: *Calculated barrier heights for Reaction 2. Results arranged relative to CCSD(T)/aug-cc-pVDZ//M06-2X/6-311++G(3df,3pd). $V_f^{\#}$ and $V_r^{\#}$ are the forward and reverse barriers, $\Delta V_f^{\#}$ and $\Delta V_r^{\#}$ show the forward and reverse deviation from the CCSD(T) values, $|\Delta|$ is the absolute average deviation. Units in kJ mol^{-1}.*

Method and Basis Set	$V_f^{\#}$	$V_r^{\#}$	$\Delta V_f^{\#}$	$\Delta V_r^{\#}$	$|\Delta|$
CCSD(T)/aug-cc-VDZ//M06-2X/6-311++G(3df,3pd)	34.0	47.0	0.0	0.0	0.0
M06-2X/6-31G(2df,p)	33.9	55.8	-0.1	8.8	4.5
M06-2X/6-311++G(3df,3pd)	34.5	59.7	0.5	12.7	6.6
M08-SO/6-31G(2df,p)	35.9	58.9	1.8	11.9	6.9
CBS-4M	35.8	59.3	1.8	12.3	7.1
CBS-QB3	31.9	59.9	-2.1	12.9	7.5
M06/6-31G(2df,p)	29.4	58.7	-4.6	11.7	8.2
G4	25.1	59.9	-8.9	12.9	10.9
G4MP2	17.7	56.6	-16.3	9.6	12.9
B3LYP/6-31G(2df,p)	11.9	54.5	-22.1	7.6	14.8

Table 6: *Calculated barrier heights for Reaction 3. Results arranged relative to CCSD(T)/aug-cc-pVDZ//M06-2X/6-311++G(3df,3pd). $V_f^\#$ and $V_r^\#$ are the forward and reverse barriers, $\Delta V_f^\#$ and $\Delta V_r^\#$ show the forward and reverse deviation from the CCSD(T) values, $|\Delta|$ is the absolute average deviation. Units in kJ mol^{-1}.*

Method and Basis Set	$V_f^\#$	$V_r^\#$	$\Delta V_f^\#$	$\Delta V_r^\#$	$|\Delta|$
CCSD(T)/aug-cc-VDZ//M06-2X/6-311++G(3df,3pd)	30.9	80.1	0.0	0.0	0.0
M08-SO/6-31G(2df,p)	29.6	89.9	-1.3	9.8	5.5
M06-2X/6-31G(2df,p)	26.3	89.3	-4.6	9.2	6.9
M06-2X/6-311++G(3df,3pd)	27.6	93.9	-3.3	13.8	8.5
CBS-QB3	27.5	98.0	-3.3	18.0	10.6
G4	18.4	90.8	-12.5	10.7	11.6
G4MP2	13.4	88.8	-17.5	-8.7	13.1
M06/6-31G(2df,p)	21.8	97.8	-9.0	17.7	13.4
CBS-4M	36.4	107.5	5.5	27.4	16.5
B3LYP/6-31G(2df,p)	5.8	94.8	-25.0	14.7	19.9

Table 7: *Calculated barrier heights for Reaction 4. Results arranged relative to CCSD(T)/aug-cc-pVDZ//M06-2X/6-311++G(3df,3pd). $V_f^\#$ and $V_r^\#$ are the forward and reverse barriers, $\Delta V_f^\#$ and $\Delta V_r^\#$ show the forward and reverse deviation from the CCSD(T) values, $|\Delta|$ is the absolute average deviation. Units in kJ mol^{-1}.*

Method and Basis Set	$V_f^\#$	$V_r^\#$	$\Delta V_f^\#$	$\Delta V_r^\#$	$|\Delta|$
CCSD(T)/aug-cc-VDZ//M06-2X/6-311++G(3df,3pd)	58.3	66.8	0.0	0.0	0.0
M06-2X/6-311++G(3df,3pd)	56.6	68.3	-1.7	1.5	1.6
CBS-QB3	57.5	71.4	-0.8	4.6	2.7
CBS-4M	58.7	72.1	0.4	5.3	2.9
M06-2X/6-31G(2df,p)	52.0	65.6	-6.3	-1.2	3.7
M08-SO/6-31G(2df,p)	56.2	74.1	-2.1	7.3	4.7
M06/6-31G(2df,p)	50.3	69.8	-8.0	3.0	5.5
G4	52.6	74.2	-5.7	7.4	6.5
B3LYP/6-31G(2df,p)	46.6	65.0	-11.7	-1.8	6.7
G4MP2	45.5	72.6	-12.8	5.8	9.3

24

Table 8: *Calculated barrier heights for Reaction 5. Results arranged relative to CCSD(T)/aug-cc-pVDZ//M06-2X/6-311++G(3df,3pd). $V_f^{\#}$ and $V_r^{\#}$ are the forward and reverse barriers, $\Delta V_f^{\#}$ and $\Delta V_r^{\#}$ show the forward and reverse deviation from the CCSD(T) values, $|\Delta|$ is the absolute average deviation. Units in kJ mol^{-1}.*

Method and Basis Set	$V_f^{\#}$	$V_r^{\#}$	$\Delta V_f^{\#}$	$\Delta V_r^{\#}$	$|\Delta|$
CCSD(T)/aug-cc-VDZ//M06-2X/6-311++G(3df,3pd)	44.2	58.5	0.0	0.0	0.0
M06-2X/6-31G(2df,p)	40.4	68.7	-3.8	10.2	7.0
CBS-4M	47.1	70.0	2.9	11.5	7.2
CBS-QB3	46.7	71.8	2.5	13.3	7.9
M06-2X/6-311++G(3df,3pd)	46.9	71.9	2.7	13.4	8.0
G4	41.6	73.1	-2.6	14.6	8.6
B3LYP/6-31G(2df,p)	40.4	75.5	-3.8	17.0	10.4
M08-SO/6-31G(2df,p)	45.7	78.5	1.5	20.0	10.7
G4MP2	34.4	71.4	-9.8	12.9	11.3

Table 9: *Calculated barrier heights for Reaction 6. $V_f^{\#}$ and $V_r^{\#}$ are the forward and reverse barriers, $\Delta V_f^{\#}$ and $\Delta V_r^{\#}$ show the forward and reverse deviation from the CCSD(T) values, $|\Delta|$ is the absolute average deviation. Results arranged relative to CCSD(T)/aug-cc-pVDZ//M06-2X/6-311++G(3df,3pd). Units in kJ mol^{-1}.*

Method and Basis Set	$V_f^{\#}$	$V_r^{\#}$	$\Delta V_f^{\#}$	$\Delta V_r^{\#}$	$|\Delta|$
CCSD(T)/aug-cc-VDZ//M06-2X/6-311++G(3df,3pd)	40.0	90.7	0.0	0.0	0.0
M06-2X/6-311++G(3df,3pd)	37.2	103.3	-2.8	12.6	7.7
G4	38.2	107.4	-1.8	16.7	9.2
CBS-QB3	41.0	108.7	1.0	18.0	9.5
M06-2X/6-31G(2df,p)	33.1	102.9	-6.9	12.2	9.5
G4MP2	34.0	103.8	-6.0	-13.1	9.6
M08-SO/6-31G(2df,p)	35.9	105.9	-4.1	15.2	9.7
CBS-4M	45.4	115.9	5.4	25.2	15.3
B3LYP/6-31G(2df,p)	31.6	113.0	-8.5	22.3	15.4
M06/6-31G(2df,p)	28.3	110.8	-11.7	20.1	15.9

25

Table 10: *Comparison of CCSD(T)/aug-cc-pVDZ//M06-2X/6-311++G(3df,3pd), M08SO/6-31-G(2df,p) and M06-2X/6-31-G(2df,p) energies. $V_f^\#$ and $V_r^\#$ are the forward and reverse barriers, $\Delta V_f^\#$ and $\Delta V_r^\#$ show the forward and reverse deviation from the CCSD(T) values. Units kJ mol^{-1}.*

	CCSD(T)/aug-cc-pVDZ		M08-SO/6-31G(2df,p)		Δ		M06-2X/6-31G(2df,p)		Δ	
	$V_f^\#$	$V_r^\#$	$V_f^\#$	$V_r^\#$	$V_f^\#$	$V_r^\#$	$V_f^\#$	$V_r^\#$	$V_f^\#$	$V_r^\#$
R1	43.1	50.2	46.9	55.1	3.8	4.9	45.1	52.4	2.0	2.2
R2	34.0	47.0	35.9	58.9	1.8	11.9	33.9	55.8	-0.1	8.8
R3	30.8	80.1	29.6	89.9	-1.2	9.8	26.3	89.3	-4.6	9.2
R4	58.3	66.8	56.2	74.1	-2.1	7.3	52.0	65.6	-6.3	-1.2
R5	44.2	58.5	45.7	78.5	1.5	20.0	41.1	68.7	-3.8	10.0
R6	40.0	90.6	35.9	105.9	-4.1	15.3	33.1	102.9	-6.9	12.2

Table 11: *Rate coefficients for bimolecular exchange reactions in the form $k = AT^n exp(-E/RT)$. Units are kmol, m^3, s, K and kJ mol^{-1}.*

No.	Reaction	A	n	E
1	$C_9H_{12} + H \rightleftharpoons C_9H_{11}\text{-}1 + H_2$			
	TST/SCT/M06-2X	2.439E+02	2.694	27.158
	TST/CCSD(T)/aug-cc-pVDZ	7.102E+04	2.035	37.345
2	$C_9H_{12} + H \rightleftharpoons C_9H_{11}\text{-}2 + H_2$			
	TST/SCT/M06-2X	2.430E+01	2.835	16.397
	TST/CCSD(T)/aug-cc-pVDZ	1.931E+04	2.116	29.123
3	$C_9H_{12} + H \rightleftharpoons C_9H_{11}\text{-}3 + H_2$			
	TST/SCT/M06-2X	2.999E+03	2.146	16.202
	TST/CCSD(T)/aug-cc-pVDZ	8.476E+03	2.043	25.656
4	$C_9H_{12} + CH_3 \rightleftharpoons C_9H_{11}\text{-}1 + CH_4$			
	TST/SCT/M06-2X	7.536E-05	4.053	29.625
	TST/CCSD(T)/aug-cc-pVDZ	6.944E-02	3.287	50.820
5	$C_9H_{12} + CH_3 \rightleftharpoons C_9H_{11}\text{-}2 + CH_4$			
	TST/SCT/M06-2X	5.075E-05	3.824	23.749
	TST/CCSD(T)/aug-cc-pVDZ	0.204E-02	3.463	35.094
6	$C_9H_{12} + CH_3 \rightleftharpoons C_9H_{11}\text{-}3 + CH_4$			
	TST/SCT/M06-2X	4.120E-04	3.857	12.629
	TST/CCSD(T)/aug-cc-pVDZ	6.00E+08	0.268	58.951

Figures
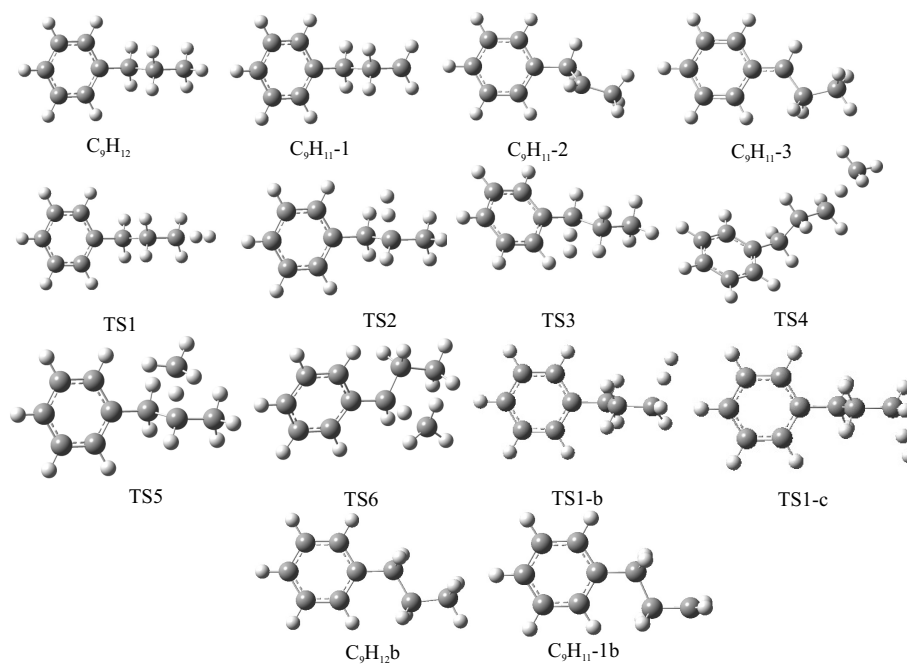
Figure 1: *Molecular and transition state structures determined at the M06-2X/6-31(2df,p) level.*
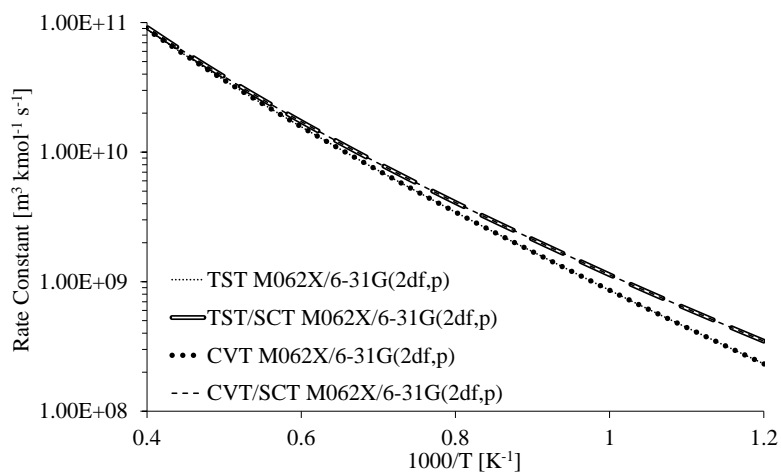
Figure 2: *Reaction rates calculated for reaction (1) C_9H_{12} + H $\rightleftharpoons$ C_9H_{11}-1 + H_2 using TST, CVT and SCT [30] at the M06-2X/6-31g(2df,p) level. Graphic illustrates the minimal differences between TST and CVT, both with and without SCT.*

28
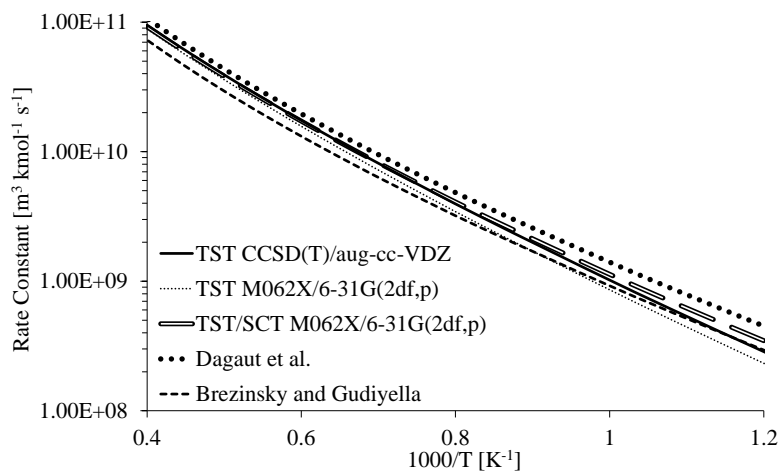
Figure 3: *Reaction rates calculated for reaction (1) C_9H_{12} + H $\rightleftharpoons$ C_9H_{11}-1 + H_2 using TST [30] at CCSD(T)/aug-cc-pVDZ and M06-2X/6-31g(2df,p) levels. Rates from Dagaut et al. [3] and Brezinsky and Gudiyella [5] are also shown.*

29
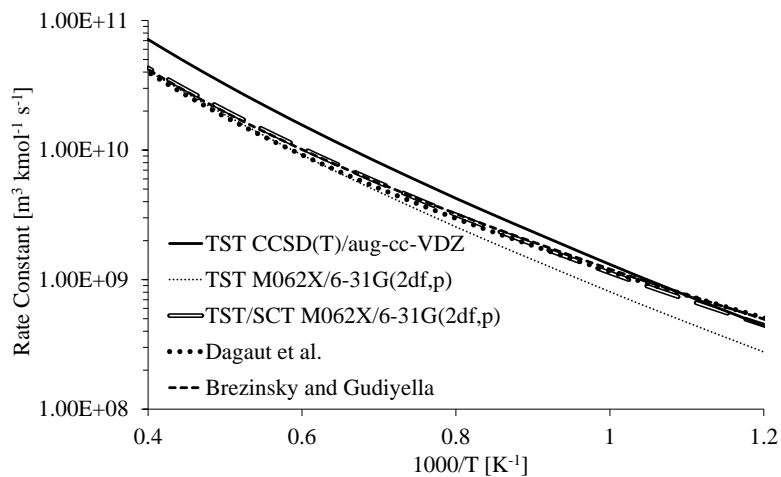
Figure 4: *Reaction rates calculated for reaction (2) C_9H_{12} + H $\rightleftharpoons$ C_9H_{11}-2 + H_2 using TST [30] at CCSD(T)/aug-cc-pVDZ and M06-2X/6-31g(2df,p) levels. Rates from Dagaut et al. [3] and Brezinsky and Gudiyella [5] are also shown.*
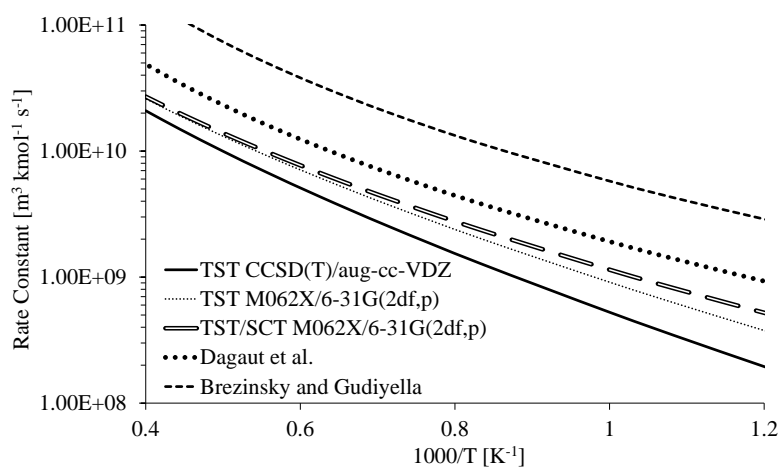
Figure 5: *Reaction rates calculated for reaction (3) $C_9H_{12} + H \rightleftharpoons C_9H_{11}$-3 + H_2 using TST [30] at CCSD(T)/aug-cc-pVDZ and M06-2X/6-31g(2df,p) levels. Rates from Dagaut et al. [3] and Brezinsky and Gudiyella [5] are also shown.*

31
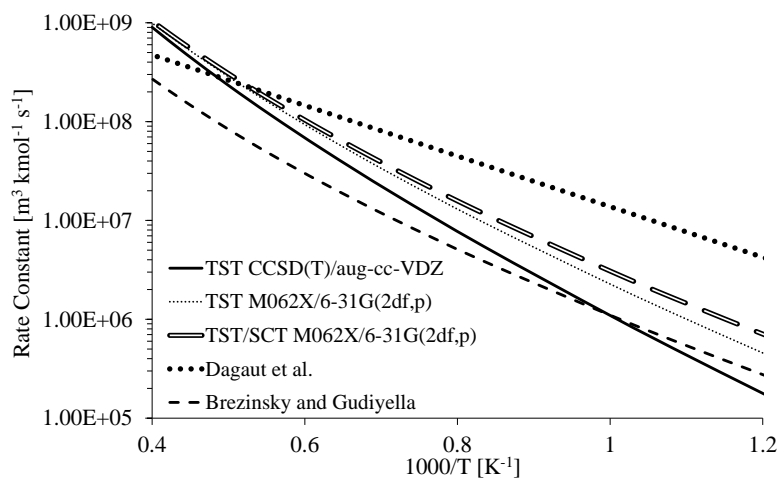
Figure 6: *Reaction rates calculated for reaction (4) $C_9H_{12} + CH_3 \rightleftharpoons C_9H_{11}\text{-}1 + CH_4$ using TST [30] at CCSD(T)/aug-cc-pVDZ and M06-2X/6-31g(2df,p) levels. Rates from Dagaut et al. [3] and Brezinsky and Gudiyella [5] are also shown.*
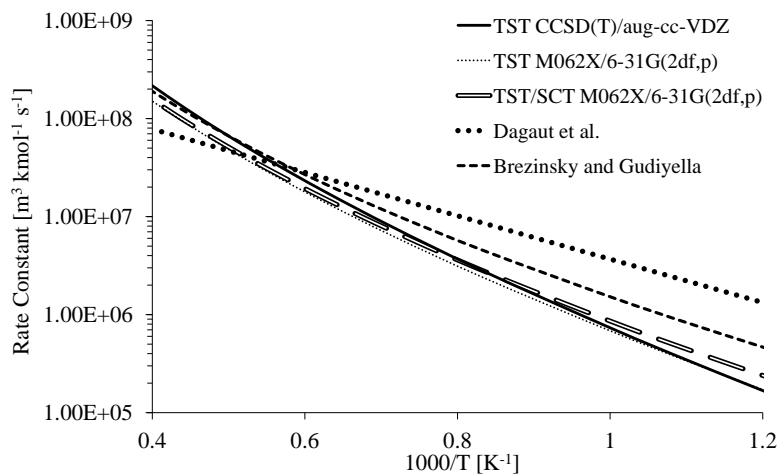
Figure 7: *Reaction rates calculated for reaction (5) $C_9H_{12} + CH_3 \rightleftharpoons C_9H_{11}$-2 + CH_4 using TST [30] at the M06-2X/6-31g(2df,p) level. Rates from Dagaut et al. [3] and Brezinsky and Gudiyella [5] are also shown.*
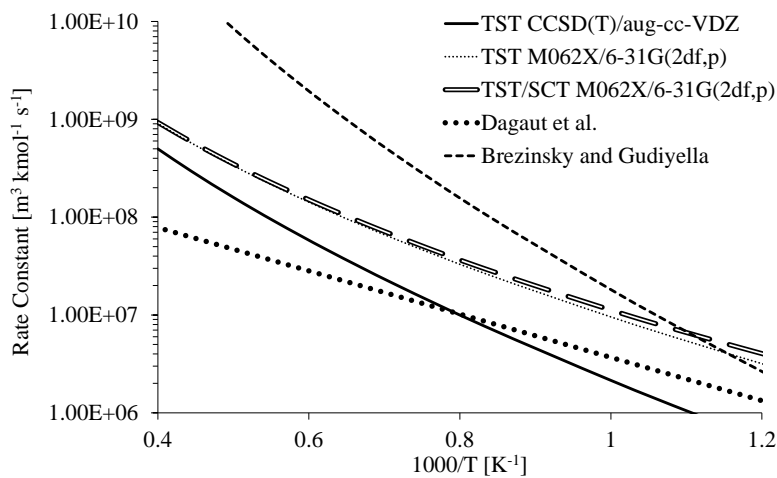
Figure 8: *Reaction rates calculated for reaction (6) $C_9H_{12} + CH_3 \rightleftharpoons C_9H_{11}$-3 + CH_4 using TST [30] at CCSD(T)/aug-cc-pVDZ and M06-2X/6-31g(2df,p) levels. Rates from Dagaut et al. [3] and Brezinsky and Gudiyella [5] are also shown.*

34